NASA Contractor Report 4036

Heat Pipe Cooling for Scramjet Engines

Calvin C. Silverstein

CONTRACT NAS1-17908
DECEMBER 1986

Date for general release December 1988

NASA

NASA Contractor Report 4036

Heat Pipe Cooling for Scramjet Engines

Calvin C. Silverstein
CCS Associates
Bethel Park, Pennsylvania

Prepared for
Langley Research Center
under Contract NAS1-17908

National Aeronautics
and Space Administration

**Scientific and Technical
Information Branch**

1986

SUMMARY

Liquid metal heat pipe cooling systems have been investigated for the combustor liner and engine inlet leading edges of scramjet engines for a missile application.

Five cooling concepts for scramjet combustor liners were analyzed, and their characteristics were compared for a short duration mission. The preferred concept consisted of a lithium-TZM molybdenum annular heat pipe surrounding a carbon-carbon combustor liner. A separate lithium reservoir is incorporated within the heat pipe structure. During the transient phase of flight, heat incident on the combustor liner is absorbed by the sensible thermal capacity of the heat pipe and the liner. During steady-state cruise, heat is absorbed by the vaporization and discharge of lithium to the atmosphere.

The heat pipe cooling system operates at a maximum temperature of 2600°F. The temperature of the combustor liner is 3400°F during steady-state operation. The peak liner temperature occurs during the transient phase of flight, and exceeds the steady-state value by 400-500°F. If the heat pipe cooling system is designed so that it remains in contact with the combustor liner throughout flight, liner temperatures can be reduced 300°F below the above levels.

For the engine inlet leading edge, heat pipe cooling is accomplished by fabricating the leading edge as a hollow structure whose inner surface is lined with a liquid-metal-filled capillary wick. Heat incident on the stagnation region and the inner surface of the leading edge is transported by the heat pipe mechanism to the outer surface and dissipated by radiation to the environment.

The leading edge which was analyzed had a radius of 0.035 in., a wedge angle of 5 deg, and was fabricated from Haynes 25 superalloy. Sodium was selected as the heat pipe fluid. With a chordwise length of 2-3 in., the peak temperature of the leading edge is limited to 1700°F or lower. Steady-state operating temperatures are about 20°F below the peak values.

It is concluded that heat pipe cooling is a viable method for limiting the temperatures of scramjet combustor liners and engine inlets to levels at which structural integrity is greatly enhanced. Current efforts to extend the operating temperature of coated carbon-carbon to the 3500-3700°F range can then be exploited to yield a combustor liner which undergoes minimal ablation during flight. Engine inlet leading edges can be fabricated from oxidation-resistant superalloys, instead of the coated refractory alloys or coated carbon-carbon which would otherwise be needed to withstand the intensive aerodynamic heating environment.

TABLE OF CONTENTS

PREFACE

The design of scramjet engines requires that engine components be protected against the severe aerothermal environment associated with hypersonic flight. Passive thermal protection methods, in which temperature- and oxidation-resistant materials are allowed to reach equilibrium temperature levels, can severely tax the maximum temperature capability of available materials. With active thermal protection systems, vulnerable structures are cooled to temperatures at which available materials may be used with confidence. If suitable cooling techniques can be devised, active cooling represents an attractive alternative to passive thermal protection.

Heat pipe cooling systems which utilize liquid metal fluids are of particular interest as a potential technique for limiting the temperature of scramjet engine components subjected to intensive aerothermal heating. With such systems, heat transport takes place automatically, without the use of external power and pumps. High heat transport rates are attainable at elevated temperatures with moderate system pressures, and system temperature drops are minimal.

The objective of the study described herein was to explore the applicability of liquid metal heat pipe cooling for those scramjet engine components for which adequate thermal protection presents the greatest challenge-the combustor liner and the inlet leading edge. The combustor liner cooling problem is treated in Part I of this report. Cooling of the inlet leading edge is addressed in Part II.

Some materials utilized in the investigation of heat pipe cooling systems for scramjet engine components are referred to by their commercial product designations, since available property data for these materials applies to specific commercial formulations. Such references do not constitute official endorsement, express or implied, of the products or their manufacturers by the National Aeronautics and Space Administration.

PART I

HEAT PIPE COMBUSTOR LINER COOLING

INTRODUCTION

Combustor liner temperatures in excess of 4000°F are characteristic of engines designed to operate at hypersonic speeds (1). No combustor liner materials are currently available which can maintain both adequate strength and resistance to corrosion/oxidation at these temperatures. A prime candidate, carbon-carbon, does exhibit good high temperature strength characteristics, but current protective coating capabilities limit maximum temperatures to around 3000°F (2). Ongoing research on carbon-carbon protective coatings is directed toward raising operational temperature capability to 3500-3700°F.

The current approach to the design of scramjet combustors for missiles is to fabricate the liner from uncooled coated carbon-carbon, with sufficient thickness to insure adequate strength after material losses from corrosion/oxidation. An alternate approach is to cool the combustor liner to a temperature at which coated carbon-carbon can exist with little or no corrosion/oxidation.

In this report, the characteristics of combustor liner cooling systems based on liquid metal heat pipe technology are examined. Liquid metal heat pipe cooling systems were considered because they are self-actuating without any requirement for external pumps or power, and are capable of heat transport at high rates and moderate pressures at elevated temperatures.

The cooling system must maintain the combustor liner temperature at prescribed levels by first removing heat incident on the liner from the combustion gas, and then dissipating the removed heat. The heat can be dissipated by sensible heating of the cooling system and surrounding structure, by vaporizing and discharging an appropriate heat sink fluid, by radiating the heat to the environment, by sensibly heating engine fuel prior to combustion, or by any combination of the above.

In an initial scoping study, carried out for the Naval Surface Weapons Center, 18 different heat pipe cooling system concepts were defined and evaluated. The results of this study are summarized in Appendix A. On the basis of relative weight and volume, five concepts were selected for further evaluation.

The heat pipe cooling system studies reported herein included the following tasks.

1. Cooling System Integrability - Additional investigations of the five cooling concepts identified in the earlier study, with emphasis on integrability of the system with the scramjet engine.

2. Conceptual Design - Selection of the preferred cooling system concept from the five candidate systems, and optimization of the resulting conceptual design.

3. Transient Behavior - Study of the temperature history of the conceptual design during a representative mission, and the influence of design parameters on peak transient temperatures.

4. Assessment of Concept Potential - Review of the heat pipe cooling system concept, its impact on scramjet engine design, and the relationship of cooling system design requirements to current technology.

OVERVIEW OF CANDIDATE DESIGN CONCEPTS

The general arrangement of the heat pipe cooling system within an engine is shown in Figures 1 and 2. The cooling system surrounds the combustor liner, and is connected to a radiating or vaporizing heat rejection system. Figure 1 illustrates how the cooling system is configured with an external heat rejection radiator. In Figure 2, the cooling system configuration is shown for a vaporizing heat sink with atmospheric discharge nozzles.

Cross-sections of the five candidate design concepts which were selected for further evaluation are illustrated schematically in Figure 3. The concepts are identified by the same designations as were used in the earlier study. For the four concepts indicated by C, the heat pipe cooling system surrounds and cools a carbon-carbon liner. With the fifth concept, designated as M-6, the internal surface of the cooling system itself acts as the combustor liner. For each case, the cooling system is constructed from TZM molybdenum, and lithium is used as the heat pipe/reservoir fluid.

In concept C-7, a heat pipe surrounding the carbon-carbon liner is connected to an external heat pipe radiator via a heat pipe transition section, as in Figure 1. Heat removed from the liner during the transient phase of the mission is absorbed by sensible heating of the cooling system and surrounding structure, while heat removed during steady-state operation is dissipated by radiation from the radiator surface.

With concepts C-8, C-5, and C-4, the transient heat load is also absorbed by sensible heating of the cooling system and surrounding structure. However, the steady-state heat load is dissipated by vaporization of lithium and its discharge into the atmosphere, as in Figure 2. These three cooling concepts differ from each other in their internal construction.

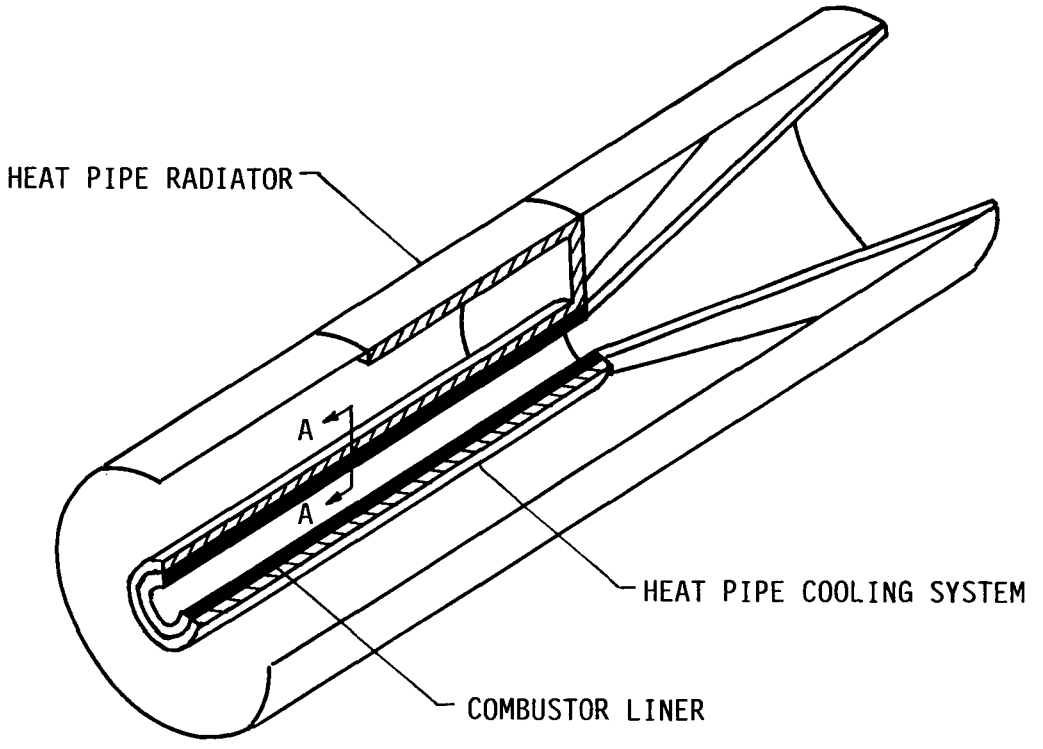

Figure 1. Cooling System Configuration With Radiation Heat Sink

Concept C-8 employs an integral heat pipe/reservoir in which the heat pipe wick and lithium reservoir are both contained within a common structure with a common vapor space. Upon opening of the discharge nozzles, the lithium vaporizes from the wick surface and is replenished by the capillary flow of liquid lithium from the reservoir.

In concept C-5, heat removed from the liner by a conventional heat pipe is transferred across a common wall to a separate lithium reservoir. Upon opening of the discharge nozzles, lithium vaporizes from the liquid-vapor interface of the reservoir, eventually depleting the reservoir of the liquid lithium.

In concept C-4, the reservoir and heat pipe wick are combined into a single entity. Upon opening of the discharge nozzles, lithium vaporizes from the liquid-vapor interface of the heat pipe wick/reservoir, eventually depleting all of the liquid lithium present.

In concept M-6, the inner surface of the heat pipe cooling system acts as the combustor liner, since there is no carbon-carbon liner present. Like concept C-5, the heat pipe structure is surrounded by a separate lithium reservoir. The heat

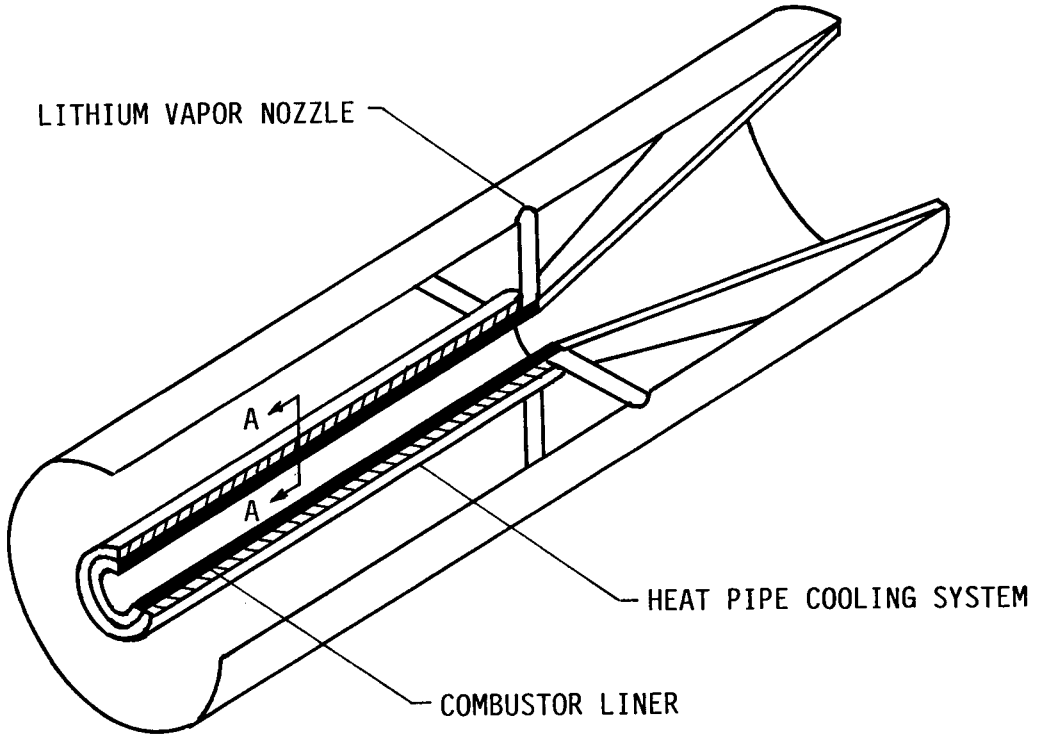

Figure 2. Cooling System Configuration With Vaporizing Heat Sink

pipe is connected to an external heat pipe radiator via a heat pipe transition section, as in Figure 1, while the vapor space of the reservoir is connected to vapor discharge nozzles, as in Figure 2. The transient heat load is dissipated by a combination of the sensible heating of the cooling system and surrounding structure, and by the vaporization and discharge of lithium from the reservoir. The steady-state heat load is dissipated by radiation from the external heat pipe radiator, as is the case for concept C-7.

STUDY ASSUMPTIONS AND DESIGN CRITERIA

The study reported herein was conducted for the most part with the same assumptions and criteria as were used in the initial NSWC study. The principal changes relate to the liner and the cooling system-liner interface.

The initial study employed a relatively thick, low conductivity protective layer of pyrolytic graphite on the carbon-carbon liner. Also, the liner and cooling system were assumed to be in perfect contact, with zero thermal resistance across

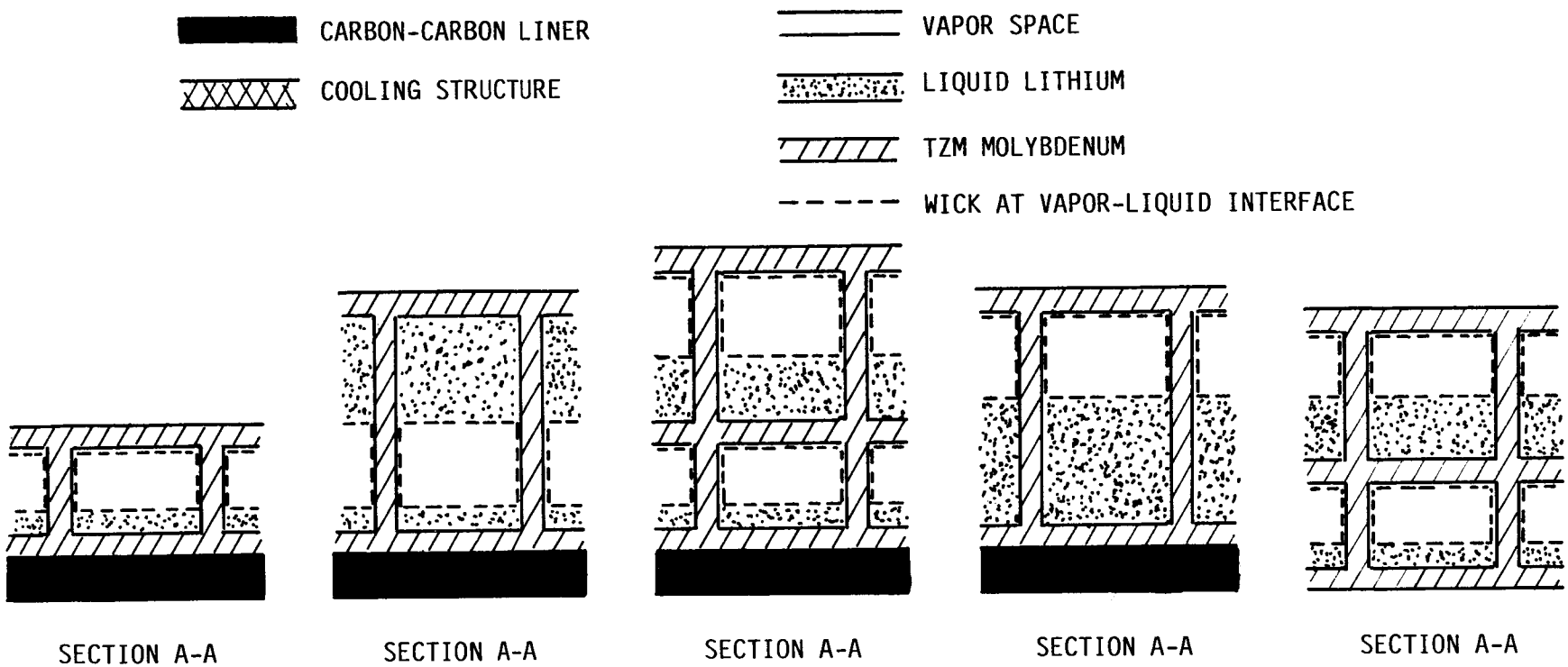

Figure 3. Cross-Sections of Heat Pipe Combustor Liner Candidate Cooling Concepts

the interface. In the present study, the carbon-carbon liner was assumed to be protected by a 0.020-in-layer of silicon carbide on the combustion gas side, and by a 0.010-in-layer of silicon carbide on surfaces exposed to air. The liner and cooling system were assumed to be separated by an air gap, across which heat flows by a combination of radiation and thermal conduction. Additional modifications included relatively minor changes in engine dimensions, and a more precise determination of equilibrium temperature on the external radiating surface.

ENGINE CONFIGURATION AND DIMENSIONS

The engine configuration used as the basis for the study is shown in Figure 4. The combustion chamber radius varies from 4.5 in. to 5.0 in. over its length of 84.0 in. The outer radius is 15.5 in. The skin thickness is 0.060 in., and is underlain by a 0.34-in. layer of MIN-K thermal insulation. When a radiative heat sink is used, the skin and insulation are displaced from the portion of the surface occupied by the radiator. A nominal thickness of 1.0 in. around the combustion chamber is allowed for the liner and heat pipe cooling system. The 20 degree (10 degree half-angle) exhaust nozzle is 59.6 in. long.

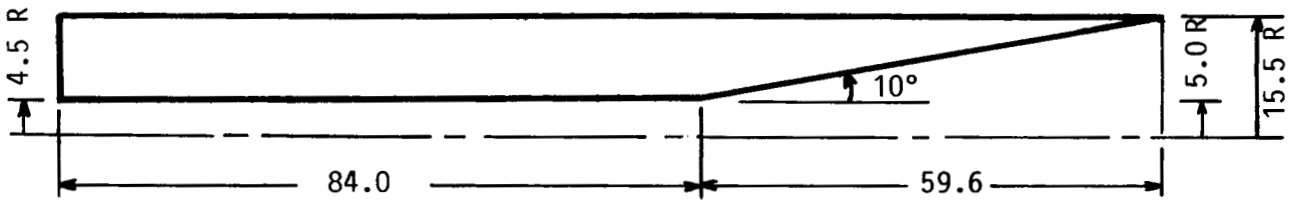

Figure 4. Engine Configuration and Dimensions

Only the combustion chamber liner is to be cooled by the heat pipe cooling system. In one design option employing a radiative heat sink, the cooling system structure was extended through the nozzle and then onto the external surface. In that instance, the nozzle was assumed to be uncooled, with no additional heat load being contributed to the heat pipe cooling system.

FLIGHT TRAJECTORY CHARACTERISTICS

Characteristics of the flight trajectory used as the basis for the study are given in Table A1 of Appendix A. Information is given on altitude, Mach number, and atmospheric pressure as a function of time, and on the average liner heat flux as a function of time and liner temperature. The total flight time

is 358 sec (rounded to 360 sec). The transient time required to approach the cruising altitude of 94,000 ft is about 72 sec.

From the data in Table A1, the vehicle acceleration and the flight path angle can be determined. The engine acceleration and component of gravity parallel to the engine axis were determined by assuming the engine axis coincident with the flight path angle. Both the engine acceleration and the component of gravity along the engine axis have the same effect on the heat pipe liquid, acting to force the liquid to the rear and increase the static head over the liquid length. In Figure 5, the total axial acceleration due to both engine acceleration and gravity is shown as a function of dimensionless time (time in sec/360). The peak axial acceleration of 2.62 g's is seen to occur at 28 sec.

COMBUSTOR PRESSURE

Detailed trajectory data on combustor pressure was not available. For purposes of analysis, the combustor pressure was assumed to vary linearly with time over the climb transient from 350 psia to 14.7 psia, and remain constant thereafter. A plot of combustor pressure versus dimensionless time is shown in Figure 6.

EQUILIBRIUM AND RECOVERY TEMPERATURES ON EXTERNAL ENGINE SURFACE

Prediction of radiative heat transfer from the surface of the external radiator (when one is used) requires that the radiation equilibrium temperature and the recovery temperature be known. The recovery temperature is the temperature in the air stream boundary layer next to the external wall. The radiation equilibrium temperature is the temperature assumed by an insulated wall surface when heat is being radiated from the surface at the same rate as the incident aerodynamic heating rate.

From Appendix B, the recovery temperature was calculated from the equation

$$T_r = T_s\left(1 + \frac{\gamma-1}{2} r M^2\right) \qquad (1)$$

where T_r = recovery temperature, R
T_s = static air temperature, R
γ = ratio of specific heats at constant pressure and constant volume
r = recovery factor = $Pr^{1/3}$ for turbulent flow (3)
Pr = Prandtl number
M = Mach number

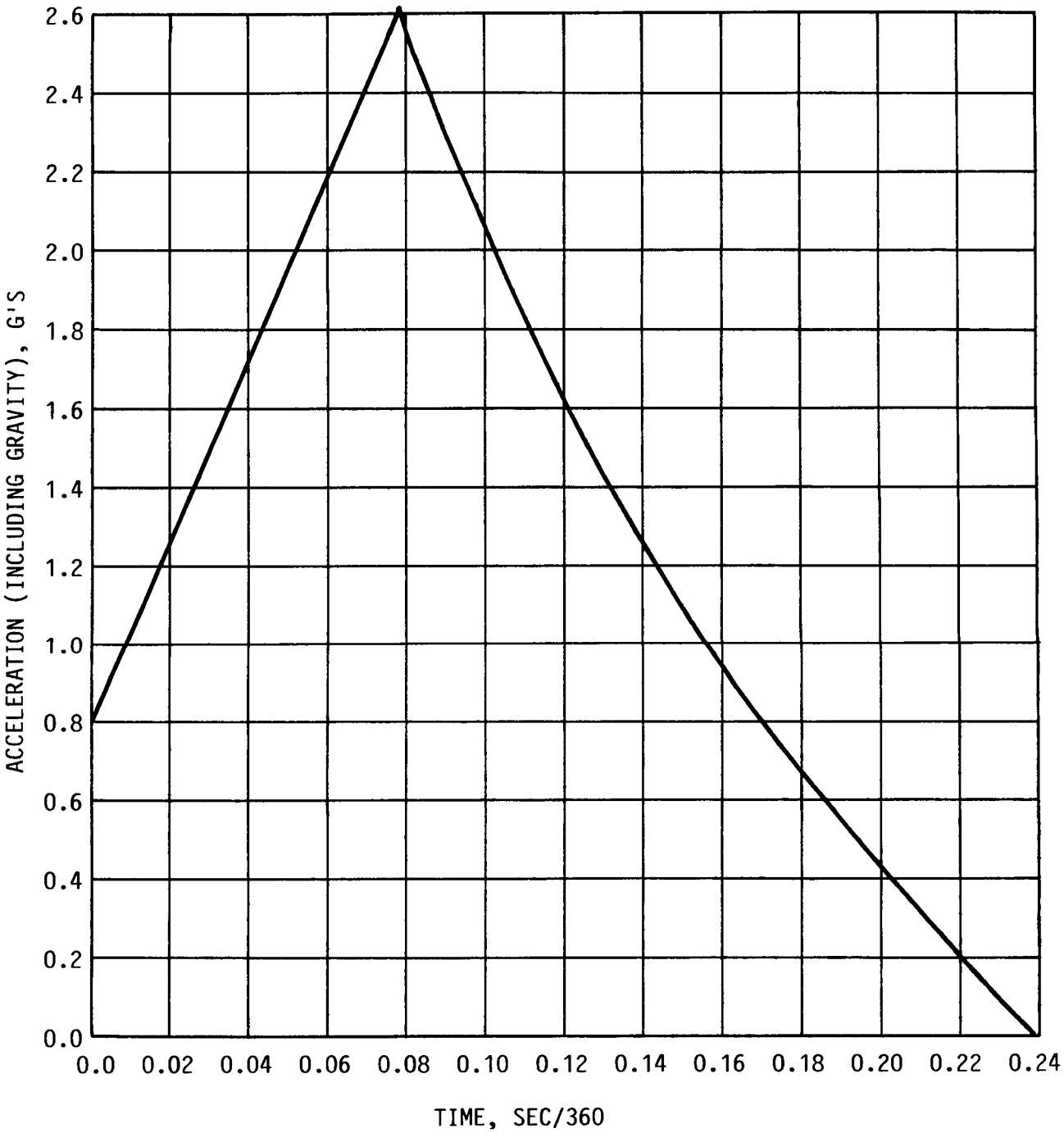

Figure 5. Axial Acceleration Versus Dimensionless Flight Time (Includes Gravity Component Along Axis)

For air, $\gamma = 1.4$ and Pr (evaluated at a mean temperature of 1880°F) = 0.722. It follows that r = 0.90.

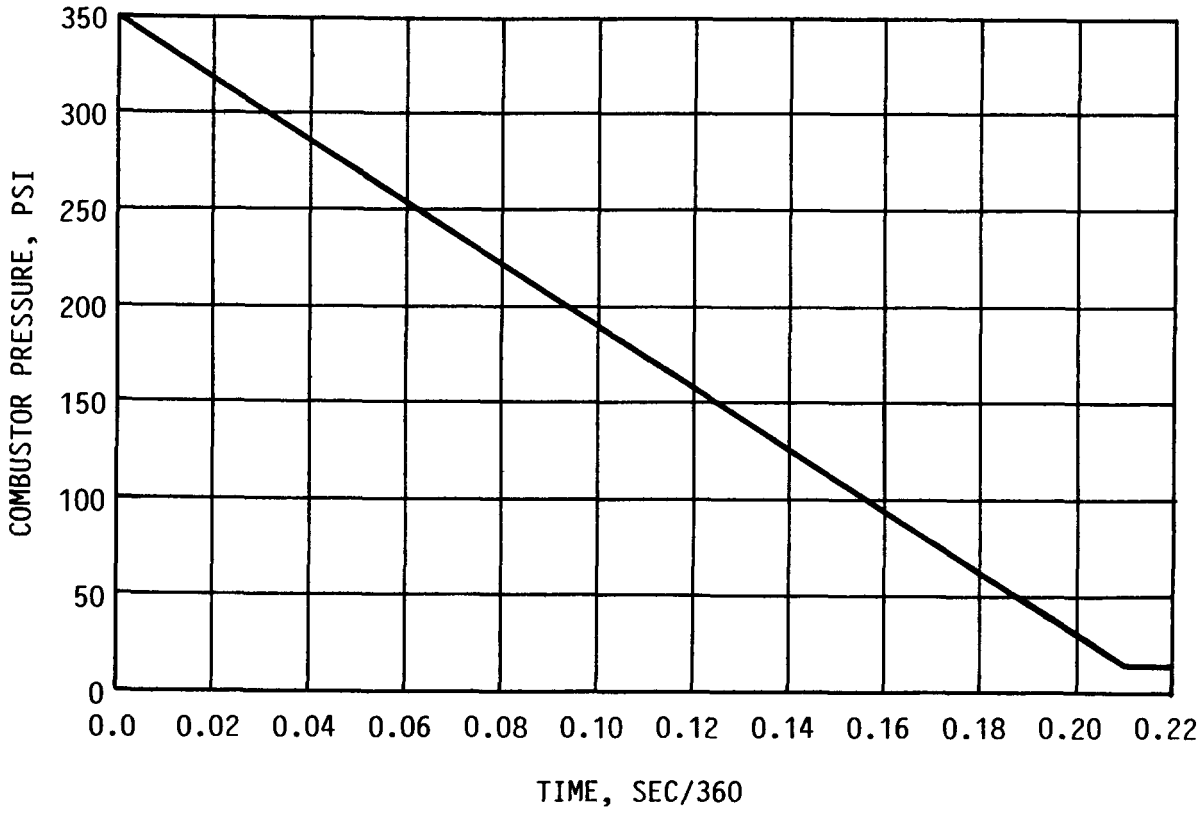

Figure 6. Variation of Combustor Pressure with Dimensionless Time

The recovery temperature was calculated as a function of mission time from the trajectory data in Appendix A.

The radiation equilibrium temperature was obtained as a function of flight time using data presented in Table I.2 of Reference 4. The data used applies to turbulent flow at a distance of 2 ft from the surface of a flat plate at an angle of attack of 0 deg. The surface emissivity was taken to be 0.8.

The recovery temperature and radiation equilibrium temperature are plotted against the dimensionless time in Figure 7.

COMBUSTOR LINER HEAT FLUX

Curves were fitted to the combustor liner heat flux data given in Table A1 of Appendix A. Two sets of curves were prepared: The initial set, termed Case A, was used to establish the steady-state liner heat flux, and to estimate the total heat load to be removed from the liner during a mission. The second set, termed Case B, matched the liner heat flux data more closely and was used in the transient analysis of cooling

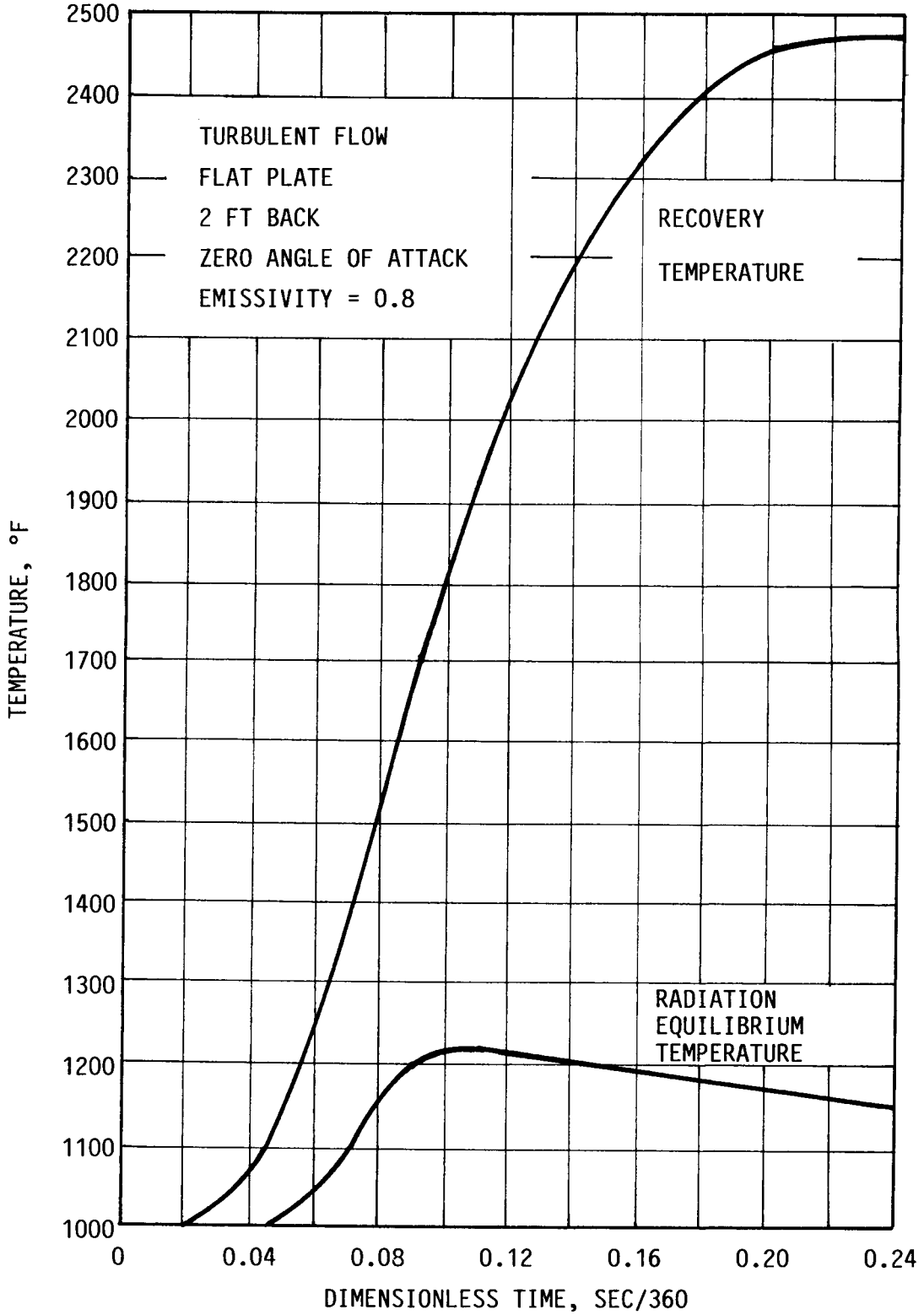

Figure 7. Recovery Temperature and Radiation Equilibrium Temperature for External Surface

system temperatures. The equations for Cases A and B are given below.

Case A

$$q_o = (1038 - 4406\tau) - (0.428 - 3.10\tau)T_o \quad ;0 \leq \tau \leq 0.10 \qquad (2)$$

$$q_o = (1038 - 4406\tau) - (0.193 - 0.767\tau)T_o \quad ;0.10 < \tau \leq 0.20 \qquad (3)$$

$$q_o = 120 - 0.0272T_o \quad ;0.20 < \tau \leq 1.00 \qquad (4)$$

Case B

$$q_o = (1040 - 2545\tau - 14{,}700\tau^2) - (0.427 - 2.818\tau)T_o \quad ;0 \leq \tau \leq 0.10 \qquad (5)$$

$$q_o = (1811 - 15{,}780\tau + 40{,}610\tau^2) - (0.468 - 4.36\tau + 11.53\tau^2)T_o \quad ;0.10 < \tau \leq 0.20 \qquad (6)$$

$$q_o = 125.9 - 0.0293T_o \quad ;0.20 < \tau \leq 1.00 \qquad (7)$$

In the above equations, T_o is the liner temperature in °F, and τ is the dimensionless time (time in sec/360 sec).

The combustor liner heat flux is plotted against dimensionless time for various liner temperatures in Figure 8, using equation sets A and B. In Figure 9, the more accurate Case B equations are plotted along with the Table A1 data. It can be seen that the heat flux at a given time decreases with increasing liner temperature. Also, at the higher liner temperatures, the heat flux is zero until some finite dimensionless time $\tau < 0.10$ has elapsed.

The dimensionless time τ_o at which the liner heat flux is zero can be found by setting Equations (2) and (5) equal to zero and solving for $\tau_o \equiv \tau$. When the heat flux is integrated over time to obtain the total heat load corresponding to a given liner temperature, τ_o is used as the lower integration limit. In Figure 10, τ_o is plotted against the recovery temperature T_o for Cases A and B.

A value of zero for the liner heat flux signifies that the effective recovery temperature of the combustion gas is equal to the liner temperature. Thus, Figure 10 also shows how the combustor recovery temperature varies with the dimensionless

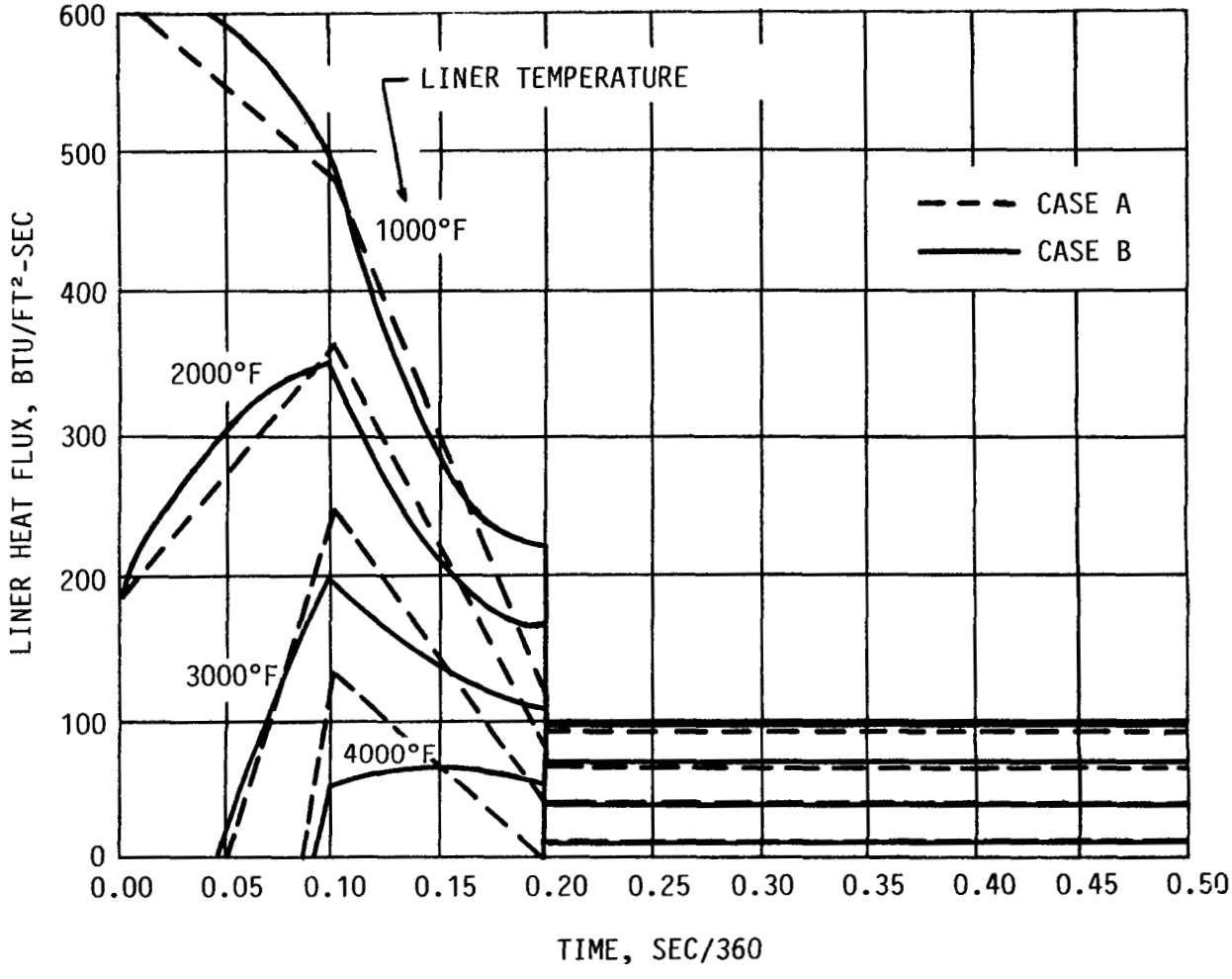

Figure 8. Liner Heat Flux from Case A and B Equations

elapsed time. For Case A, the combustor recovery temperature is 2425°F at $\tau = 0$, and 3500°F at $\tau = 0.0714$.

MATERIALS

The combustor liner is fabricated from carbon-carbon coated with silicon carbide. The heat pipe cooling system is fabricated from TZM molybdenum, with a W-3 (molybdenum disilicide) coating on surfaces exposed to air. The heat pipe and heat sink fluids are both lithium. Heat transfer from the cooling system to surrounding fuel is limited by thermal insulation. For temperatures up to 2000°F, MIN-K is used; for temperatures above 2000°F, ZIRCAR (zirconium oxide) is used. The fuel tank was assumed to be fabricated from titanium. The fuel was assumed to be Shelldyne H.

Thermophysical properties of these materials are given in Appendix C.

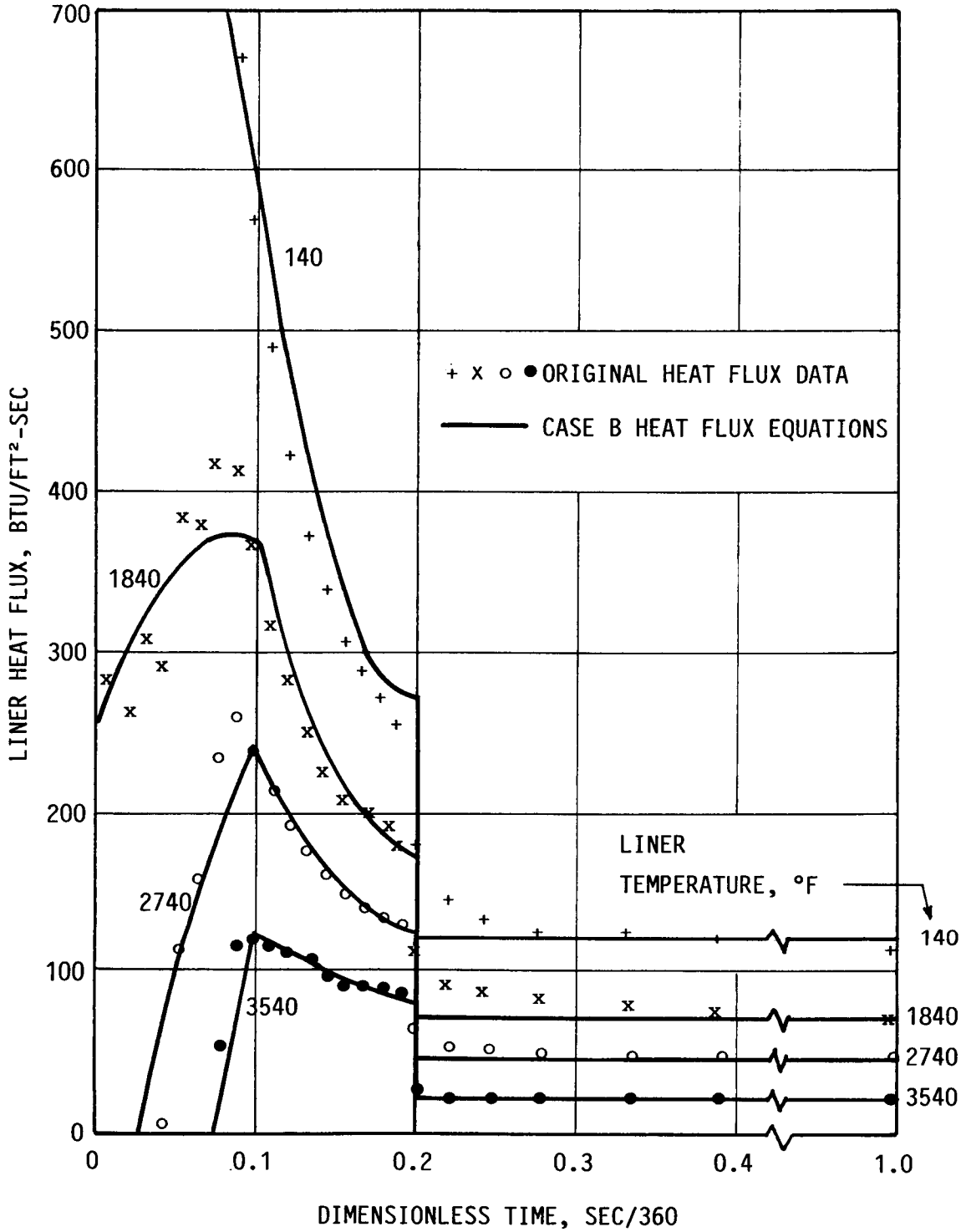

Figure 9. Liner Heat Flux Data and Case B Curves

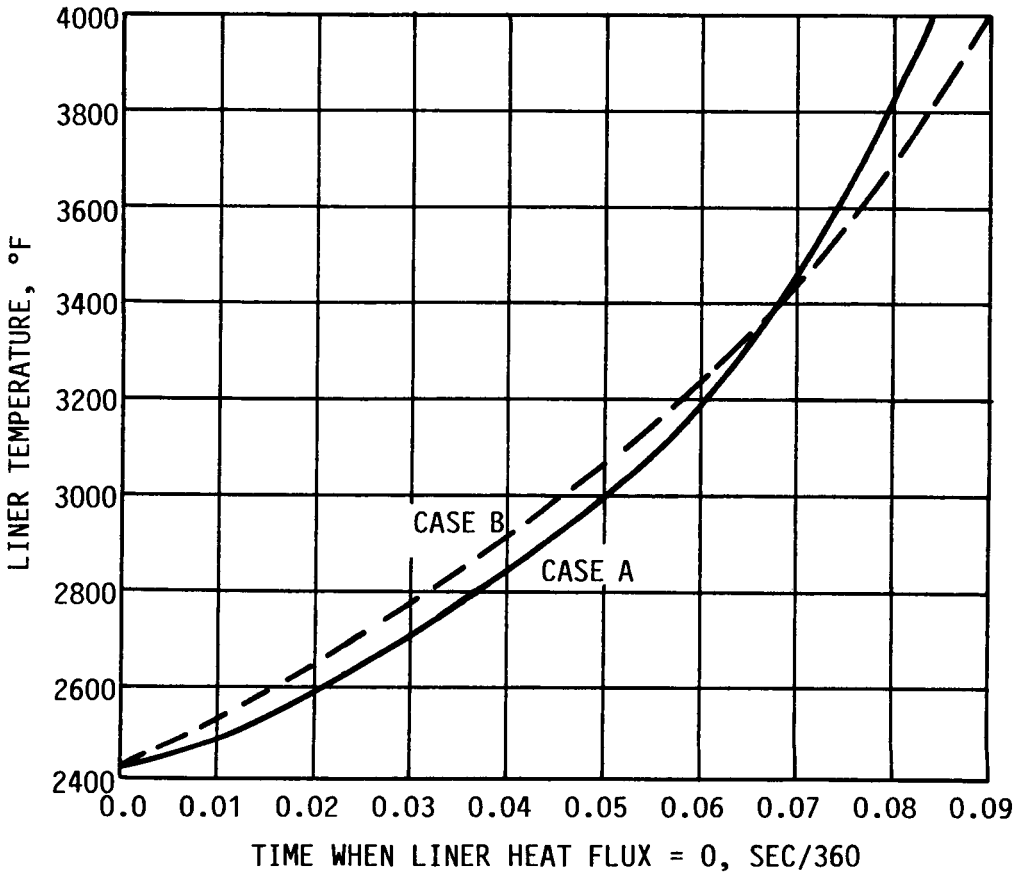

Figure 10. Liner Temperature Versus Dimensionless Time When Liner Heat Flux Is Zero (See Figure 8)

ANALYSIS OF CANDIDATE COOLING SYSTEMS

Characteristics of the candidate cooling systems having a significant influence on integrability with a scramjet engine were determined, based on steady-state cruise conditions. Included were: cooling system weight, volume, dimensions, and configuration.

Certain dimensions arrived at from the study summarized in Appendix A were retained in the current analysis, including the vapor space thickness, heat pipe wick thickness, and the thickness of the structural walls and ribs. The principal design parameters to be calculated included: system operating temperature, the spacing between structural ribs, the additional amount of lithium or structure required to absorb the combustor liner heat load, the area of the heat pipe radiator (when used), the number and size of lithium discharge nozzles (when used), and thermal insulation requirements.

System temperatures were calculated for steady-state cruise conditions, using liner heat fluxes given by Equation (4). The transient and total heat loads were calculated by integrating the liner heat flux curves over the transient and total mission times for a specified liner temperature, using Case A equations (2), (3), and (4), and then multiplying by the liner area of 17.41 ft^2. Integration started at the dimensionless time τ_o given by Case A of Figure 10.

Heat transport limits were not calculated, since the vapor space and wick dimensions determined from the heat pipe heat transport limit considerations in the earlier study were deemed adequate. Heat pipe heat transport limits were considered, however, in the subsequent conceptual design task.

CONCEPT C-7

Concept C-7 utilizes the sensible thermal capacity of the heat pipe, the carbon-carbon liner, and a secondary carbon-carbon structure to absorb the transient heat load, and an external heat pipe radiator to dissipate the steady-state heat load. The heat pipe is the same as used in the previous study, and its cross-section is shown in Figure 11.

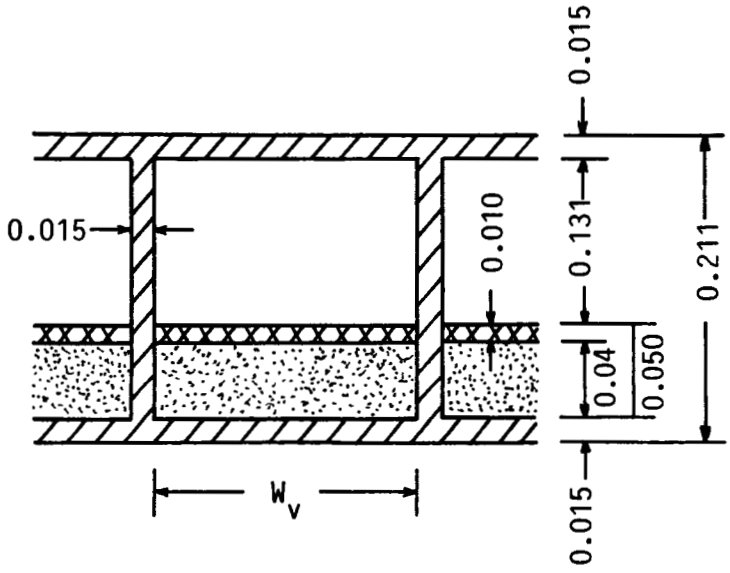

Figure 11. Heat Pipe Cross-Section for Concept C-7

The overall thickness is 0.211 in., and includes a 0.050 in. two-layer wick and a 0.131 in. vapor space. The vapor space width W_v is to be determined. The heat pipe is integrated with the liner as shown in Figure 12. Gas gaps separate the heat pipe from the carbon-carbon liner and from a secondary

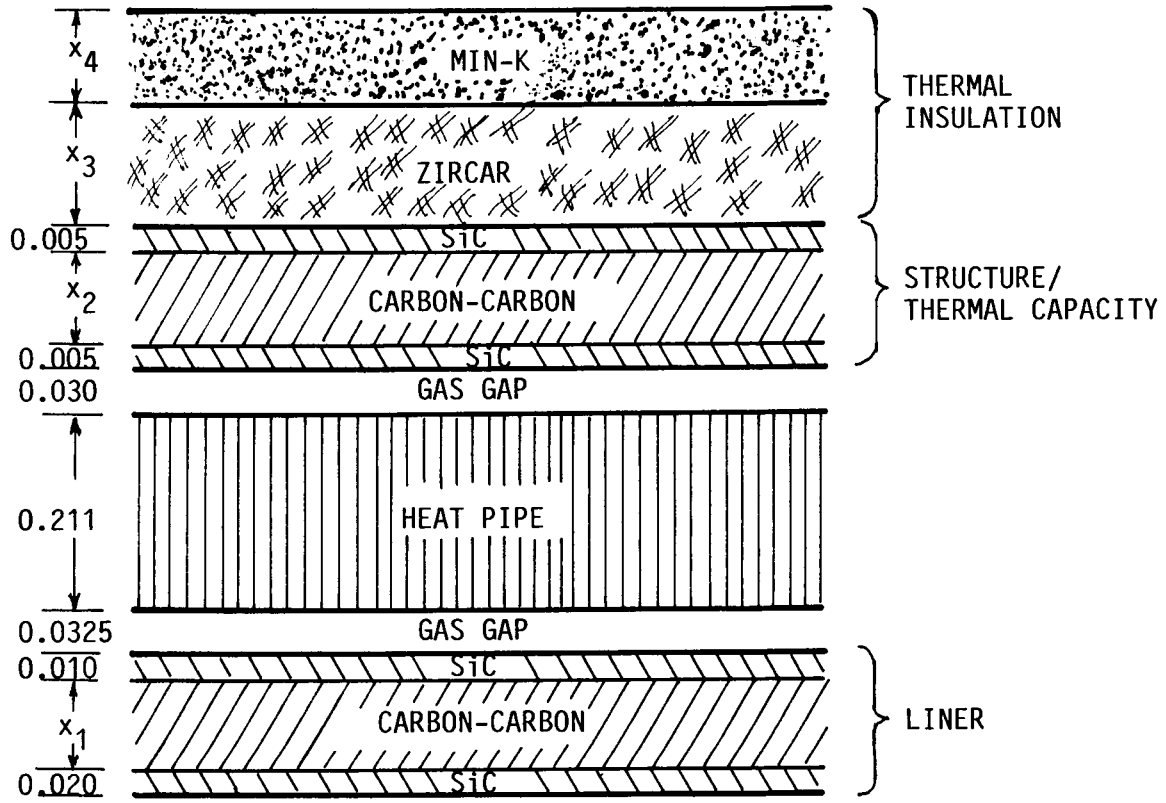

Figure 12. Cooling System Configuration for Concept C-7

carbon-carbon layer. The carbon-carbon liner, of thickness x_1, is coated with 0.020 in. of silicon carbide (SiC) on the combustion gas side and 0.010 in. of SiC on the gas gap side. The secondary carbon-carbon layer, of thickness x_2, is coated with 0.005 in. of SiC on each side. Thermal insulation borders the secondary layer on its outer surface.

The TZM heat pipe extends beyond the combustor to the engine exterior, where it serves as the heat dissipation radiator. Exterior TZM surfaces are coated with a thin (0.003 in.) layer of molybdenum disilicide. The carbon-carbon thicknesses x_1 and x_2 are to be determined. The thickness of the first gas gap corresponds to the difference in radius which develops between the liner and the heat pipe when heated from 90°F to 3000°F. The thickness of the second gas gap was taken to be approximately the same as that of the first gap.

Design Options

Two design options were initially considered for concept C-7. In Option A, the carbon-carbon liner and TZM heat pipe "float"; that is, they are exposed to combustion gas pressure on both sides. Hence, neither the liner nor the heat pipe are

required to withstand the high hoop stress associated with containment of the combustion gas. Instead, the containment function is provided by the second carbon-carbon layer of thickness x_2.

In Option B, the liner acts as the pressure vessel, withstanding the hoop stress imposed by the pressurized combustion gas. The gaps on either side of the heat pipe are then at atmospheric pressure, so that again there is no pressure differential across the heat pipe thickness to produce a hoop stress. Layer x_2 serves no structural function in Option B, but is included to augment the thermal capacity of the engine structure.

Although the heat pipe is not subjected to a hoop stress in either option, a pressure differential will exist between the heat pipe interior and exterior. Therefore, the heat pipe walls will be subjected to bending stress for both options.

Provision must be made for heat pipe access to the exterior surface. The most direct path is radially through the engine mid-section. An alternate path, which does not impact the engine interior structural design, would run through the engine exhaust nozzle and then to the exterior. Since preliminary analysis showed an increase in heat pipe weight of about 50% for access to the engine exterior via the exhaust nozzle compared to access via the engine mid-section, only mid-section access was considered further.

Cooling System Heat Transfer

The basic criterion followed in establishing the operating temperature of the heat pipe cooling system was that the steady-state liner temperature not exceed 3500°F. The heat pipe temperature is equal to the liner temperature minus the temperature drop across the liner and the gas gap. Initially, the factors affecting heat transfer across the gas gap, and the associated temperature drops were considered. Then, the effects of liner design parameters on operating temperature were analyzed. The gas in the gap was assumed to be air.

Air Gap Heat Transfer - Heat transfer across the air gap occurs by a combination of radiation and conduction, and is given by the equation

$$q_5 = \left(\frac{\varepsilon}{2-\varepsilon}\right)\sigma(T_5^4 - T_6^4) + \frac{k_g}{\delta}(T_5 - T_6) \qquad (8)$$

where q_5 = incident liner heat flux
ε = emissivity on each side of air gap
δ = air gap thickness
k_g = mean thermal conductivity of air in gap

T_5 = absolute temperature on liner side of gap
T_6 = absolute temperature on heat pipe side of gap
σ = universal radiation constant
$= 0.476 \times 10^{-12}$ Btu/ft^2-sec-R^4

In Figure 13, the temperature on the cooler side of an air gap (i.e., the heat pipe temperature) is plotted as a function of hot side temperature (i.e., the temperature on the cool side of the liner) and gap thickness. The liner heat flux is fixed at 24.8 Btu/ft^2-sec, corresponding to a liner temperature of 3500°F. The emissivity of the surfaces on both sides of the gap is 0.8. The liner thickness varies with the hot side temperature here in order to maintain the liner temperature and heat flux constant.

At a given hot side temperature, the cold side temperature varies over a range defined by gap thicknesses of zero and infinity. A gap thickness of zero signifies zero thermal resistance between the surfaces, and the cold and hot side temperatures are identical. A gap thickness of infinity signifies maximum thermal resistance between the surfaces, with heat transfer solely by radiation. The cold side temperature is then at a minimum.

The effective gap width between two surfaces in contact at zero pressure with surface finishes in the 10 to 40 microinch range lies approximately between 0.0001 in. and 0.001 in. (5). Conduction heat transfer dominates in this gap thickness range, and the cold side temperature is at most 100°F lower than the hot side temperature.

If the carbon-carbon liner and TZM heat pipe are initially in contact at room temperature and allowed to expand freely as the temperature rises to operating levels, a gap of 0.0325 in. develops. Radiation heat transfer dominates for gap thicknesses of this magnitude or larger. The cold side temperature is then at most around 100°F hotter than the temperature which would be attained for a gap thickness of infinity (i.e., radiation heat transfer only).

Even when radiation is the dominant heat transfer mode, the cold side temperature is only a few hundred degrees below that of the hot side. Consider a hot side temperature of 3100 °F. If the two surfaces have a 40 microinch finish and are in contact, the cold side temperature is 3000°F. If the gap thickness is 0.0325 in., the cold side temperature is 2635°F.

The effectiveness of conductive heat transfer across a small air gap is dependent on the air behaving as a continuum. This condition is generally satisfied if the gap thickness δ is 50 to 100 times larger than the mean free path λ of the air. For air at 14.7 psia and 2600°F, the mean free path, as calculated from Equation (36) of Reference 6 in conjunction with air

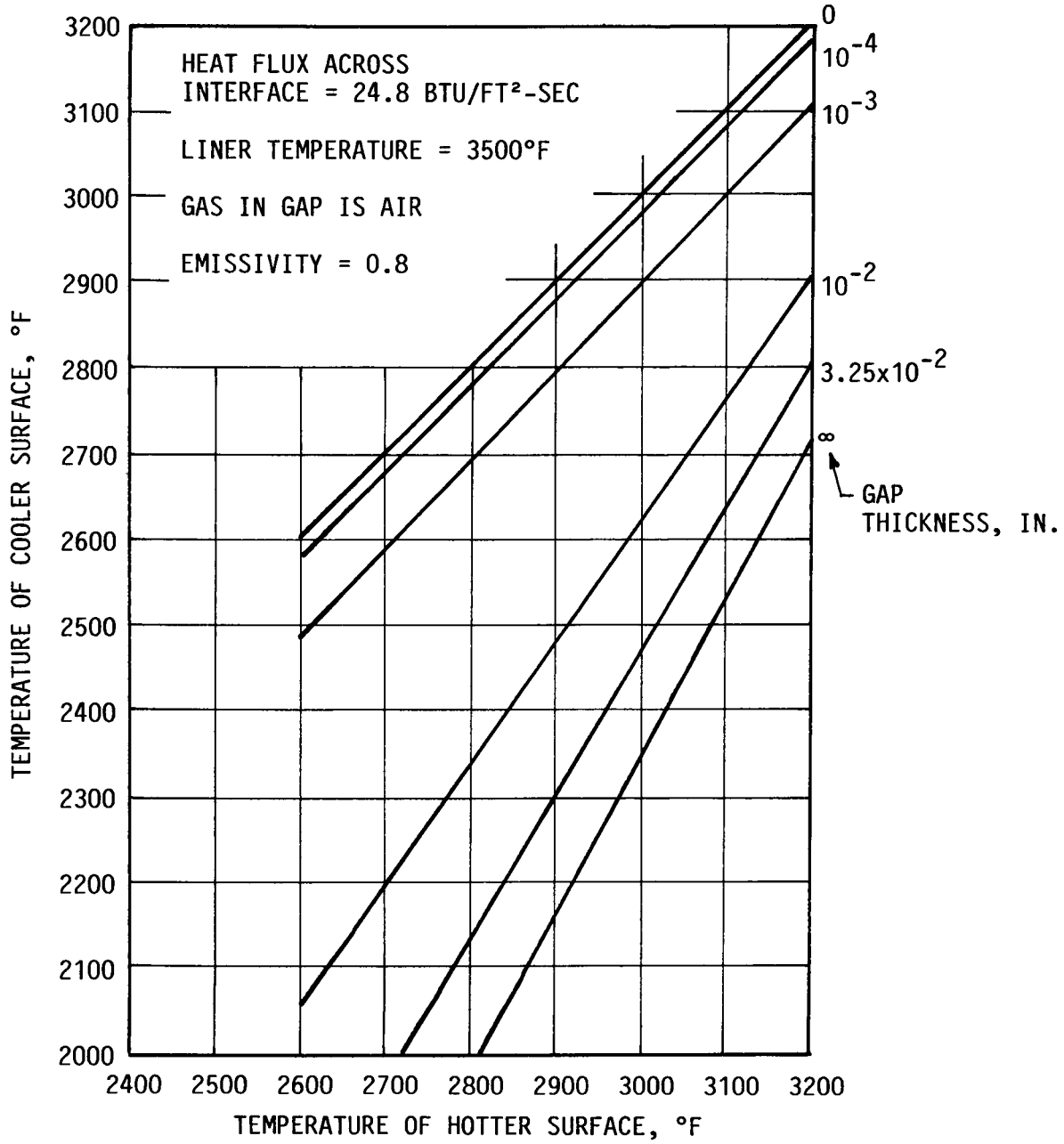

Figure 13. Surface Temperature Due to Heat Transfer Across Air Gap By Radiation and Conduction

density data, is 1.93×10^{-5} in. The ratio δ/λ for the 0.0325 in. gap is then 1684, assuring continuum heat transfer.

However, the ratio δ/λ is proportional to pressure. At cruising altitude, where the atmospheric pressure is 0.21 psia, the ratio δ/λ drops to 24, indicating that heat transfer is more characteristic of the transitional region between free molecular and continuum flow. The liner temperature for a given heat pipe temperature may then be somewhat higher than

given heat pipe temperature may then be somewhat higher than predicted on the basis of continuum conductive heat transfer across the air gap.

Operating Temperature - The heat pipe operating temperature is equal to the liner temperature less the sum of the temperature drops across the liner and the gas gap. The temperature across the liner thickness can be found from:

$$T_o - T_5 = \frac{y q_o}{k_1} \tag{9}$$

where q_o = liner heat flux
y = liner thickness
k_1 = liner mean thermal conductivity (carbon-carbon)
T_o = liner temperature on hot side
T_5 = liner temperature on cold side

Since the thermal conductivities of carbon-carbon and silicon-carbide are similar at elevated temperatures, the thermal conductivity of carbon-carbon was used to represent the conductivity of the entire liner.

The heat pipe/radiator temperature T_6 was then found from Equation (8). The radiator area required to dissipate the heat transferred to the liner was calculated from Equations (B6) and (B8) of Appendix B. In calculating the heat pipe/radiator temperature and the radiator area, air was assumed to be the gap gas, and the following values were used. (See Figure 7.)

Emissivity = 0.8 (gap surfaces and radiator surface)
Radiator equilibrium temperature = 1130°F
Recovery temperature on radiator surface = 2472°F
Liner area = 17.41 ft^2

In Figure 14, the heat pipe/radiator temperature and ratio of radiator area to liner area are shown as functions of liner temperature and liner thickness. Generally, the heat pipe/radiator temperature should be as high as is feasible to maximize the sensible thermal capacity per unit mass and the radiator heat flux. Offsetting these advantages of high operating temperature are the decreasing strength of the TZM containment and the increasing vapor pressure of the lithium heat pipe/heat sink fluid.

For purposes of analysis, a heat pipe/radiator temperature of 2800°F was selected. The associated lithium vapor pressure is 52.93 psia. The 2800°F temperature is not necessarily an optimum value, but provides a common basis for comparison of the various candidate cooling concepts which utilize a carbon-carbon liner.

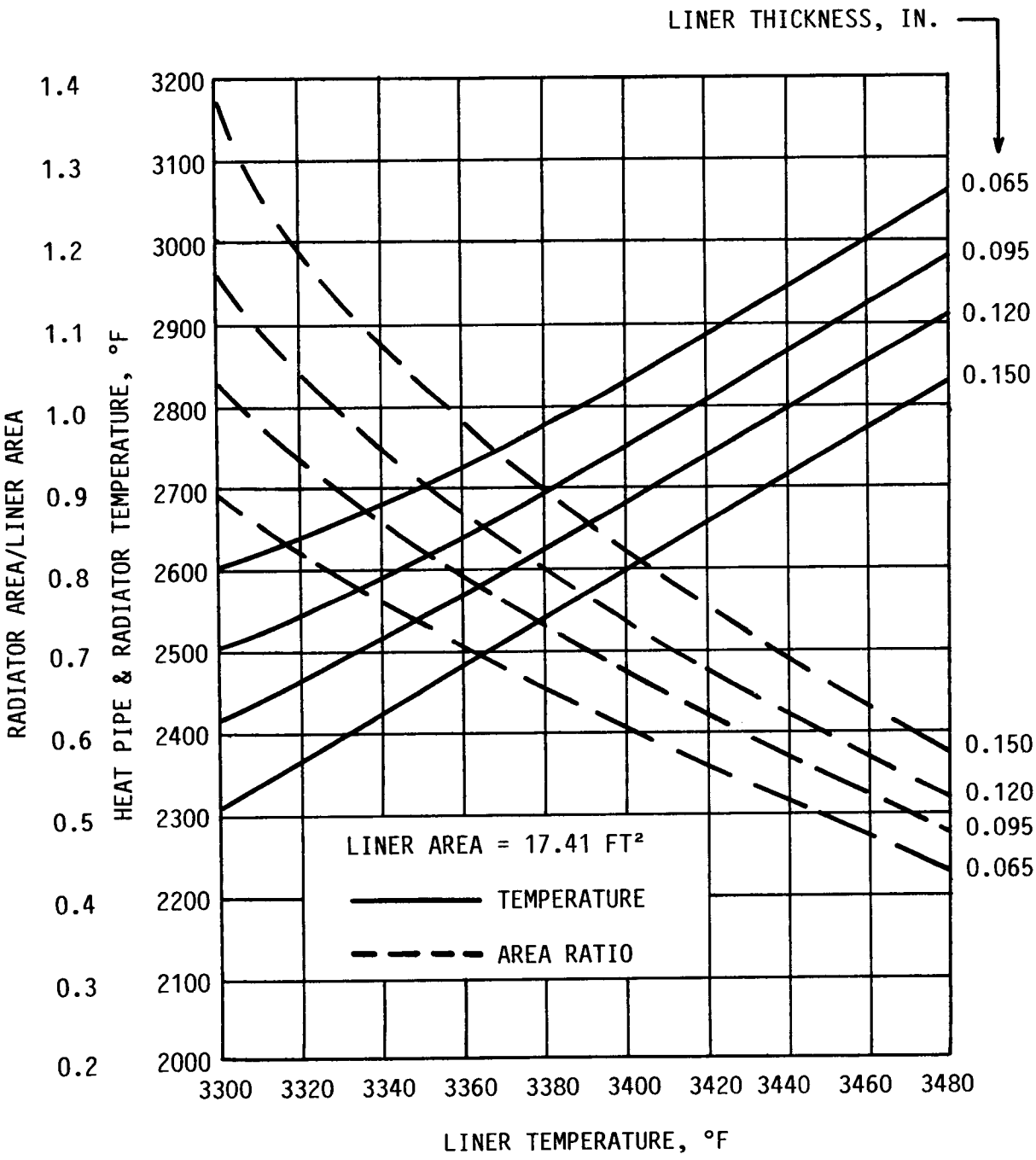

Figure 14. Radiator Temperature and Area for Cooling Concept C-7

For Option A, the floating liner, a liner thickness of 0.095 in. (including the SiC coatings) was selected. Although not subject to hoop stress, the Option A liner should nonetheless have adequate thickness to provide a reasonably stiff, vibration-resistant structure. For Option B, the structural liner, a liner thickness of 0.150 in. (including the SiC coat-

ings) was selected. The Option B liner thickness is adequate to withstand the hoop stress imposed by the combustion gas, as will be indicated below.

Heat dissipation characteristics corresponding to the selected temperature and liner thicknesses are given in Table 1.

Table 1. Heat Dissipation Characteristics for Concept C-7

Characteristic	Option A	Option B
	Floating Liner	Structural Liner
Heat Pipe/Radiator Temperature, F	2800	2800
Liner Thickness, in.	0.095	0.150
Liner Temperature, F	3419	3472
Cruise Liner Heat Flux, Btu/ft²-sec	27.0	25.5
Radiator Area, ft²	10.97	10.36
Transient Heat Load, Btu	86,500	84,600
Total Heat Load, Btu	218,100	210,000

The heat loads shown in Table 1 were found by integrating Case A Equations (2), (3), and (4) from $\tau = \tau_o$ to $\tau = 0.20$ for the transient heat load, and from $\tau = \tau_o$ to $\tau = 1.00$ for the total heat load, in each case multiplying by the liner area. The dimensionless time τ_o was found from Figure 10. It was assumed in the integrations that between $\tau = 0$ and $\tau = \tau_o$ the liner temperature is equal to the combustion gas recovery temperature, resulting in zero net heat flux and zero contribution to the heat load during this interval.

Rib Spacing

The pressure difference between the gas which surrounds the heat pipe and the heat pipe vapor pressure will produce bending stresses in the heat pipe walls and tensile or compressive stresses in the heat pipe ribs. The spacing W_v between heat pipe ribs (see Figure 11) must be selected so that the allowable stress is not exceeded in the walls or ribs. From Equations (17) and (19) of Reference (6), the rib spacing W_v can be expressed as

For wall bending: $$W_v = (\sqrt{2s/\Delta P} - 1)t_w \qquad (10)$$

For rib compression or tension: $W_v = (s/\Delta P - 1)t_w$ (11)

where t_w = wall and rib thickness
s = allowable stress
ΔP = difference between external pressure and heat pipe vapor pressure

As long as $s/\Delta P > 2$, the allowable rib spacing will be less for wall bending than for rib compression or tension. Since $s/\Delta P > 2$ for all conditions of interest and the smaller rib spacing must be selected, the heat pipe rib spacing was found from Equation (10). The rib spacing W_v should correspond to the time when the ratio $s/\Delta P$ is a minimum. A conservative approach was used to estimate the time dependence of the heat pipe temperature on which s and ΔP are dependent.

First, the liner temperature was assumed to vary with time approximately as shown in Figure 10 until the steady-state cruise temperature was reached, after which the liner temperatures remains constant. The heat pipe temperature was assumed to be about 600°F below the liner temperature. The allowable stress was taken to be 1/2 the mean tensile strength of TZM (7). The ratio $s/\Delta P$ could then be calculated as a function of mission time.

For the floating liner of Option A, where the heat pipe is surrounded by combustion gas, the minimum $s/\Delta P$ was found to be 59.5 at 25 sec. For the structural liner of Option B, where the heat pipe is surrounded by air at the pressure corresponding to the engine altitude, the minimum $s/\Delta P$ was found to be 208.6 at 72 sec. From Equation (10), the resulting rib spacings W_v are:

Option A, Floating Liner	$W_v = 0.149$ in.
Option B, Structural Liner	$W_v = 0.291$ in.

When the external pressure on the heat pipe walls exceeds the heat pipe vapor pressure, buckling of the ribs is of possible concern. The pressure differential required to buckle the heat pipe ribs can be found from Equation (20) of Reference (6).

$$\Delta P = \frac{\pi^2}{3} E \left(\frac{t_w}{H}\right)^2 \left(\frac{t_w}{W_v + t_w}\right) \quad (12)$$

where E = elastic modulus of TZM
t_w = rib thickness
H = rib height

For the floating liner of Option A, the ΔP for buckling is lowest at the heat pipe temperature of 2800°F. For the structural liner of Option B, the external (air) pressure exceeds

the heat pipe vapor temperature only at mission startup, when the heat pipe temperature is assumed to be about 600°F below the liner temperature of 2425°F, or about 1825°F. The calculated buckling pressure differential for the two options is shown below.

	Temperature,°F	ΔP for Buckling, psi	Maximum ΔP, psi
Option A, Float. Liner	2425	28,300	349
Option B, Struct. Liner	1825	65,000	12

It is clear that buckling of the heat pipe ribs is not a problem for either option.

Radiator Orientation

The combustor heat pipe is connected to the external heat pipe radiator via a heat pipe transition section. The radiator may be oriented forward or aft, as indicated in Figure 15. With the forward orientation, the heat pipe wick is located on the exterior side of the radiator, facilitating the return of condensed vapor via a liquid flow path of minimal length. With the aft orientation, an additional length of wick must be added to the exterior side of the radiator, either doubling the liquid flow path length in the radiator or requiring the addition of bridging wicks (not shown) between the exterior and interior sides.

In either case, if the flow paths through the combustor heat pipe, the transition section, and the radiator are continuous, the two right angle bends will increase the total frictional pressure drop in the heat pipe fluid. From Reference (8), based on the equivalent length of straight pipe for a 90 deg bend in 0.375 in. O.D. brass tubing with a bend radius equal to the tube radius, it was estimated that the two right angle bends will increase the effective frictional length of the heat pipe structure by 19.6 in.

The preferred configuration for concept C-7 is the forward-facing radiator orientation of Figure 15.

Segmented Heat Pipe Structure

As an alternative to the continuous heat pipe structures shown in Figure 15, the combustor heat pipe, transition section, and radiator heat pipe could be fabricated as individual subsections joined together at overlapping joints. This procedure limits the maximum frictional flow path length to

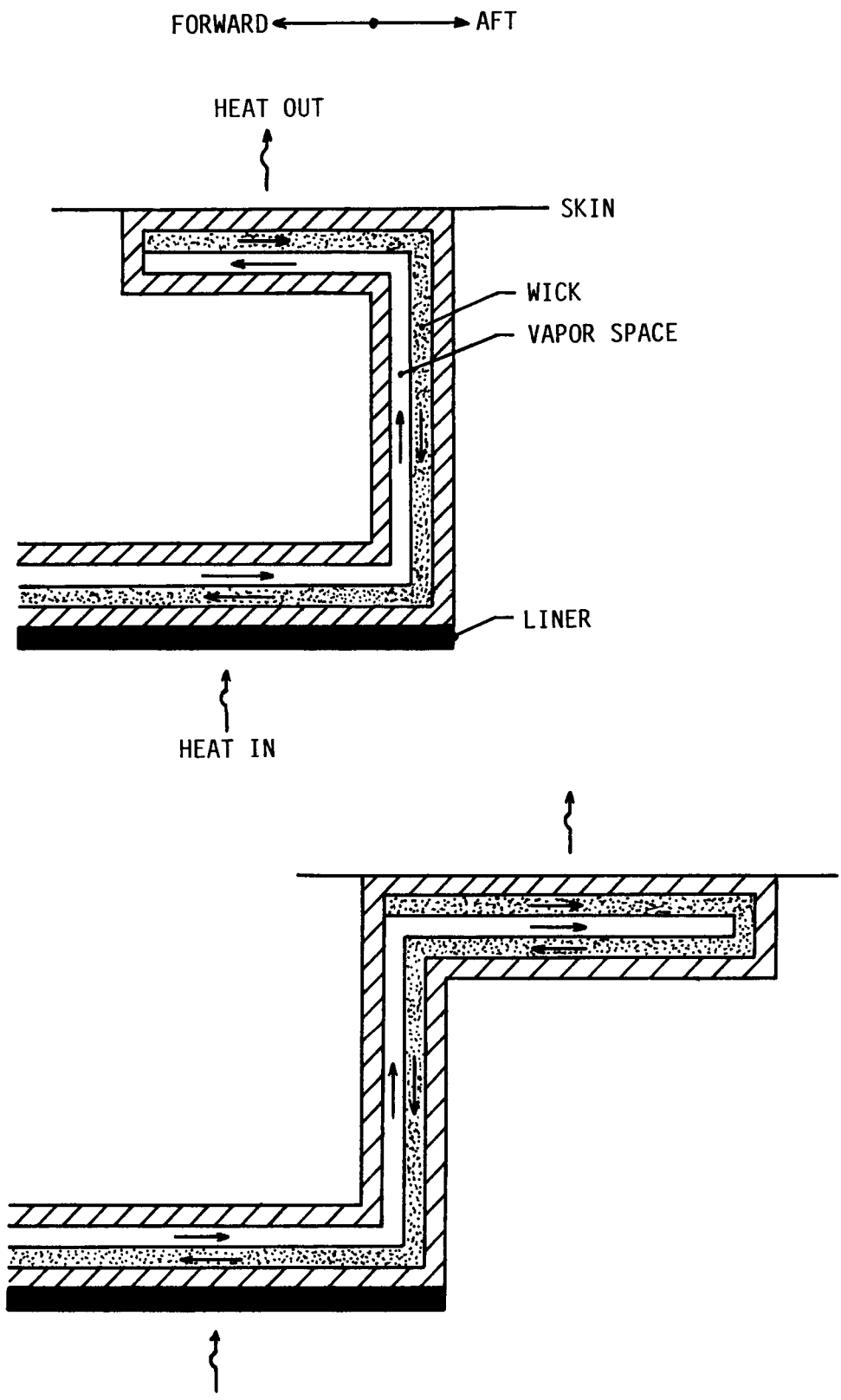

Figure 15. Heat Pipe Radiator Orientations

that in the combustor section (84.0 in.), thus reducing capillary pumping requirements. However, a substantial weight penalty will accompany this fabrication mode, resulting from the extra weight of overlapping joints and a lower temperature radiator.

For example, consider an overlapping joint at the combustor-transition junction whose area is 10% of the combustor liner area (17.41 ft^2). As indicated in Figure 16, the heat transferred across this joint will flow through two 0.015 in. TZM walls, a 0.050 in. wick, and, most probably, a minimal thickness wick opposite the primary wick. The minimal thickness wick, assumed to have a thickness of 0.010 in., may be required to assure the orderly return of vapor which condenses on the nonwick side of the heat pipe structure during the climb transient.

Assuming that 65% of the wick volume is lithium and 35% is TZM, the temperature drop across the overlapped joint is 177°F. If this were the only joint, the radiator temperature would drop to 2800 - 177 = 2623°F, requiring an increase in radiator size and weight of 24%. Adding this to the 10% weight increase due to the overlap, total cooling system weight would increase by 34%. A second comparable joint at the transition-radiator junction would further increase cooling system weight by a comparable percentage. A continuous heat pipe structure is therefore preferable to one with overlapping joints.

Pressure Drop Due to Acceleration

The acceleration which occurs during the climb transient produces a static head in the liquid lithium in the heat pipe wick, which is manifested as an additional liquid pressure drop. The magnitude of the pressure drop ΔP_a due to acceleration is given by

$$\Delta P_a = w_l x n \tag{13}$$

where w_l = density of liquid lithium
x = component of liquid length along acceleration vector
n = number of g's of acceleration

The engine acceleration, assumed to be parallel to the engine axis, is given in Figure 5. The component of gravity parallel to the engine acceleration also contributes to the liquid pressure drop, and hence has been added to the engine acceleration. The acceleration peaks at a dimensionless time of 0.078 (actual time of 28 sec) and has a total magnitude, including the effect of gravity, of 2.62 g's.

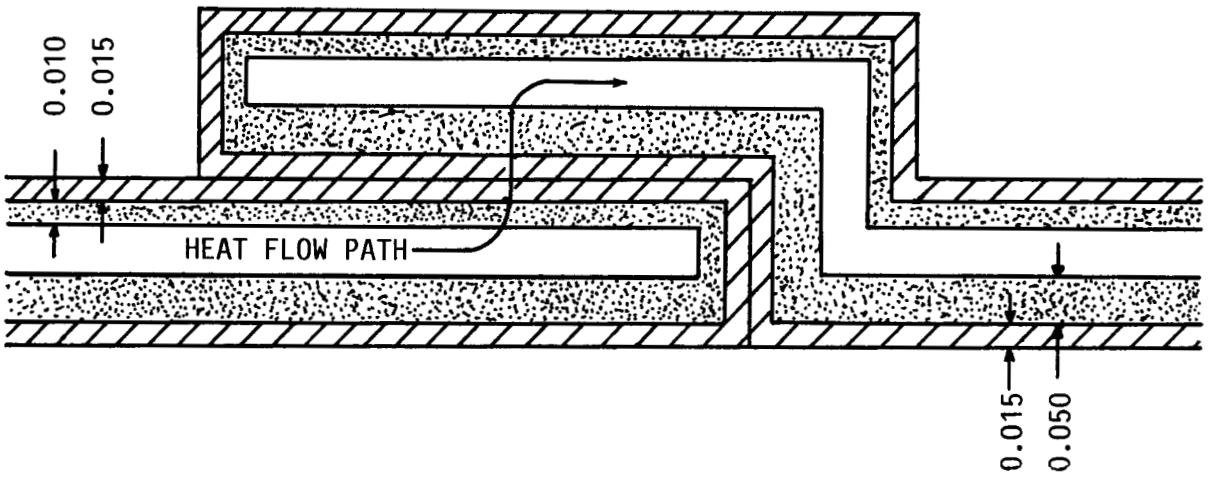

Figure 16. Overlapping Joint at Combustor-Transition Junction

The magnitude of ΔP_a is also dependent on the heat pipe temperature (since the lithium density is a function of temperature) and the position of the continuum front which advances into the unheated portion of the heat pipe. Since the time dependence of temperature and the continuum front position are not known in the steady-state analysis, the peak pressure drop due to acceleration could not be established precisely.

An estimate of the peak ΔP_a was made from Equation (13) by using the peak acceleration, the liquid lithium density at the steady-state temperature of 2800°F, and a liquid column length equal to the combustor length of 84.0 in. The resulting acceleration head was 3.24 psi. For lithium at 2800°F, it may be shown that an effective wick pore diameter of 37 microns is required to just offset this pressure drop.

A pore diameter of 20 microns, producing a maximum capillary pressure of 6.02 psi, would permit a frictional pressure drop of 6.02 - 3.24 = 2.78 psi due to flow of the heat pipe fluid. The earlier study described in Appendix A indicated that this frictional pressure drop would be adequate for heat transport at the steady-state rate, provided that an open liquid flow channel with no internal structure was used. Determination of the actual frictional pressure drop at peak acceleration would require that a transient thermal analysis be performed.

Thickness of Secondary Carbon-Carbon Layer, Thermal Capacity, and Weight

The secondary carbon-carbon layer of thickness x_2 (see Figure 12), acts as the containment vessel for the pressurized

combustion gas in Option A. The secondary layer also provides the additional sensible thermal capacity needed to absorb the transient heat load in both Options A and B.

The thickness of the secondary carbon-carbon layer was found from sensible thermal capacity considerations. The sensible thermal capacity is defined as the quantity of heat needed to raise the temperature of a given component from 90°F to its mean steady-state operating temperature. The sensible thermal capacity of the secondary carbon-carbon layer was found by subtracting the thermal capacity of the other cooling system components during the climb transient from the transient heat load given in Table 1. Since the sensible thermal capacity is equal to the product of specific heat, density, temperature rise, and volume, the thickness of the secondary carbon-carbon layer can be found if its sensible thermal capacity is known.

The total thermal capacity of the other components is equal to the sum of the sensible thermal capacity of the complete heat pipe (combustor section, transition section, and radiator section) plus the carbon-carbon liner, and the heat dissipated from the radiator during the transient climb period.

The latter contribution to thermal capacity occurs while a hot continuum front, originating in the combustor section of the heat pipe, moves to the end of the radiator. Its magnitude was estimated by assuming that the front, at a temperature of 2800°F, requires 36 sec to traverse the radiator section of the heat pipe. On the average, 1/2 of the radiator is functional during this period, which results in a heat dissipation of approximately 8500 Btu.

Values of the secondary carbon-carbon layer thickness and related thermal capacity parameters for Concept C-7 are given in Table 2. Associated weight data are given in Table 3.

From Tables 2 and 3, it is evident that there is little difference in the total thickness and weight of carbon-carbon for the floating and structural liners. However, the heat pipe is about 14 lb lighter for the structural liner of Option B, primarily because of wider rib spacing.

Hoop Stress

The tensile or hoop stress experienced by a cylindrical structure which encloses a pressurized gas is, from Equation (15) of Reference (6),

$$s = (\bar{r}/t)\Delta P \qquad (14)$$

Table 2. Sensible Thermal Capacity Parameters for Concept C-7		
Item	Option A, Floating Liner	Option B, Structural Liner
Sensible Thermal Capacity, Btu		
Heat Pipe*	32,100	29,700
C-C Liner + 2nd C-C Layer	54,400	54,900
Total	86,500	84,600
Carbon-Carbon Thickness, in.§		
Liner, x_1	0.065	0.120
2nd Layer, x_2	0.215	0.156
Total	0.280	0.276

* Includes estimated 8500 Btu dissipated by radiation during transient.

§ Doesn't include thickness of SiC protective coating.

where s = tensile stress in wall
t = wall thickness
$\bar{r}$ = mean wall radius
ΔP = net pressure difference across wall thickness

The hoop stress was conservatively calculated for the floating and structural liners according to the following assumptions.

- o ΔP is equal to the maximum combustor gas pressure of 350 psia
- o Only the carbon-carbon in the containment wall resists the ΔP

Then, for the floating liner, $\bar{r}$ = 5.54 in. and t = 0.215 in. for the second, structural layer, and the hoop stress is 9020 psi.

For the structural liner, $\bar{r}$ = 5.08 in. and t = 0.120 in., and the hoop stress is 14,800 psi.

Table 3. Heat Pipe and Carbon-Carbon Weight for Concept C-7, lb		
Item	Option A, Floating Liner	Option B, Structural Liner
Heat Pipe		
TZM	82.8	69.1
Lithium	3.0	3.0
Total	85.8	72.1
Carbon-Carbon*		
Liner	18.3	26.6
2nd Layer	37.6	28.3
Total	55.9	54.9
Heat Pipe + Carbon-Carbon		
Total	141.7	127.0
* Includes weight of protective SiC coating.		

These maximum hoop stress figures may be compared to a tensile strength of about 32,000 psi for ACC-4 carbon-carbon (9). Thus, the thickness of the structural carbon-carbon member is adequate to withstand imposed pressure loads for both design options.

Heat Leakage

Thermal insulation is required between the heat pipe cooling system and the engine interior to limit heat leakage to acceptable levels. The criterion adopted for establishing permissible heat leakage was the maximum allowable temperature rise in the engine fuel during a mission, which was taken to be 300°F.

An approximate analysis to determine the end-of-flight fuel temperature as a function of total heat leakage was conducted according to the following assumptions.

- o The fuel and fuel tank have the same temperature
- o The heat leakage rate is constant
- o The fuel consumption rate is constant

The heat leakage over a time increment dt may then be written

$$\frac{Q_o}{T_c} dt = W_{fo}(1 - \frac{t}{T_c})c_f dT + W_t c_t dT \qquad (15)$$

where Q_o = total heat leakage over flight
T_c = flight time
t = elapsed flight time
W_{fo} = initial fuel weight
c_f = specific heat of fuel
W_t = fuel tank weight
c_t = specific heat of fuel tank
T = fuel and fuel tank temperature

Letting

$$T_r = \frac{Q_o}{W_{fo}c_f}$$

$$\beta = \frac{W_t c_t}{W_{fo}c_f}$$

$$\tau = \frac{t}{T_c}$$

Equation (15) may then be written in the form

$$d(T/T_r) = \frac{d\tau}{1 + \beta - \tau} \qquad (16)$$

Upon integrating Equation (16) between $\tau = 0$ and $\tau = 1$,

$$\frac{\Delta T}{T_r} = \ln(1 + \beta) - \ln\beta \qquad (17)$$

where ΔT = the fuel and fuel tank temperature rise.

ΔT from Equation (17) was evaluated as a function of the total heat load Q_o (see T_r), for an initial fuel load of 600 lb of Shelldyne H and a 20 lb titanium fuel tank. A mean temperature of 200°F was assumed for determining thermal properties. Thermal property data for these materials are given in Appendix C. Results are shown in Figure 17. A heat leakage of 12,000 Btu produces a temperature rise of 240°F in the fuel, an acceptable figure. Therefore, a heat leakage of 12,000 Btu was used to size the thermal insulation.

If Equation (16) is integrated between $\tau = 0$ and τ, the result is

$$\frac{\Delta T}{T_r} = \ln(1 + \beta) - \ln(1 + \beta - \tau) \qquad (18)$$

ΔT from Equation (18) is plotted as a function of τ in Figure 18 for the 600 lb initial fuel weight, the 20 lb fuel tank, and a heat leakage of 12,000 Btu.

Thermal Insulation

Thermal insulation is provided around the secondary carbon-carbon layer, under the radiator heat pipe inner wall and the engine skin, and on both sides of the transition section. The thermal insulation model is illustrated in Figures 19 and 20.

The heat leakage rate was assumed to be constant over the total flight time. For temperatures of 2000°F or less, MIN-K was specified as the thermal insulation material. For temperatures above 2000°F, ZIRCAR (zirconia felt) was specified. Properties of these materials are given in Appendix C.

The objective of the thermal insulation analysis was to determine the thicknesses of MIN-K and ZIRCAR required to limit the total heat leakage to a specified level. The allowable heat leakages Q_i from the interior and Q_o from the exterior were specified separately. The flight time T_c is 360 sec.

In the combustor section, the heat pipe temperature T_o, the radius of the heat pipe outer wall R_i, and the air gap and secondary carbon-carbon layer thicknesses x_1 and x_2 are known. The temperatures at the ZIRCAR/MIN-K interface and at the MIN-K /fuel tank interface were specified as indicated. The heat transfer rate across each segment of the model is the same, and was formulated in terms of the thermal radiation and/or conduction equations appropriate to each segment. From this information, the temperatures T_1 and T_2 across the carbon-carbon layer and the ZIRCAR and MIN-K thicknesses x_3 and x_4 can be calculated.

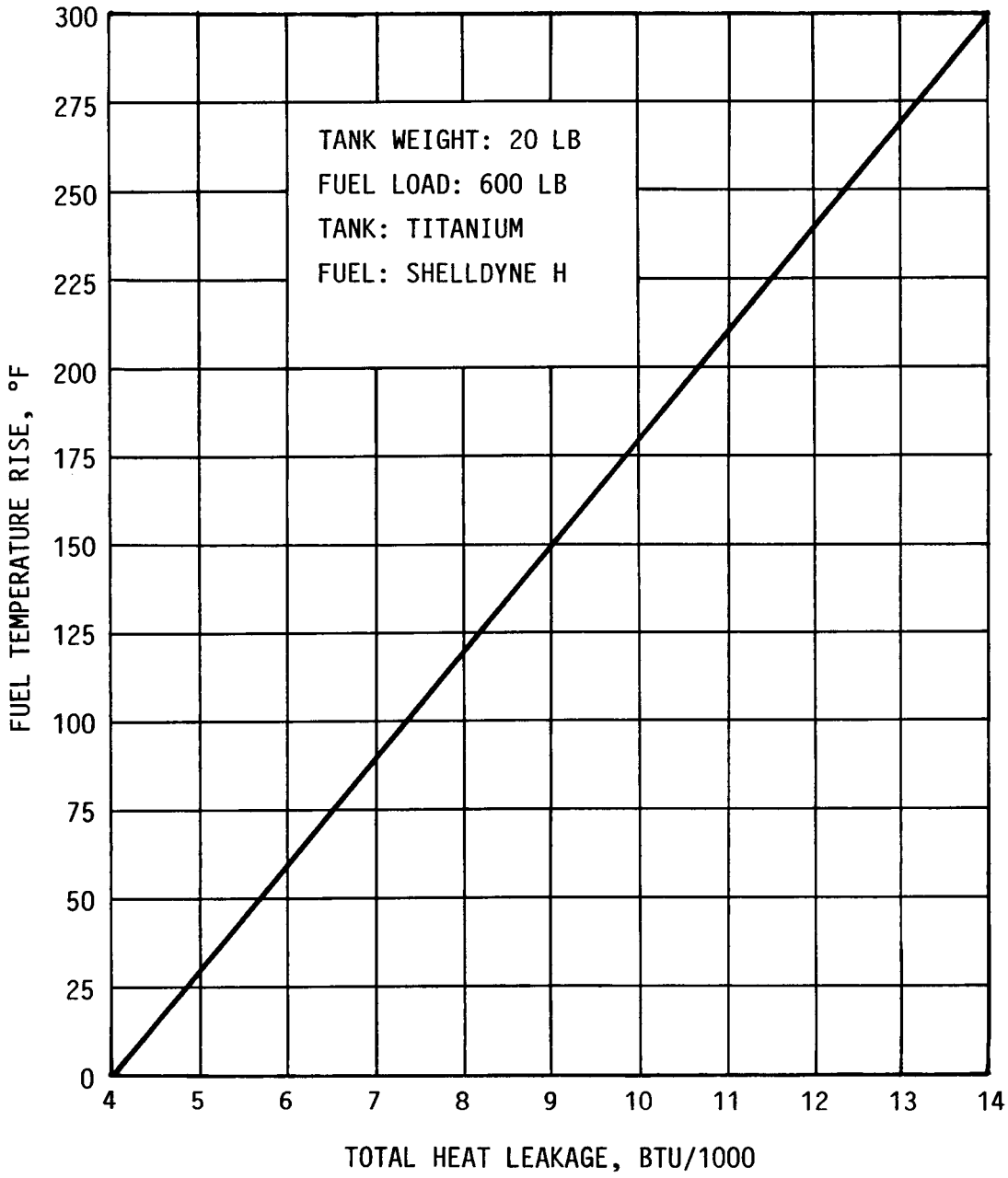

Figure 17. Fuel Temperature Rise Versus Heat Leakage Into Fuel

On the engine surface, the heat leakage to the interior is equal to that from the inner surface of the heat pipe radiator plus that from the inner surface of the skin which extends over the remaining length of the combustor. The heat leakage per unit length was taken to be the same in the combustor and radiator sections.

In the radiator section, the interface temperatures have already been established, thus enabling the insulation thick-

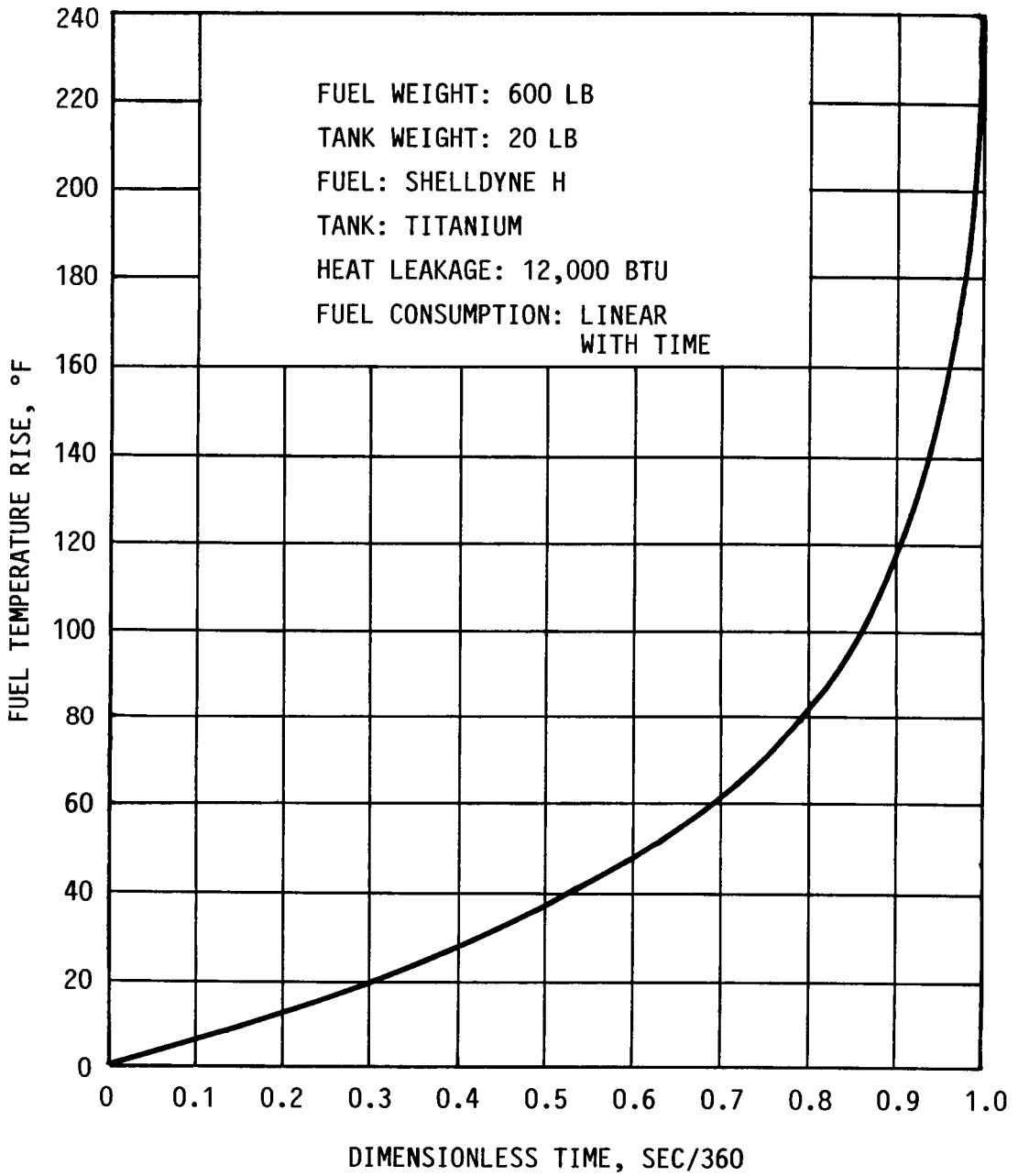

Figure 18. Rise in Fuel Temperature with Dimensionless Time

ness to be calculated. In the skin section, the skin temperature was taken to be the steady-state radiation equilibrium temperature of 1130°F, enabling the thickness of MIN-K under the skin to be determined for a specified heat leakage per unit length of the skin section.

The annular transition section between the combustor and radiator heat pipes is insulated on both sides with ZIRCAR and MIN-K, as shown in Figure 20. The heat leakage per unit area

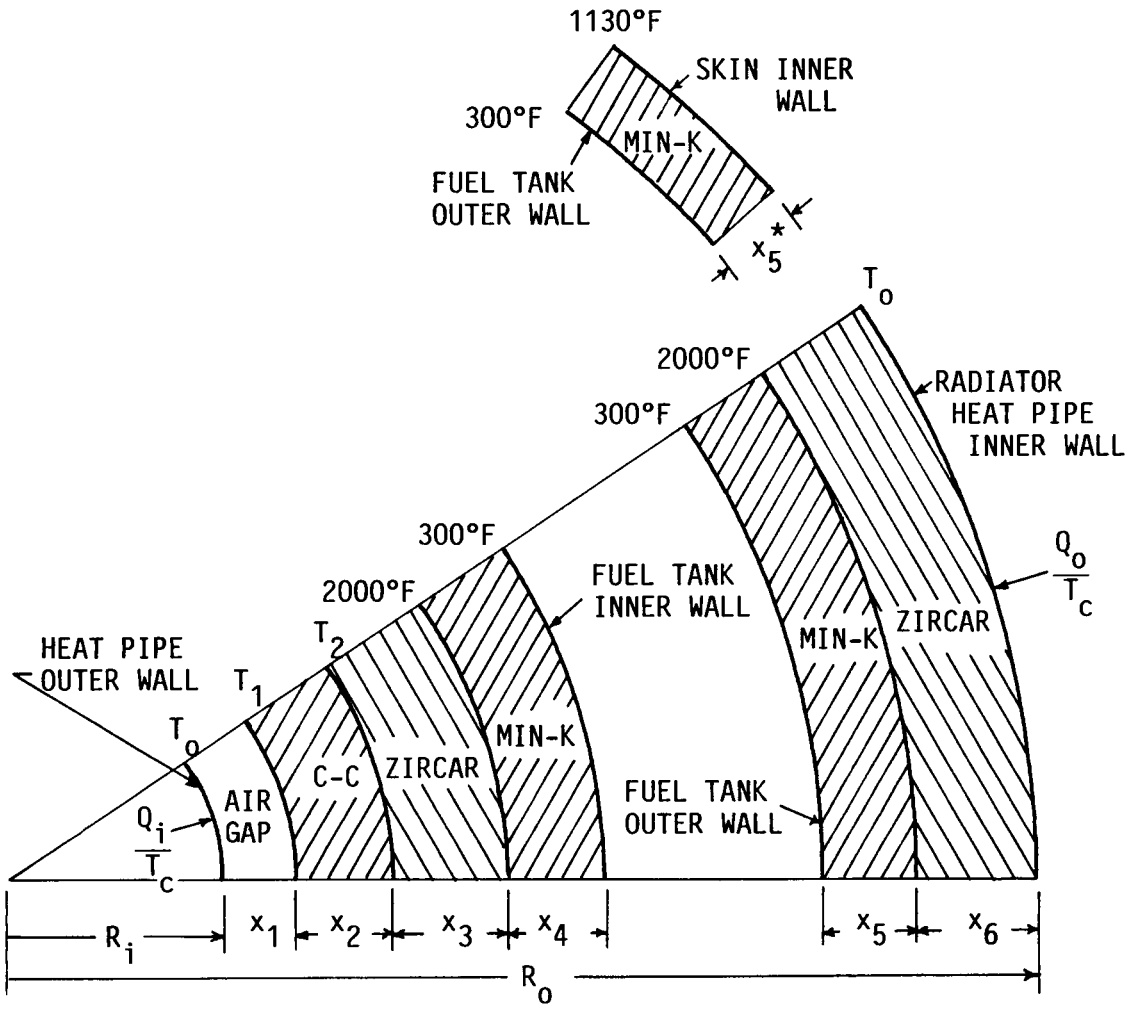

Figure 19. Thermal Insulation Model for Combustor, Radiator, and Skin

was taken to be the same as that in the radiator section. T_o is the heat pipe temperature, and the interface temperatures are as indicated. From this information, the thicknesses x_7 and x_8 and the heat leakage Q_t from the transition section can be calculated.

The total heat leakage Q_{tot} is given by

$$Q_{tot} = Q_i + Q_o + Q_t \tag{19}$$

where

$$Q_o = \left(\frac{L_c - L_r}{L_c}\right) Q_s + \frac{L_r}{L_c} Q_i \tag{20}$$

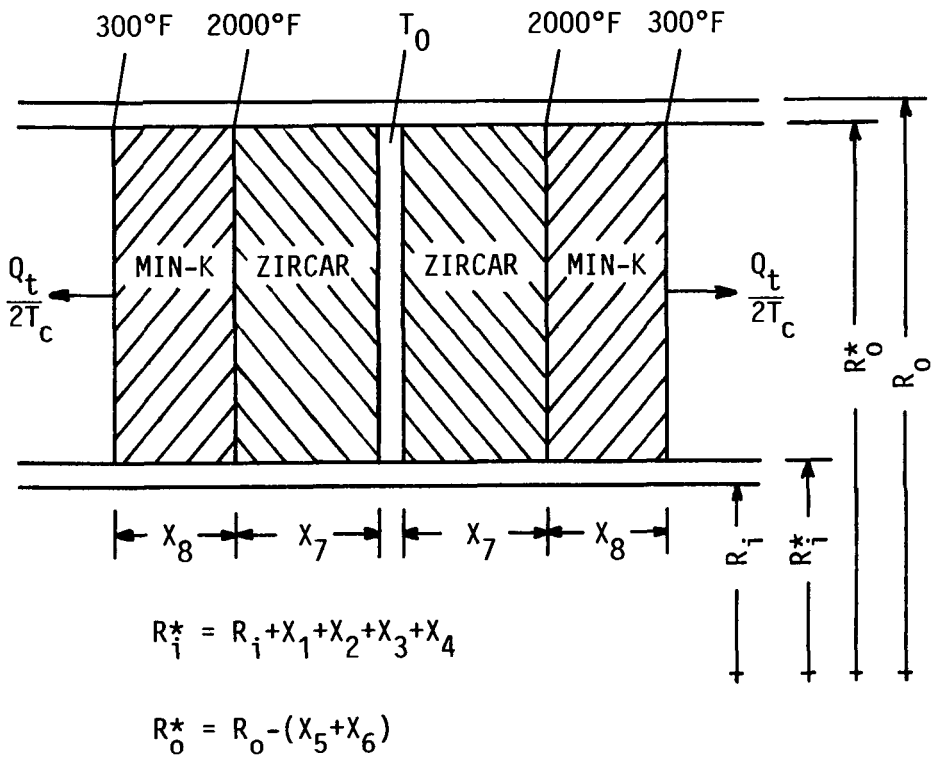

Figure 20. Thermal Insulation Model for Transition Section

In these equations,

Q_i = heat leakage from combustor heat pipe
Q_o = heat leakage from skin and radiator heat pipe
Q_t = heat leakage from transition section
Q_s = heat leakage from skin over combustor length L_c = 2000 Btu
L_c = combustor length
L_r = radiator length

The thickness of MIN-K required to limit the heat leakage from the skin to the specified 2000 Btu over the entire combustor length is 0.34 in. The insulation thickness does not change even when the radiator is present, since the heat leakage per unit length of the skin section is taken as constant.

Calculations were performed to find the thermal insulation thicknesses around the combustor heat pipe, under the radiator heat pipe, and on either side of the heat pipe transition section, as a function of the total heat leakage. The thermal insulation calculations were performed only for the structural liner of Option B, which is the preferred design option for concept C-7 because of its lower weight. Results are listed in

Table 4 for a total heat leakage of approximately 12,000 Btu.

Table 4. Thermal Insulation Parameters for Concept C-7, Option B (Structural Liner)

Q_i = 8000 Btu (heat leakage from combustor heat pipe)
Q_e = 3092 Btu (heat leakage from skin & radiator heat pipe)
Q_t = 1048 Btu (heat leakage from heat pipe transition section)
Q_{tot} = 12,140 Btu (total heat leakage)

T_1 = 2778 F (inner surface of second C-C layer)
T_2 = 2764 F (outer surface of second C-C layer)

x_3 = 0.28 in. (ZIRCAR around combustor heat pipe)
x_4 = 0.11 in. (MIN-K around combustor heat pipe)
x_5 = 0.27 in. (MIN-K under radiator heat pipe)
x_6 = 0.84 in. (ZIRCAR under radiator heat pipe)
x_7 = 0.84 in. (ZIRCAR on heat pipe transition section)
x_8 = 0.29 in. (MIN-K on heat pipe transition section)

Using the information in Table 4, the weight and thermal capacity of the thermal insulation were calculated. Results are given in Table 5.

Almost 35 lb of thermal insulation is required, about 70% of which is used around the transition section and the radiator. The thermal capacity is about 11,000 Btu. The thermal capacity of the insulation was not included in the total sensible thermal capacity of the cooling system. Because of the low thermal conductivity of the insulation materials, it is believed that only a small fraction of the available thermal capacity will actually be utilized during the critical transient phase of flight.

Overall System Characteristics

A preliminary layout of Concept C-7 with the Option B structural liner is shown in Figure 21. A summary of total cooling system weight is given in Table 6, along with the excess volume and displaced fuel weight. The latter items provide a convenient means for assessing the relative impact of the cooling system on engine volume.

Table 5. Weight and Thermal Capacity of Thermal Insulation for Concept C-7, Option B (Structural Liner)

Location	Weight, lb			Thermal Cap., Btu		
	ZIRCAR	MIN-K	Total	ZIRCAR	MIN-K	Total
Liner	7.03	3.05	10.08	2416	873	3289
Transition	7.71	2.84	10.55	2672	813	3485
Radiator	10.42	3.44	13.86	3611	984	4595
Total	25.16	9.33	34.49	8699	2670	11,369

Excess volume is defined as the increase in volume of the heat pipe cooling system over that of comparable components for a reference uncooled combustor liner. The components for the reference uncooled liner include:

A. A carbon-carbon liner and associated thermal insulation extending over the combustor length.

B. The engine skin and associated thermal insulation extending over the combustor length.

In the reference system, component group A is contained within a 1-in.-thick annulus whose inner boundary is the combustor wall, and component group B is contained within a 0.40-in.-thick annulus whose outer boundary is the exterior surface of the engine.

Displaced fuel weight is defined as the weight of fuel which would be lost if the excess volume were accommodated at the expense of fuel.

CONCEPTS C-8, C-5, AND C-4

Concepts C-8, C-5, and C-4 all utilize a sensible lithium heat sink, in addition to the sensible thermal capacity of the heat pipe and the carbon-carbon liner, to absorb the transient heat load. There is no radiator or secondary carbon-carbon layer, and only the structural liner (Option B) has been considered.

The steady-state heat load is dissipated by evaporating and discharging lithium vapor to the atmosphere through exhaust nozzles, after all the available sensible thermal capacity has

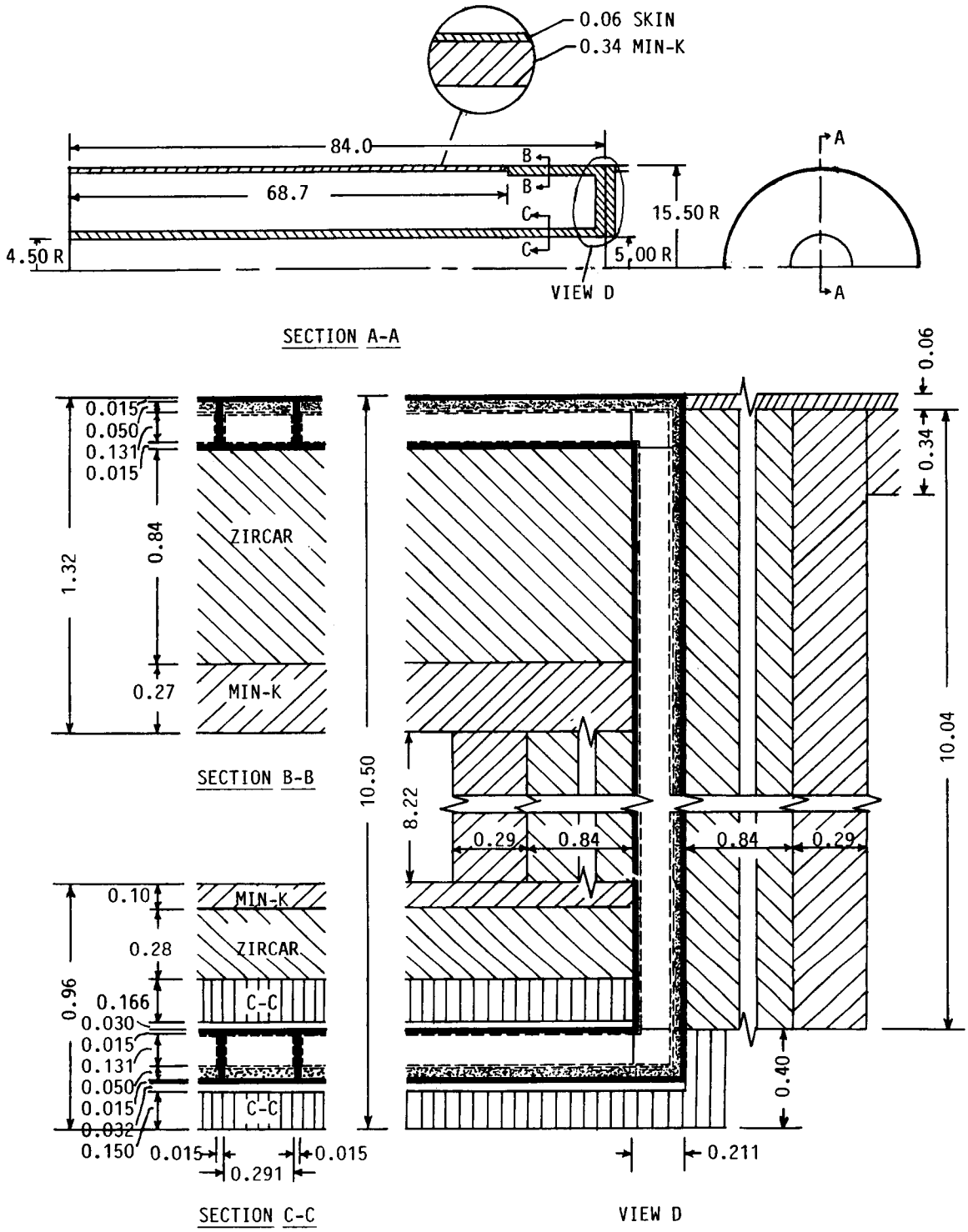

Figure 21. Preliminary Layout of Cooling Concept C-7, Option B

Table 6. Weight, Excess Volume, and Displaced Fuel Weight for Concept C-7, Option B (Structural Liner)	
Weight, lb	
Heat Pipe	72.1
Carbon-Carbon Liner	26.6
2nd Carbon-Carbon Layer	28.3
Thermal Insulation	34.5
Total	161.5
Excess Volume, in^3	
2540	
Displaced Fuel Weight, lb	
93.7	

been utilized (i.e., when the system has been heated to the steady-state operating temperature). The vapor is discharged upon failure of rupture plates in the nozzles, which are designed to fail at the vapor pressure corresponding to the operating temperature. Because of their similarity, these concepts are discussed as a single group. A schematic illustrating the concepts is shown in Figure 22. They differ in the manner in which the lithium heat sink is incorporated into the cooling system.

In Concept C-8, the lithium heat sink reservoir is incorporated with the heat pipe wick into a single containment structure. During steady-state operation, lithium evaporates into the vapor space from the heat pipe wick, flows to the exhaust nozzles, and is discharged. Liquid in the wick is replenished by flow from the reservoir along thin capillary wicks on the rib walls (not shown). After the reservoir has been fully depleted of liquid, the liquid in the wick is then depleted.

In Concept C-5, a common wall separates a conventional heat pipe from a lithium reservoir with a vapor space. The heat pipe serves to transport heat to the reservoir. During

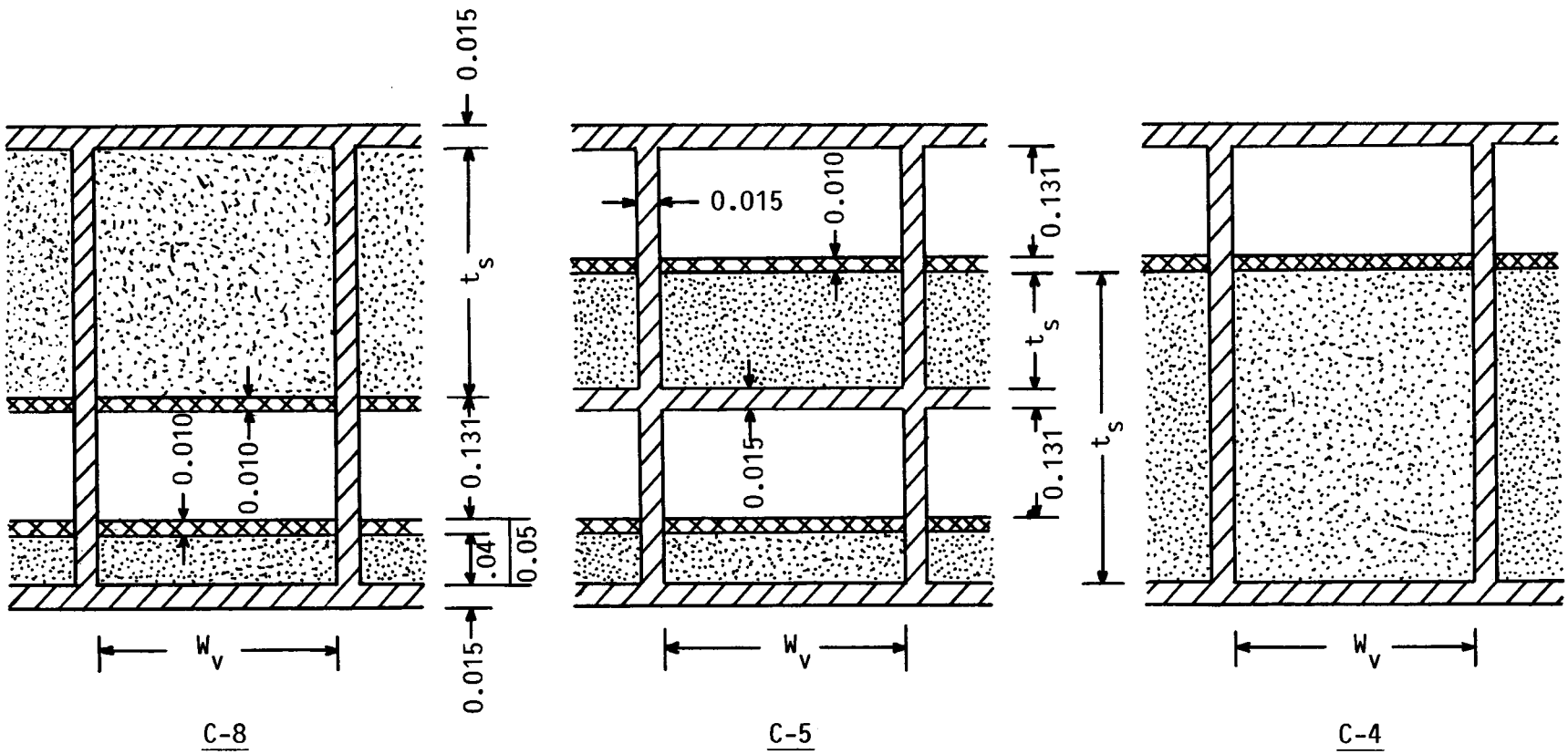

Figure 22. Cross-Sections of Cooling Concepts C-8, C-5, and C-4

steady-state operation, liquid evaporates from the reservoir into the reservoir vapor space, flows to the exhaust nozzles, and is discharged. The process continues until all the liquid in the reservoir has been depleted. The liquid in the heat pipe wick remains undepleted.

In Concept C-4, the lithium reservoir and the heat pipe wick are one and the same. During steady-state operation, lithium evaporates from the "thick" wick into the vapor space, flows to the nozzles, and is discharged.

In all cases, a fine-pored, 65% porosity, 0.010-in.-thick wick layer is used at the liquid-vapor interface to provide the capillary pressure needed to offset the liquid pressure drop produced by acceleration during the climb transient. The remainder of the liquid volume is filled with a low density, 90% porosity metal felt with relatively coarse pores to provide a stable liquid-vapor interface as liquid is depleted during discharge of the lithium vapor. The metal felt is also used in the heat pipe wick of Concept C-5, even though the wick is not depleted.

The operating temperature was taken to be 2800°F, the same as for Concept C-7, which also leads to the same rib spacing. The principal design characteristics to be determined include: the reservoir thickness, the characteristics of the lithium discharge nozzles, and the thermal insulation thickness. Then the cooling system weight and excess volume can be established.

Reservoir Thickness

The thickness of the lithium reservoir is determined by the thermal capacity required to absorb the heat load incident on the combustor liner during flight. The reservoir must be large enough so that the sensible thermal capacity of the contained TZM and lithium, when added to that of the heat pipe structure and liner, is sufficient to absorb the transient heat load. Additionally, the latent thermal capacity of the lithium, when vaporized and discharged, must be sufficient to absorb the steady-state heat load.

The required reservoir thickness t_s was found by finding an expression for the total thermal capacity , sensible and latent, of the heat pipe cooling system and the carbon-carbon liner as a function of t_s. This expression was then equated to the total heat load and solved for t_s. Results obtained for the reservoir thickness t_s, along with cooling system weights and thermal capacities, are listed in Table 7 for concepts C-8, C-5, and C-4. The weight and thermal capacity of the discharge nozzles and thermal insulation is not included in the results shown in Table 7.

Table 7. Thickness, Weight, and Thermal Capacity* for Concepts C-8, C-5, and C-4

Component	Concept		
	C-8	C-5	C-4
	Thickness, in		
Reservoir**	0.425	0.415	0.473
Heat Pipe + Reservoir	0.646	0.782	0.644
	Weight, lb		
TZM	97.2	115.0	96.8
Lithium	15.1	14.8	15.2
Carbon-Carbon Liner	26.6	26.6	26.6
Total	138.9	156.4	138.6
	Thermal Capacity, Btu		
TZM	18,485	21,817	18.370
Lithium (Sensible)	40,174	39,336	40,242
Lithium (Latent)	122,065	119,519	122,270
Carbon-Carbon Liner	29,222	29,248	29,222
Total Sensible	87,881	90,401	87,834
Total	209,946	209,920	210,104

* Discharge nozzles and thermal insulation not included.

** Does not include 0.010 in. screen wick at liquid-vapor interface.

In each case, the total thermal capacity is about equal to the total heat load of 210,000 Btu, and the total sensible thermal capacity exceeds the transient heat load of 84,600 Btu by a few thousand Btu's. The latter situation means that the discharge of lithium vapor will be initiated several seconds

after the start of the steady-state cruise period, a perfectly acceptable procedure.

Discharge Nozzles

Vaporized lithium is discharged to the atmosphere through four equispaced TZM nozzles, which extend radially from the combustor to the engine exterior. The nozzles are attached to a plenum at the rear end of the heat pipe cooling system, into which the vapor space of the lithium reservoir opens. The interior surface of the plenum is lined with a single layer of 200 mesh TZM screen coupled to the reservoir, so that the vapor in the plenum is saturated and in equilibrium with the reservoir liquid.

The nozzle geometry is illustrated in Figure 23. The thickness p of the plenum and nozzles is 0.5 in. The plenum height corresponds to the height of the heat pipe/reservoir system under consideration. The nozzle geometry is essentially the same for each concept, except that the distance from the nozzle throat to the exterior is adjusted to allow for differences in plenum height. The remaining nozzle dimensions are the same for each concept. Rupture plates in the plenum wall at the entrance to each nozzle are designed to open at 52.9 psi, the vapor pressure of lithium at the steady-state design temperature of 2800°F.

The nozzle entrance width n was taken to be 2.0 in., and the distance l from the throat to the exterior was taken to be 9.0 in. Other key nozzle dimensions, the throat width d_t and the exit width d_e, were determined from calculations of the required nozzle throat area A_t and exit area A_e. The area of a given nozzle at any given downstream pressure P_2 can be found from the following modified form of the continuity equation:

$$A_2 = \frac{q_o A_1 v_2}{4\kappa V_2} \tag{21}$$

where q_o = liner heat flux
A_1 = liner area
κ = heat of vaporization at operating temperature
v_2 = specific volume of lithium vapor at pressure P_2
V_2 = velocity of lithium vapor at pressure P_2

The velocity V_2 is given by (10)

$$V_2 = [2g(h_1 - h_2)]^{1/2} \tag{22}$$

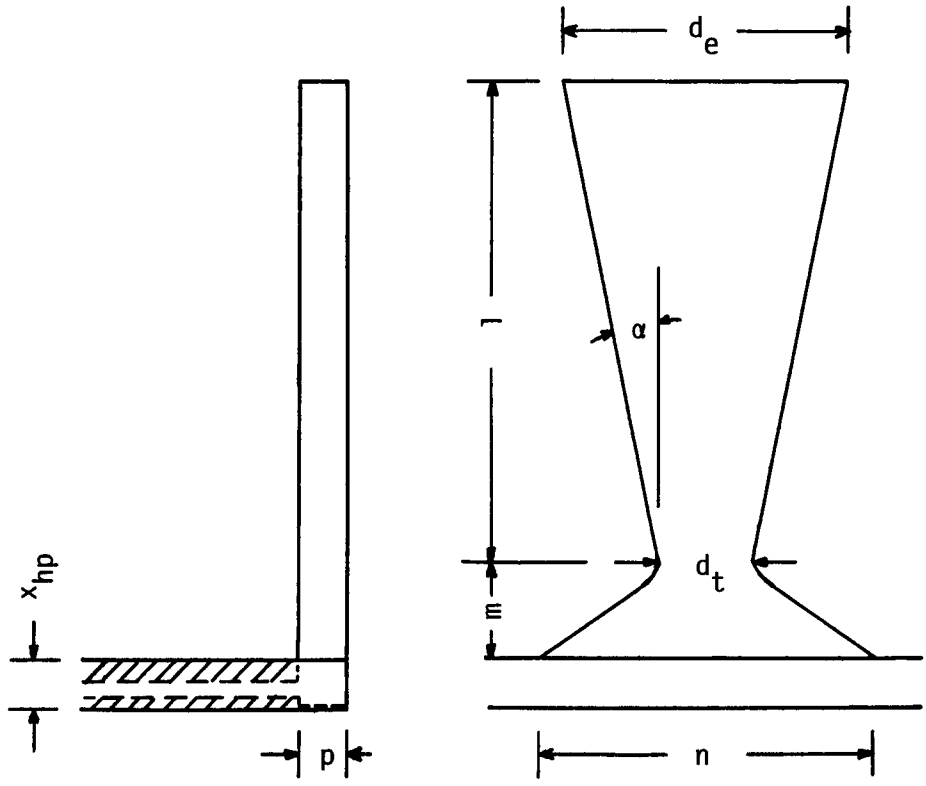

Figure 23. Lithium Discharge Nozzle Geometry

where g = acceleration of gravity
h_1 = enthalpy of lithium vapor at nozzle entrance
h_2 = enthalpy of lithium vapor at pressure P_2

Equation (22) assumes that the nozzle entrance velocity is negligible compared to V_2, a valid condition for the design considered here. The nozzle efficiency is also assumed to be 100%.

The specific volume v_2 can be approximated by

$$v_2 = x_2 v_{g2} \tag{23}$$

where v_{g2} = specific volume of saturated lithium vapor at pressure P_2
x_2 = lithium vapor quality (weight fraction of vapor) at pressure P_2

The nozzle areas at various downstream pressures P_2 were calculated as a function of P_2 for the isentropic (constant entropy) expansion of lithium vapor. The enthalpy, quality, and temperature at P_2 were found from a Mollier (h-s)

diagram for lithium given in Reference (11). The specific volume of saturated lithium vapor was obtained from a curve of v_{g2} versus T_2, also given in Reference (11).

The nozzle area A_2 versus downstream pressure P_2 is shown in Figure 24. The minimum area, at the nozzle throat, occurs at a pressure of 22.5 psi. Because the curve is very flat in the vicinity of the throat, the throat pressure was assumed to be 20 psi, with little effect on throat area. The nozzle exhaust pressure was taken to be 0.411 psia, corresponding to the atmospheric pressure after 60 sec of flight. Since the atmospheric pressure during steady-state cruise is 0.211 psia, the lithium vapor issuing from the nozzles will be somewhat underexpanded.

Once the nozzle throat and exit areas have been determined, the throat and exit widths d_t and d_e are found by dividing the respective areas by the nozzle thickness of 0.5 in.

In Table 8, the various lithium vapor properties at the nozzle entrance, throat, and exit are indicated, along with the vapor velocities and areas. The data in Table 8 apply for concepts C-8, C-5, and C-4. Information on nozzle dimensions for the three concepts under consideration is given in Table 9.

The nozzle dimensions are the same for each concept with the exception of the throat-to-exit length l and the half-angle α. These dimensions change to accommodate the varying plenum height x_{hp} for the three concepts within the fixed liner-to-exterior dimension of 10.50 in. Also, the dimensions with asterisks are internal dimensions. Since the nozzle walls are fabricated from 0.030 in. TZM, the external dimensions are 2 x 0.030 = 0.060 in. wider than the internal dimensions.

The four equispaced nozzles occupy 7% of the external circumference. If directed to the rear, the flow issuing from the four nozzles would generate a thrust of 20.2 lb.

The approximate weight of the four nozzles and vapor plenum is 1.7 lb, and their volume is about 26.3 in^3.

Thermal Insulation

Less thermal insulation is required with concepts C-8, C-5, and C-4, since there is no high temperature radiator on the engine surface to be insulated. Instead, the outer skin over the entire combustor length is insulated with 0.34 in. of MIN-K, resulting in 2000 Btu of heat leakage to the interior. The thicknesses of ZIRCAR and MIN-K required around the heat pipe/reservoir in the combustor section were found using the same model as was used for concept C-7. (See Figure 19.)

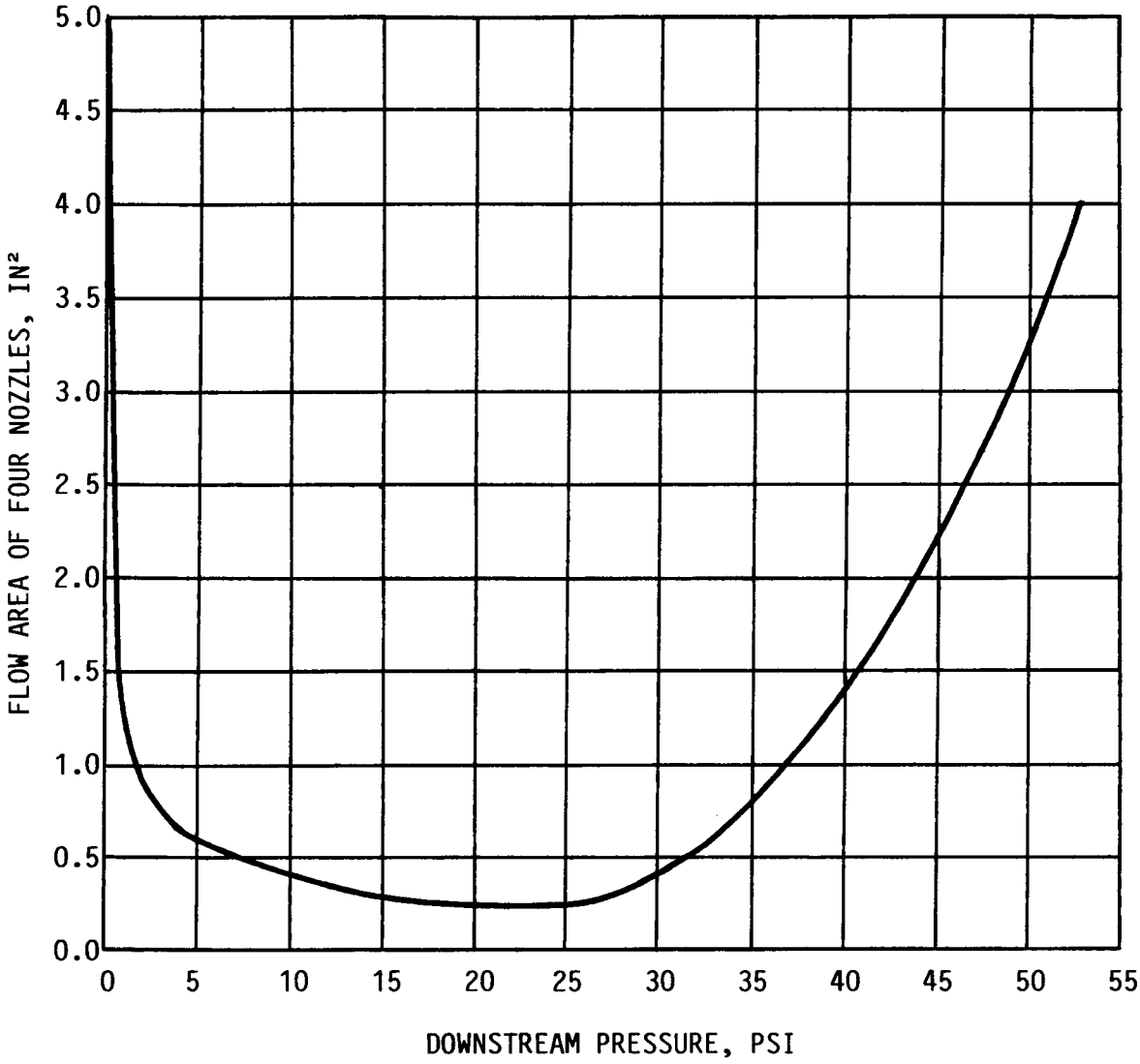

Figure 24. Nozzle Area Versus Downstream Pressure for Lithium Vapor Nozzle

To obtain the same total heat leakage of about 12,000 Btu, the heat leakage from the heat pipe/reservoir was specified to be 12,000 - 2,000 = 10,000 Btu. Since there is no secondary carbon-carbon layer, the thickness x_2 in the model was taken to be 0.0001 in., which approximates zero. The lithium discharge nozzles were insulated with the same thicknesses of ZIRCAR and MIN-K as were used to insulate the heat pipe transition section in concept C-7.

Insulation thicknesses and associated heat leakages are given in Table 10. The weight and thermal capacity of the thermal insulation are given in Table 11. Results are similar for each concept. About 10 lb of insulation is required, with a thermal capacity of about 3300 Btu. The relatively small

Table 8. Discharge Nozzle Data for Concepts C-8, C-5, and C-4

Item	Entrance	Throat	Exit
Temperature, F	2800	2500	1740
Pressure, psia	52.9	20.0	0.411
Enthalpy, Btu/lb	11,220	10,510	8440
Entropy, Btu/lb-R	5.444	5.444	5.444
Quality, %	100.0	92.5	71.1
Specific Volume of Saturated Vapor, ft^3/lb	81.97	208.3	7143
Specific Volume, ft^3/lb	81.97	192.7	5079
Vapor Velocity, ft/sec	162.3	5963	11,800
Vapor Flow Rate, lb/sec	0.0138	0.0138	0.0138
Flow Area, in^2	1.000	0.056	0.852

Table 9. Nozzle Dimensions for Concepts C-8, C-5, and C-4 (See Figure 23)

Dimension	Concept		
	C-8	C-5	C-4
n, in.*	2.00	2.00	2.00
d_t, in.*	0.111	0.111	0.111
d_e, in.*	1.705	1.705	1.705
m, in.	1.00	1.00	1.00
l, in.	8.672	8.536	8.674
α, deg	5.25	5.33	5.25
x_{hp}, in.	0.646	0.782	0.644
p, in.*	0.50	0.50	0.50

* Internal dimensions. For external dimensions, add 0.060 in.

Table 10. Heat Leakage and Thermal Insulation Thickness for Concepts C-8, C-5, and C-4

Item	C-8	C-5	C-4
Q_i(heat from h.pipe/reser.), Btu	10,000	10,000	10,000
Q_e(heat from skin), Btu	2,000	2,000	2,000
Q_n(heat from nozzles), Btu	114	114	114
Q_{tot}(total heat leakage), Btu	12,114	12,114	12,114
T_2(temp. at ZIRCAR inner s.), F	2,775	2,775	2,775
x_3(ZIRCAR arnd h.pipe/reser.), in.	0.24	0.24	0.24
x_4(MIN-K arnd h.pipe/reser.), in.	0.09	0.09	0.09
x_5(MIN-K under skin), in.	0.34	0.34	0.34
x_8(ZIRCAR on nozzles), in.	0.84	0.84	0.84
x_9(MIN-K on nozzles), in.	0.29	0.29	0.29

thermal capacity of the insulation was not taken into account in establishing cooling system thermal capacity requirements.

Heat Transport Characteristics

Heat transport characteristics of the cooling systems were briefly examined, based on the requirement that heat pipe heat transport limits not be exceeded. These limits were established using References 6, 12, and 13.

During steady-state operation, lithium evaporates from the heat pipe, and the vapor flows axially along the vapor space to the discharge nozzles. Liquid lithium flow is in the radial direction only, and its pressure drop is negligible.

The axial heat flux is 113 Btu/in^2-sec, well below the sonic limit (axial heat flux at which the vapor velocity becomes sonic) of 1510 Btu/in^2-sec at the operating temperature of 2800°F. Entrainment will not occur if the pore size at the liquid-vapor interface in less than 550 micron, a design requirement which is easily met. The axial pressure drop of 0.33 psi in the flowing vapor can be sustained by the capillary pressure developed in wick pore sizes of less than 370 micron, another readily met design criterion. For example, the pore size of the 90% TZM felt proposed for the body of the heat pipe wick and reservoir is estimated to be 200 micron, based on

Table 11. Weight and Thermal Capacity of Thermal Insulation for Concepts C-8, C-5, and C-4

Location	Weight, lb			Thermal Capac., Btu		
	ZIRCAR	MIN-K	Total	ZIRCAR	MIN-K	Total
C-8						
Heat pipe/reser.	6.30	2.59	8.89	2171	804	2975
Nozzles	0.84	0.31	1.15	303	79	382
Total	7.14	2.90	10.04	2474	883	3357
C-5						
Heat pipe/reser.	6.45	2.65	9.10	2223	758	2981
Nozzles	0.84	0.31	1.15	303	79	382
Total	7.29	2.96	10.25	2526	837	3363
C-4						
Heat pipe/reser.	6.30	2.59	8.89	2171	741	2912
Nozzles	0.84	0.31	1.15	303	79	382
Total	7.14	2.90	10.04	2474	820	3294

comparison with 89% porosity sintered stainless steel fiber. (See p. 70, Reference 6.)

The superheat in the wick of concept C-8 is 10°F. In the reservoir of concept C-5, through which liner heat must flow to the vaporizing interface, the superheat is 85°F. In the combined heat pipe wick/reservoir of concept C-4, the superheat is 97°F.

During steady-state operation, the diameter of curvature of the liquid-vapor interface will be at least 370 micron. For this condition, at an operating temperature of 2800°F and with a nucleation site radius of 3 micron, boiling will not be initiated until the superheat reaches 114°F. Therefore, steady-state boiling is not expected with any of the cooling

concepts, although the margin for error is smallest for C-4.

During the climb transient, there is no axial vapor flow. However, the engine acceleration, along with gravity, produces a substantial axial liquid pressure drop to be offset by capillary pressure in the wick pores. At 2800°F and a peak acceleration (including gravity) of 2.62 g's, the liquid pressure drop is 3.03 psi, requiring the wick pore size to be less than 40 micron. For this reason, a thin (0.010 in.) layer of TZM screen is used at the liquid-vapor interface of both the heat pipe wick and reservoir. The porosity of this wick layer is taken to be 65% with an effective pore size of 20 micron, obtained by drawing down several layers of 400 mesh screen.

Since liner heat fluxes during the climb transient may exceed the steady-state value by a substantial multiple, the possibility of boiling during the transient must be considered. At the lower cooling system temperatures encountered during the transient, the superheat required for the initiation of boiling increases considerably. No problems are expected with concept C-8 because of its thin wick. However, boiling conceivably could be a problem with concepts C-5 and C-4 because of the thicker reservoir structures through which heat must pass in order to reach the vapor space.

For example, in Figure 25 the actual superheat in the reservoir of concept C-4, and the superheat required for boiling, are plotted as a function of vapor temperature for a heat flux of 180 Btu/ft^2-sec. If the vapor temperature at this heat flux should exceed 1950°F, the actual superheat will exceed that for boiling. Whether boiling will in fact occur in the thick reservoir structures of concepts C-5 and C-4 depends on their transient temperature and heat flux histories.

Overall System Characteristics

Preliminary layouts of concepts C-8, C-5, and C-4 are shown in Figure 26. A summary of total cooling system weights is given in Table 12, along with excess volumes and displaced fuel weights.

CONCEPT M-6

Concept M-6 differs from the previously considered cooling concepts in two important respects. First, the heat pipe structure itself acts as the combustor liner, and thus there is no separate carbon-carbon liner. Second, thermal capacity required during the climb transient which exceeds that available from the heat pipe structure is supplied by a vaporizing lithium heat sink. The steady-state heat load is dissipated from an external heat pipe radiator in the same manner as was employed in concept C-7.

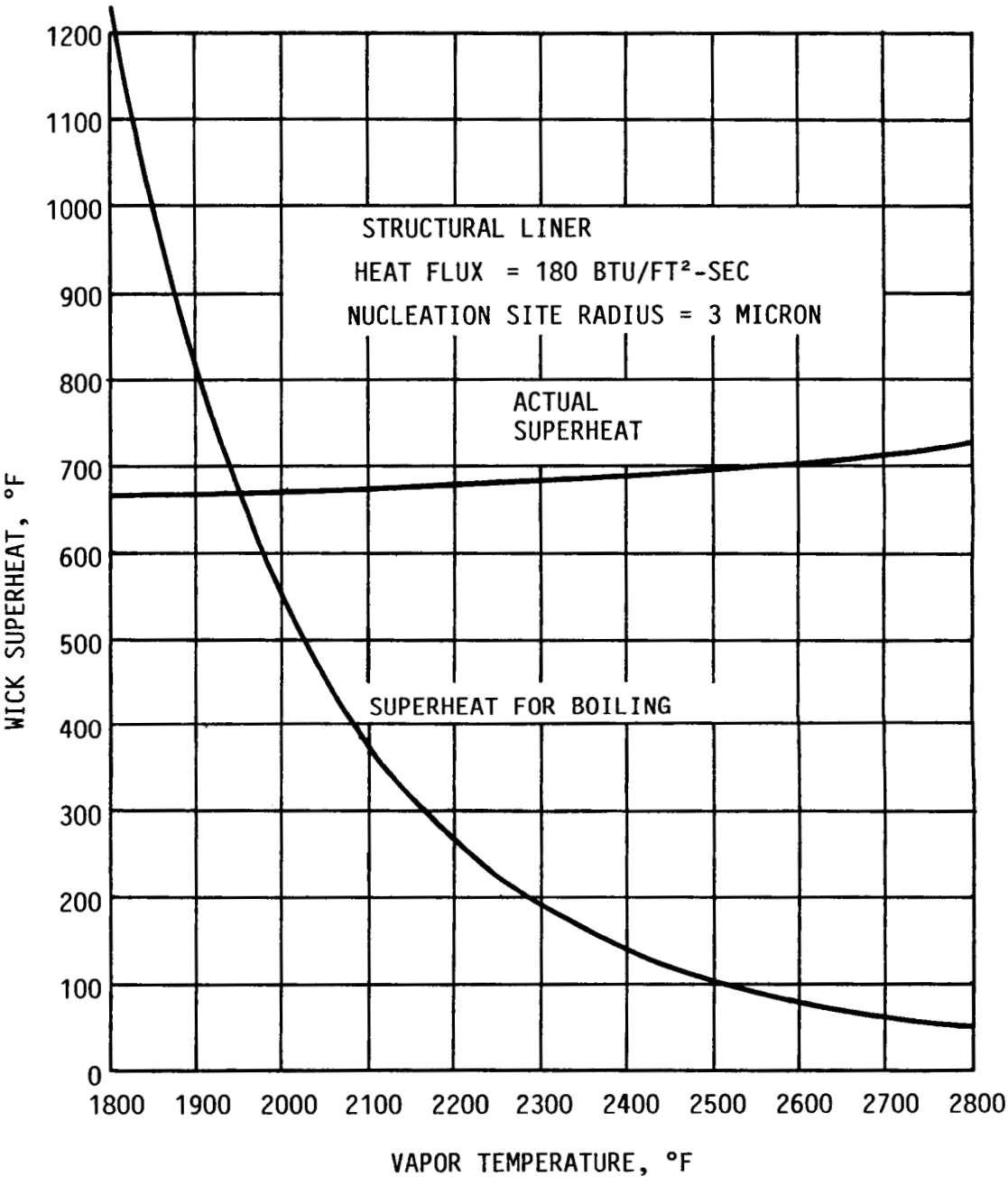

Figure 25. Conditions for Boiling with Concept C-4

By using the heat pipe structure directly as the combustor liner, the relatively high-thermal-resistance air gap between the liner and the heat pipe structure, which is characteristic of the other concepts, is eliminated. Since the heat pipe structure is now directly exposed to combustion gas pressure, it must be designed to withstand the resulting hoop stress.

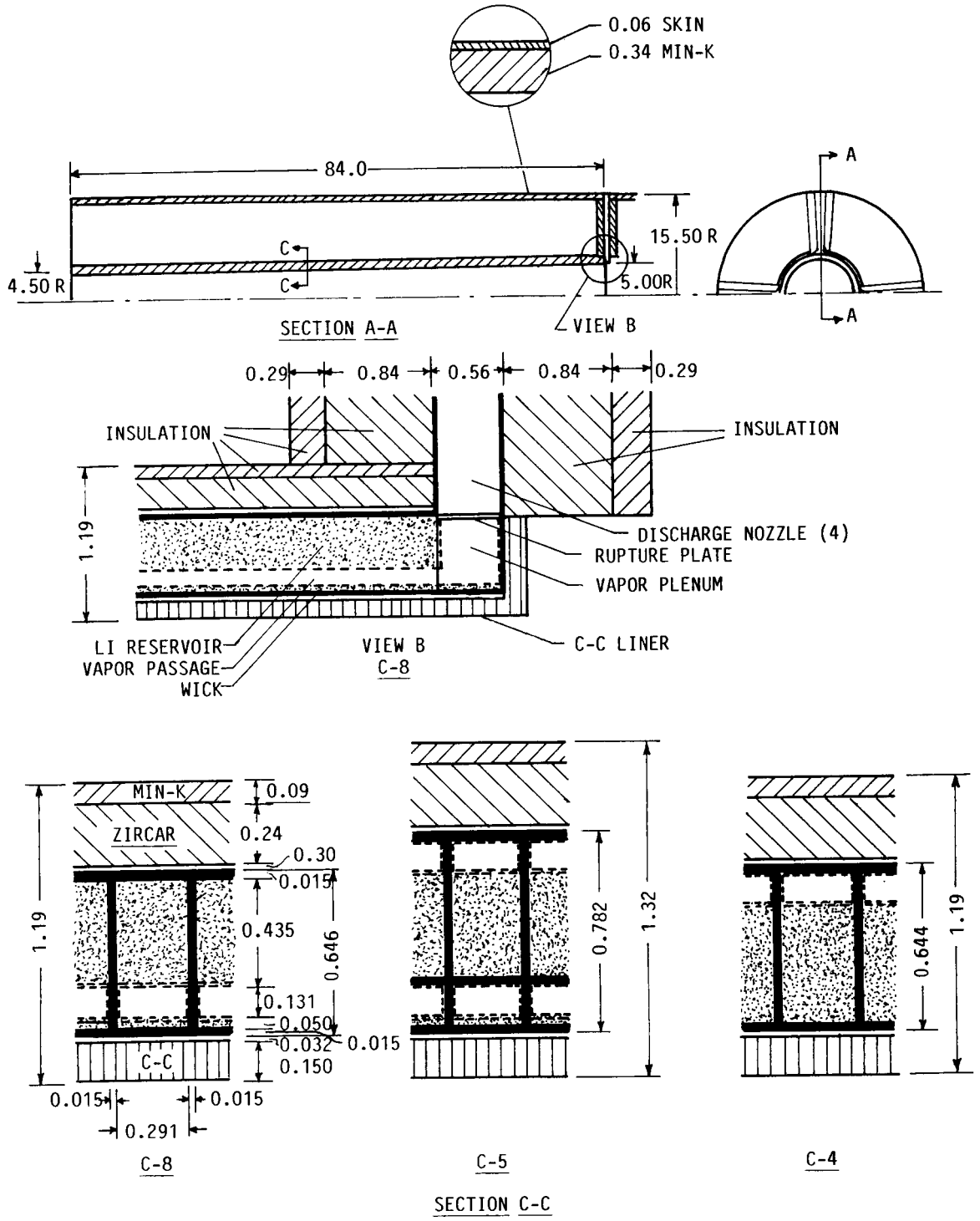

Figure 26. Preliminary Layout of Concepts C-8, C-5, and C-4

Table 12. Weight, Excess Volume, and Displaced Fuel Weight for Concepts C-8, C-5, and C-4

Item	C-8	C-5	C-4
Weight, lb			
Heat Pipe/Reservoir	112.3	129.8	112.0
Carbon-Carbon Liner	26.6	26.6	26.6
Nozzles and Plenum	1.7	1.7	1.7
Thermal Insulation	10.0	10.3	10.0
Total	150.6	168.4	150.3
Excess Volume, in^3			
Cooling System	735.0	1163.1	725.2
Displaced Fuel Weight, lb			
Cooling System	27.1	42.9	26.8

The operating temperature for concept M-6 was set at 3000°F, the highest practical steady-state level for a lithium-TZM heat pipe. At this temperature, the lithium vapor pressure is 95.8 psia. A protective W-3 silicide coating (14) covers exposed TZM surfaces.

The cross-section of the M-6 cooling system in the combustor is shown in Figure 27. The configuration is similar to that of C-5, except that the heat pipe section extends all the way to the external radiator. The vapor space of the lithium heat sink reservoir connects with the vapor discharge nozzles. All of the dimensions are specified as shown, with the heat sink thickness t_s, the rib spacing W_v, and the wall thickness t_w to be determined.

The porosity of the TZM screens at the liquid-vapor interfaces is 0.65. The porosity of the TZM felt within the reservoir is 0.90. The wick itself is an all-liquid channel. The rib spacing and wall thickness are determined from stress considerations, and the heat sink thickness from thermal capa-

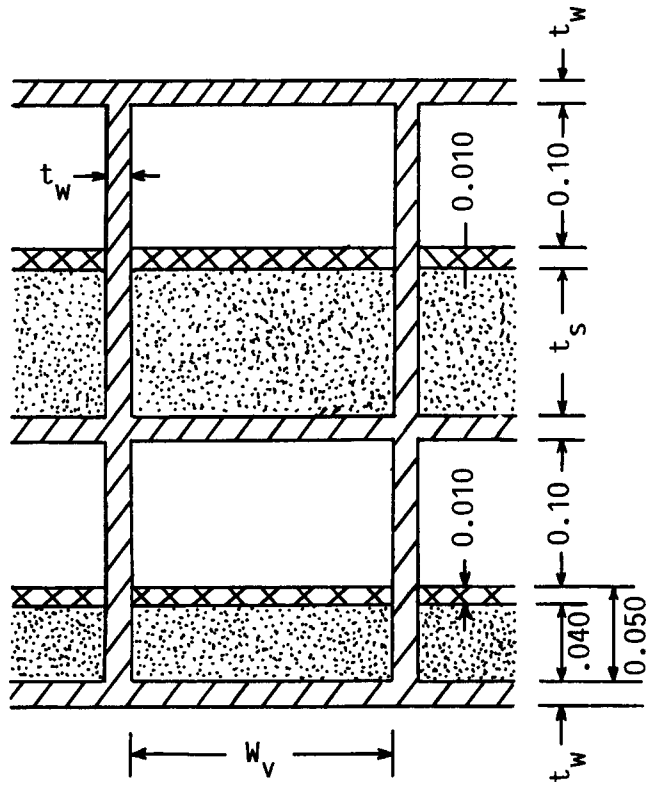

Figure 27. Cross-Section of Cooling Concept M-6

city considerations. Additional information needed to characterize concept M-6 includes: radiator area, discharge nozzle dimensions, and thermal insulation needs.

Wall Thickness and Rib Spacing

The walls must have sufficient thickness to avoid excessive hoop and bending stresses. Using the maximum combustion gas pressure of 350 psi, a mean radius of 5 in., 0.060 in. walls in the heat pipe and heat sink, and assuming that the stress is equally applied to the three walls, the hoop stress from Equation (14) is 9720 psi.

The pressure differential between the combustion gas and the heat pipe vapor produces bending stress in the inner wall. With ΔP equal to 350 - 100 = 250 psi, an allowable bending stress s of 7000 psi, and wall and rib thicknesses t_w of 0.060 in., the rib spacing W_v is found to be 0.389 in. from Equation (10). The center-to-center rib spacing is then 0.389 + 0.060 = 0.449 in.

Adding the bending stress of 7000 psi to the hoop stress gives 16,720 psi, a figure greater than the tensile strength of

15,000 psi for TZM at 3000°F. The system temperature will likely be less than 3000°F, and the tensile strength greater than 15,000 psi, at the start of flight when the maximum combustor pressure is encountered. Nonetheless, the above analysis indicates that a wall thickness in excess of 0.060 in. may be needed.

There is no hoop stress in the radiator section of the heat pipe, and the pressure differential across the walls (vapor pressure minus atmospheric pressure) is about 100 psi. Using the same center-to-center rib spacing of 0.449 in. and an allowable stress of 7000 psi, it may be shown with Equation (10) that the rib spacing W_v = 0.411 in. and the wall and rib thicknesses t_w = 0.038 in.

These calculated dimensions are summarized below.

	Combustor Heat Pipe/ Heat Sink	Radiator Heat Pipe
Wall & rib thickness t_w, in.	0.060	0.038
Spacing between ribs W_v, in.	0.389	0.411

Radiator Area

The radiator area required to dissipate the steady-state heat load was found from Equations (B6) and (B8) of Appendix B. The following data were used in the equations:

Radiator temperature T_4 = 3460 R
Radiation equilibrium temperature T_e = 1590 R
Recovery temperature T_r = 2932 R
Liner heat flux q_l = 38.3 Btu/ft^2-sec
Liner area A_l = 17.41 ft^2

The radiator area A_r is then 11.98 ft^2. The area of the annular heat pipe transition section between the combustor and radiator is 4.70 ft^2. Assuming that the radiator extends completely around the engine, its axial length is then 17.7 in.

Reservoir Thickness

The thickness t_s in the lithium reservoir was determined from thermal capacity conditions. At 3000°F, the transient and total heat loads are 128,500 Btu and 318,400 Btu, respectively. There must be sufficient sensible and latent thermal capacity in the cooling system to absorb the transient heat load. The

steady-state heat load is dissipated by the radiator.

An expression for the total system thermal capacity was calculated, with the reservoir thickness t_s a variable to be determined, and set equal to the transient heat load of 128,500 Btu. The total system thermal capacity includes: sensible thermal capacity of the TZM, sensible thermal capacity of the lithium, latent heat of vaporization of the lithium in the heat sink reservoir, and the heat radiated to the environment from the radiator prior to steady-state operation. The latter figure was estimated to be 12,000 Btu. The thermal capacity of the nozzles and thermal insulation is relatively small, and was not included.

Upon solving for t_s, the thickness of lithium in the reservoir was found to be 0.148 in. Once t_s has been determined, the thicknesses, weights, and thermal capacities can be calculated. Results are given in Table 13.

The total thermal capacity is seen in Table 13 to be about equal to the transient heat load of 128,500 Btu. About 27% of the thermal capacity is due to the latent heat of vaporization of the lithium which evaporates from the reservoir.

Discharge Nozzles

The discharge nozzle geometry is similar to that shown in Figure 23. The vapor discharge temperature was assumed to be equal to the operating temperature of 3000°F. The actual vapor discharge temperature is lower than this figure because of the temperature drop between the inner surface of the heat pipe and the lithium in the reservoir. The discharge of lithium vapor starts after all the available sensible thermal capacity has been utilized, including heat dissipated from the radiator while it is being heated fully to the operating temperature. This occurs when 93,600 Btu of heat has been absorbed, after 50.4 sec of flight.

From the Case A 3000°F curve of Figure 8, the liner heat flux at 50.4 sec is 175 Btu/ft^2-sec. The nozzles were designed to discharge lithium vapor at the flow rate corresponding to this heat flux. The nozzle exhaust pressure was taken to be 0.571 psia, which is the atmospheric pressure at the time vapor discharge is initiated.

Nozzle characteristics were calculated using the same techniques and equations described in the discharge nozzle section for concepts C-8, C-5, and C-4. However, the vapor velocity was modified to the form

$$V_{2o} = V_2(1 + \delta)^{1/2} \qquad (24)$$

Table 13. Thickness, Weight, and Thermal Capacity for Concept M-6*	
Thickness, in.	
Reservoir**	0.148
Heat Pipe/Reservoir	0.588
Radiator Heat Pipe	0.226
Weight, lb	
TZM	297.1
Lithium	7.4
Total	304.5
Thermal Capacity, Btu	
TZM	60,510
Lithium (sensible)	20,950
LIthium (latent)	34,900
Radiation During Transient	12,000
Total	128,360

* Discharge nozzles and thermal insulation not included.

** Does not include 0.010 in. screen at liquid-vapor interface.

where V_2 is calculated from Equation (22), δ is defined by

$$\delta = (V_1/V_2)^2 \tag{25}$$

and V_1 is the exit velocity from the reservoir vapor space. In the prior calculations, δ was negligible. Because of the relatively high vapor flow rate (resulting from the initiation of vapor discharge during the climb transient), 16 nozzles were used.

In Table 14, the various lithium vapor properties at the nozzle entrance, throat, and exit are indicated, along with the vapor velocities and areas. Information on nozzle dimensions is given in Table 15.

Table 14. Discharge Nozzle Data for Concept M-6

Item	Entrance	Throat	Exit
Temperature, F	3000	2770	1790
Pressure, psia	95.7	50.0	0.571
Enthalpy, Btu/lb	11,276.3	10,760	8270
Entropy, Btu/lb-R	5.3176	5.3176	5.3176
Vapor Quality, %	100.0	94.5	68.8
Specific Volume of Saturated Vapor, ft^3/lb	47.62	89.29	5263
Specific Volume, ft^3/lb	47.62	84.38	3621
Vapor Velocity, ft/sec	329	5085	12,271
Vapor Flow Rate, lb/sec	0.0240	0.0240	0.0240
Flow Area, in^2	0.500	0.0573	1.0194

Table 15. Nozzle Dimensions for Concept M-6 (See Figure 23)

n, in.*	1.00
d_t, in.*	0.115
d_e, in.*	2.039
m, in.	1.00
l, in.	8.91
α, deg	6.16
x_{hp}, in.	0.588
p, in.*	0.50

* Internal dimensions. For external dimensions, add 0.060 in.

Actual nozzle dimensions will be somewhat larger than indicated in Table 15 because the saturated lithium vapor is at a lower temperature, and hence lower pressure and density, than the assumed temperature of 3000°F.

The 16 equispaced nozzles occupy 33.5% of the external engine circumference. The nozzles and vapor plenum are fabricated from 0.030 in. sheet TZM. The approximate weight of the 16 nozzles and the plenum is 5.6 lb, and they occupy a volume of about 91.0 in^3.

Thermal Insulation

Thermal insulation requirements for concept M-6 are similar to those for concept C-7. Insulation is applied around the heat pipe/reservoir surrounding the combustor, the heat pipe transition section and adjacent nozzles, and under the heat pipe radiator on the engine surface. The remainder of the surface over the combustor section not occupied by the radiator is insulated with 0.34 in. of MIN-K. The same thermal insulation model as was used for concept C-7 is also used for M-6. (See Figures 19 and 20.) However, since there is no secondary carbon-carbon layer, the thickness x_2 was taken to be 0.0001 in., an approximation to zero.

The results of calculations to determine the insulation thicknesses and associated heat leakages are given in Table 16. The calculations were based on a total nominal heat leakage to the interior of 12,000 Btu.

The weight and thermal capacity of the thermal insulation are given in Table 17. The thermal insulation under the skin is not included.

About 45 lb of thermal insulation is required, with a thermal capacity of over 15,000 Btu. The thermal capacity of the insulation was not taken into account in establishing cooling system thermal capacity requirements. Because the thermal conductivity of the thermal insulation is low, only a small fraction of the thermal capacity may be available to absorb sensible heat during the climb transient.

Overall System Characteristics

A preliminary layout of concept M-6 is shown in Figure 28. A summary of total cooling system weights is given in Table 18, along with the excess volume and displaced fuel weight.

Table 16. Heat Leakage and Thermal Insulation Thickness for Concept M-6

Q_i(heat leakage from heat pipe/reservoir), Btu	8,000
Q_e(heat leakage from skin and radiator), Btu	3,266
Q_t(heat leakage from transition /nozzles), Btu	996
Q_{tot}(total heat leakage), Btu	12,262
T_2(temperature at ZIRCAR inner surface), °F	3,000
x_3(ZIRCAR thickness around heat pipe/reservoir), in.	0.39
x_4(MIN-K thickness around heat pipe/reservoir), in.	0.11
x_5(MIN-K thickness under radiator), in.	0.26
x_6(ZIRCAR thickness under radiator), in.	1.12
x_8(ZIRCAR around transition section/nozzles), in.	1.12
x_9(MIN-K around transition section/nozzles), in.	0.29

Table 17. Weight and Thermal Capacity of Thermal Insulation for Concept M-6

Location	Weight, lb			Thermal Cap., Btu		
	ZIRCAR	MIN-K	Total	ZIRCAR	MIN-K	Total
Heat pipe/reservoir	9.89	3.11	13.00	3,575	890	4,465
Transition/Nozzles	9.42	2.68	12.10	3,405	767	4,172
Radiator/Skin	15.91	3.75	19.66	5,751	1,073	6,824
Total	35.22	9.54	44.76	12,731	2,730	15,461

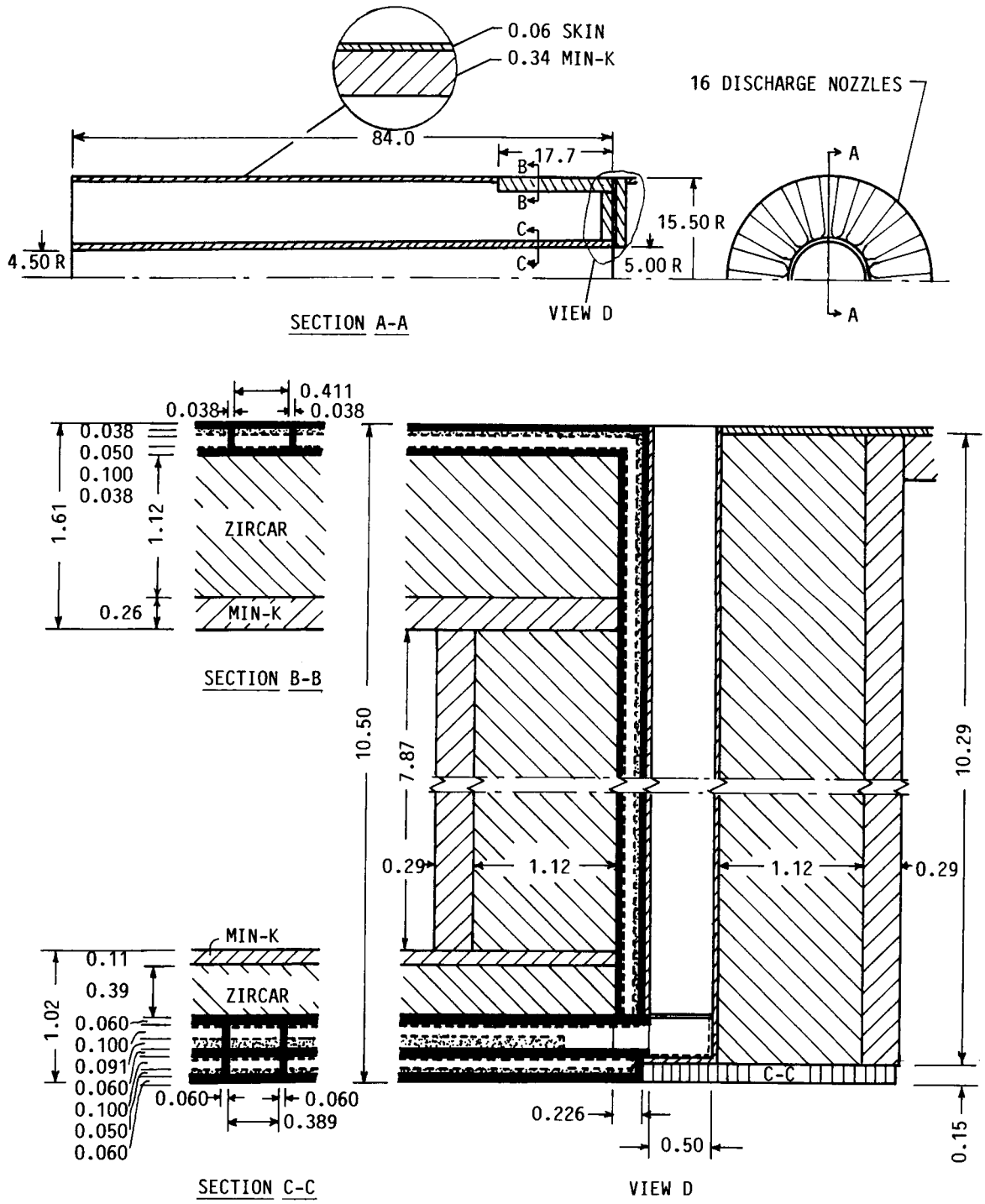

Figure 28. Preliminary Loyout of Cooling Concept M-6

Table 18. Weight, Excess Volume, and Displaced Fuel Weight for Concept M-6	
Item	Weight, lb
Heat Pipe/Reservoir	304.5
Nozzles and Plenum	5.6
Thermal Insulation	44.8
Total	354.9
Excess Volume, in^3	
3835.7	
Displaced Fuel Weight, lb	
141.5	

COMPARISON OF CANDIDATE COOLING CONCEPTS

In Figure 29, important characteristics of the five candidate cooling concepts are given. Preliminary layouts of the concepts have been presented in Figures 21, 26, and 28. The features of the various concepts will now be discussed and compared.

CONCEPT M-6

In concept M-6, a vaporizing lithium heat sink supplements sensible heat sinks during absorption of the transient heat load, and an externally-mounted radiator is used to dissipate the steady-state heat load. Lithium vapor is discharged to the atmosphere through 16 radially-oriented nozzles, starting at 50 sec when the liner heat flux is 175 Btu/ft^2-sec. An annular disk transition section adjacent to the nozzles connects the inner conical combustor heat pipe with the outer cylindrical radiator heat pipe. Vapor passages penetrate the transition section, connecting the vapor discharge plenum to the nozzle plenum.

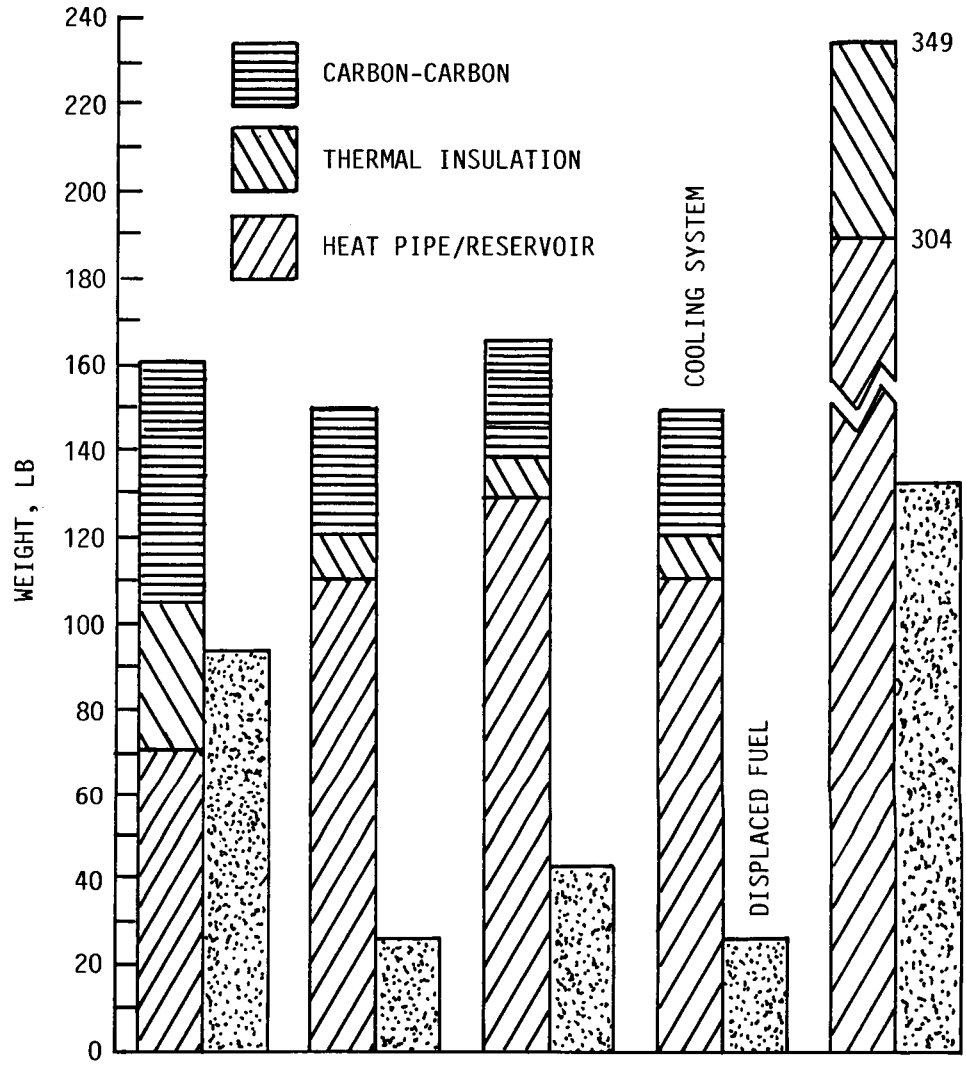

CONCEPT	C-7	C-8	C-5	C-4	M-6
CARBON-CARBON LINER	X	X	X	X	
C-C HEAT SINK	X				
COMB. HEAT PIPE	X	X	X	X	X
RAD. HEAT PIPE	X				X
VAP. HEAT SINK		X	X	X	X
LINER TEMP., °F	3472	3472	3472	3472	3000
HP/RES. TEMP., °F	2800	2800	2800	2800	3000
HEAT LOAD, BTU/1000	210	210	210	210	318
TRAN. HT. LD., BTU/1000	85	85	85	85	129
HEAT LEAK., BTU/1000	12	12	12	12	12
RADIATOR AREA, FT^2	10.4				12.0

Figure 29. Comparison of Candidate Cooling Concepts

The system weight and displaced fuel weight of concept M-6 are substantially greater than that of the other concepts. This occurs for a number of reasons. Here, the heat pipe structure acts as the combustor liner, and hence its walls must be appreciably thicker to withstand the hoop stress imposed by combustion gas pressure. This effect is accentuated by the relatively low tensile strength of TZM at the liner/heat pipe temperature of 3000°F.

The heat load is higher due to the lower liner temperature (compared to the other concepts), requiring a greater system thermal capacity and hence more weight and volume. More insulation is required because of the higher heat pipe temperature (compared to the other concepts). Finally, since the vaporizing heat sink is used here to augment system sensible thermal capacity during the transient, the discharge nozzles must be sized to accommodate a vapor discharge rate almost five times that for steady-state operation, and a larger expansion ratio.

Concept M-6 was eliminated from further consideration because of its high weight and volume.

CONCEPT C-7

Concept C-7 utilizes the sensible thermal capacity of the heat pipe and surrounding structure to absorb the transient heat load, and an external radiator to dissipate the steady-state heat load. A structural carbon-carbon liner withstands the hoop stress produced by combustion gas pressure. An additional layer of carbon-carbon is added to insure sufficient sensible thermal capacity to absorb the transient heat load. An annular disk transition section connects the inner heat pipe which surrounds the combustor liner with the outer heat pipe radiator.

The overall weight of the C-7 system is about 15 lb greater than that of concepts C-8 and C-4, and the equivalent displaced fuel weight is about 65 lb greater. The larger system volume implied by the latter figure results from the additional thermal insulation required for the radiator and the transition section. As a result, the overall insulation requirement is more than three times that of the nonradiator concepts.

The design of concept C-7 utilizes an open channel for liquid lithium in the heat pipe wick. A more preferable porous liquid flow channel would require the wick thickness to be increased by a factor of around five due to the higher friction of a porous channel, substantially increasing heat pipe weight and volume and increasing the susceptibility of the liquid lithium in the wick to boiling. However, overall system weight and volume should change very little because the higher thermal capacity of the thicker wick would probably eliminate the need for the supplemental carbon-carbon heat sink.

For very long missions or where extensive re-usable capability is required, concept C-7 may well be the preferred choice, since its weight and volume are invariant with time and fluid replenishment is not needed. For the mission under consideration here, the higher weight and volume of concept C-7, along with its more complex configuration, render it less attractive than the vaporizing heat sink systems.

CONCEPTS C-8, C-5, AND C-4

Concepts C-8, C-5, and C-4 all use a vaporizing lithium heat sink to dissipate the steady-state heat load, in conjunction with a structural carbon-carbon liner. The transient heat load is absorbed by the sensible thermal capacity of the cooling system and associated structure. In each case, when the design temperature (2800°F) and vapor pressure (52.9 psi) are reached at the end of the transient, rupture plates in four adjacent nozzles yield, discharging lithium vapor to the atmosphere.

These concepts differ in the manner in which heat is transferred to the lithium heat sink reservoir. In concept C-5, heat is transferred to the reservoir from the carbon-carbon liner via a separate heat pipe structure. In concept C-8, the heat pipe and lithium reservoir are integrated into a single structure. In concept C-4, the heat pipe wick and the lithium reservoir are the same entity. In each case, both the heat pipe wick and the lithium reservoir contain a TZM felt of 90% porosity to stabilize the liquid.

Concept C-5 employs a perfectly viable cooling system design approach, incorporating tested heat pipe technology. However, its weight and the equivalent weight of displaced fuel are significantly greater than for concepts C-8 and C-4. Also, substantial superheat will be developed in the reservoir section, raising the possibility of boiling.

In addition to having lower weight and volume than C-5, concepts C-8 and C-4 utilize a simpler structure, without an internal wall. The structure of C-4 is even simpler than that of C-8, requiring but one wick. However, for evaporation to occur at the liquid-vapor interface, incident heat must flow through the lithium reservoir/wick. The temperature drop through this thickness represents the superheat in the liquid lithium. If boiling in the reservoir is to be avoided, the actual superheat must be less than the superheat at which boiling is initiated. It has been shown that boiling is not likely during steady-state conditions. The likelihood of boiling during the climb transient cannot be established without knowledge of heat flux and temperature histories.

Boiling in the lithium reservoir, particularly if initiated at the high heat fluxes encountered during the tran-

sient, will be accompanied by large, possibly destructive, fluctuations in temperature and pressure. Since analysis could not discount the possiblility of boiling, concept C-4 could not be considered further, despite its design simplicity and competitive weight and volume.

Concept C-8, along with C-4, exhibits the lowest system and displaced fuel weight of all the candidate concepts. By incorporating the lithium reservoir and heat pipe wick into a single containment, as is done in concept C-8, significant weight and volume savings and a relatively simple internal design result. Additionally, the thin (0.050 in.) heat pipe wick in concept C-8 assures that boiling will not be a problem.

PREFERRED COOLING CONCEPT

On the basis of the considerations which have been presented herein, concept C-8 was selected as the preferred cooling system concept which best meets specified design criteria.

CONCEPTUAL DESIGN

In the previous section, concept C-8 was selected as the preferred concept for further investigation, from among the candidate concepts which were considered. Concept C-8 utilizes an integral heat pipe/reservoir structure around a carbon-carbon combustion liner coupled to four lithium vapor discharge nozzles. (Figure 26.)

A conceptual design based on concept C-8 was developed. The conceptual design operates at a temperature at which cooling system thickness, weight, and displaced fuel weight are minimized. Also, design characteristics were analyzed in more detail than for the candidate cooling concepts.

A sketch of the cooling system cross-section for the conceptual design is shown in Figure 30. The vapor space width W_v, the vapor space thickness t_v, and the reservoir thickness t_s are variable parameters to be determined as a function of operating temperature. All of the other dimensions are fixed as indicated. Also fixed are the thickness of the carbon-carbon liner and the thickness of the two air gaps on either side of the cooling system. The thicknesses of the ZIRCAR and MIN-K thermal insulation layers around the cooling system are variable parameters, to be determined as a function of temperature.

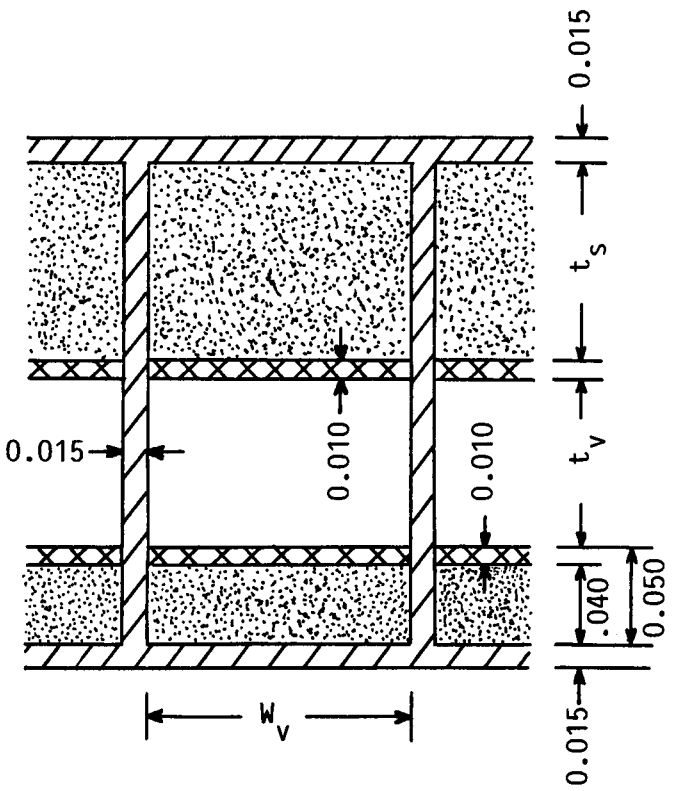

Figure 30. Cross-Section of Conceptual Design

HEAT PIPE VAPOR TEMPERATURE

The initial step in the analysis was to determine the relationship between the liner temperature and the temperature of the heat pipe vapor. First, the steady-state liner heat flux was calculated from Equation (4). Then, the temperature drop across the liner thickness was calculated from the standard heat conduction equation. The temperature drop across the air gap between the liner and the heat pipe/reservoir was then found using Equation (8). The temperature drop across the heat pipe wall and wick was taken to be 15°F, a figure which is accurate within 3 to 5°F over the liner temperature range considered.

From the above information the heat pipe vapor temperature was determined as a function of the liner temperature, as shown in Figure 31. As the liner temperature drops from 3500°F to 3250°F, the vapor temperature drops by more than 700°F from 2835°F to 2122°F. Using Figure 31, Figure 10, and integrating Case A Equations (2),(3), and (4), the heat load as a function of vapor temperature was also determined.

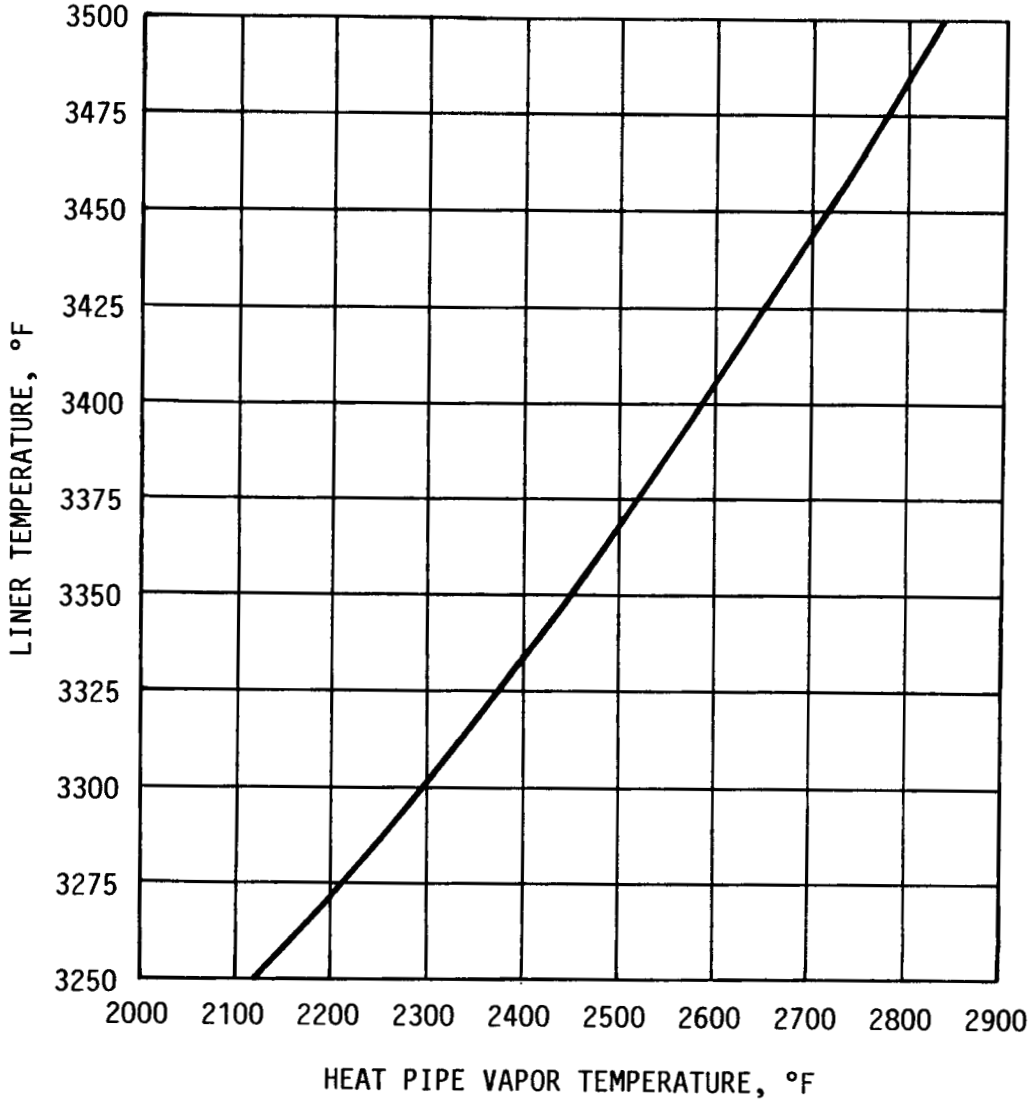

Figure 31. Liner Temperature Versus Heat Pipe Vapor Temperature for Conceptual Design

RIB SPACING

The spacing between ribs as a function of heat pipe vapor temperature was found from Equation (10). The allowable stress was taken as 1/2 the tensile stress of TZM, and ΔP is the difference between the heat pipe vapor pressure and the external steady-state atmospheric pressure of 0.21 psi. As the vapor temperature drops from 2835°F to 2122°F, the rib spacing increases from 0.26 in to 4.17 in.

VAPOR SPACE THICKNESS

The thickness of the vapor space as a function of vapor temperature was established from consideration of heat pipe capillary pumping, sonic, and entrainment limits. Capillary pumping limit equations were developed using References 6 and 13. Equations for the sonic, entrainment, and boiling limits were obtained from Reference 12.

During steady-state cruise, lithium vapor flows axially through the vapor flow passages and then is discharged to the atmosphere through the exhaust nozzles. During this phase of operation, as liquid lithium is depleted from the reservoir, the liquid-vapor interface moves into the coarse-pored reservoir layer. Capillary pumping is then determined by the capillary pressure capability of the coarse pores, rather than the fine pores in the thin screen layer adjacent to the vapor space.

The coarse-pored layer is fabricated from TZM felt of 90% porosity and, has an effective pore size of 190 micron. Therefore, the diameter of curvature at the liquid-vapor interface for capillary pumping cannot be less than 190 micron. The diameter of curvature varies inversely with the capillary pressure, which in this case is equal to the axial vapor pressure drop. (Liquid flow is in the radial direction, and its pressure drop is negligible.)

Since the flowing lithium vapor is saturated and in equilibrium with its adjacent liquid, the vapor temperature is a direct function of the vapor pressure. Therefore, the vapor pressure drop must be limited to keep the vapor temperature from decreasing excessively during vapor flow. For lithium, the temperature of saturated vapor drops 2-3°F for each per cent drop in vapor pressure.

In establishing the vapor space thickness from capillary pumping considerations, the following criteria were used.

1. The diameter of curvature must not fall below 220 micron.

2. The vapor pressure drop must not exceed 3%.

When these criteria were applied, the resulting vapor space thicknesses varied from 0.11 in. at a vapor temperature of 2835°F to 0.50 in at 2122°F.

Using these values of vapor space thickness, the axial heat flux, sonic limit, and the maximum pore size for no entrainment were calculated as a function of vapor temperature. Over the vapor temperature range from 2835°F to 2122°F, the axial heat flux varied from 132 Btu/in^2-sec to 35 Btu/in^2-sec, while the sonic heat flux ranged from 1668 Btu/in^2-sec to 128

Btu/in^2-sec. Since the axial heat flux is always less than the sonic heat flux, the sonic limit was not encountered.

Over the same vapor temperature range, the pore size above which entrainment of the liquid by its vapor can be expected varies from a minimum of 282 micron to a maximum of 729 micron. Since the actual pore size is 190 micron, the entrainment limit was not encountered.

WICK THICKNESS

The thickness of the heat pipe lithium-filled wick was maintained constant at 0.050 in. The inner 0.040 in. of the wick is fabricated from TZM felt of 90% porosity, and the outer 0.010 in. is fabricated from TZM screen of 65% porosity. Calculations were carried out to compare the superheat due to steady-state heat flow through the wick with the superheat required for boiling in the wick. The boiling superheat calculations were performed for a diameter of curvature of 40 micron, the approximate minimum value which is encountered during the climb transient. (See below.) A nucleation site radius of 3 micron was assumed.

Over the vapor temperature range of 2835°F to 2122°F, the wick superheat varied from 9.9°F to 12.1°F, while the superheat for boiling varied from 89.5°F to 1074°F. Since the wick superheat was always well below the superheat for boiling, the boiling limit was not encountered.

PORE SIZE AT INNER WICK LAYER

As was indicated above, the minimum diameter of curvature during steady-state operation is at least 220 micron. Therefore, the coarse-pored TZM felt with 190 micron pores is adequate to meet steady-state capillary pumping requirements.

A second, fine-pored wick layer is needed to meet capillary pressure requirements during the climb transient. During this period, the flow of both vapor and liquid is in the radial direction along a very small flow path, and frictional pressure drops can be neglected. However, a substantial static liquid pressure drop develops as the result of engine acceleration and gravity. The magnitude of this static pressure drop was calculated as a function of vapor pressure for the maximum combined engine/gravity acceleration of 2.62 g's, along with the diameter of curvature needed for capillary pressure to offset the pressure drop.

Over the usual vapor temperature range, the static pressure drop varied from 3.01 psi to 3.33 psi while the diameter of curvature varied from 39.4 micron to 46.5 micron. The effective wick pore diameter must be less than the diameter of curvature. Therefore, the effective pore size for the inner

wick was set at 30 micron, to be achieved by drawing down several layers of 400-mesh screen.

RESERVOIR THICKNESS

As in the earlier studies, the reservoir thickness t_s was established by equating the cooling system and liner thermal capacity to the total thermal load. Expressions were developed for the lithium and TZM volumes as a function of the rib spacing, vapor space thickness, and reservoir thickness. The rib spacing and vapor space thickness are already known as a function of vapor space temperature.

The volumes for each constituent were then multiplied by the product of the density and unit thermal capacity (heat absorbed per pound when heating to a given vapor temperature) to obtain the total thermal capacity. Expressions used to calculate the temperature-dependent thermal properties are given in Appendix C.

The thermal capacity for lithium includes both sensible and latent heat components. The thermal capacity for TZM, lithium, and the liner were added together and equated to the total heat load corresponding to the vapor temperature under consideration. The resulting expression was then solved for the reservoir thickness, from which the combined heat pipe/reservoir thickness, component weights, and thermal capacities could then be calculated.

As the vapor temperature temperature dropped from 2835°F to 2122°F, the reservoir thickness increased from 0.384 in. to 0.618 in. The increase is due primarily to the higher heat load at lower vapor (and liner) temperatures. The combined heat pipe/reservoir thickness increased from 0.584 in. to 1.208 in. The weight of the combined heat pipe/reservoir (not including the liner, nozzles, plenum, or thermal insulation) ranged from a minimum of 110 lb at 2588°F to a maximum of 139 lb.

The total thermal capacity (equal to the total heat load) varied from 205,000 Btu at a heat pipe vapor temperature of 2835°F to 331,000 Btu at 2122°F. The thermal capacity during the climb transient ranged from 94,000 Btu at 2835°F to a minimum of 93,000 Btu at 2588°F to a maximum of 104,000 Btu at 2122°F. Over the same temperature range, the transient heat load increased from 83,000 Btu to 104,000 Btu.

The transient thermal capacity was greater than or equal to the transient heat load over the entire vapor temperature range considered. The design operating temperature was then always reached, and the discharge of lithium vapor initiated, at or somewhat after the time when steady-state cruise conditions are reached. This is a desirable situation, since the

steady-state and total cruise times are then at least equal to the design values.

THERMAL INSULATION

Thermal insulation requirements were calculated using the same model previously employed for concept C-8. (See Figure 19.) For each vapor temperature considered, the temperature at the inner ZIRCAR surface was found, along with the thickness of the ZIRCAR and MIN-K layers. The ZIRCAR was used for insulation temperatures of 2000°F and above, and the MIN-K for temperatures up to 2000°F.

As before, insulation requirements were determined for a total interior heat leakage of 12,000 Btu, of which 10,000 Btu originates from the heat pipe/reservoir and 2000 Btu from the engine skin. Again, 0.34 in. of MIN-K was used under the skin. Once the insulation thicknesses were calculated, insulation volumes, weights, and thermal capacities could be determined.

The temperature at the inner ZIRCAR surface ranged from 29°F below the vapor temperature when the vapor temperature was 2835°F to 52°F below the vapor temperature at 2122°F. The weight of ZIRCAR dropped from 6.5 lb at 2835°F to approximately zero at 2122°F. The weight of MIN-K varied from 2.57 lb at 2835°F to a minimum of 2.56 lb at 2588°F to a maximum of 3.04 lb at 2122°F. The thermal capacity of ZIRCAR varied from 2255 Btu at 2835°F to zero at 2122°F. For MIN-K, the thermal capacity varied from 735 Btu at 2835°F to a minimum of 733 Btu at 2588°F to a maximum of 870 Btu at 2122°F.

DISCHARGE NOZZLES

The size, weight, and insulation requirements of the four lithium vapor discharge nozzles were calculated over the vapor temperature range of interest. The nozzle geometry and calculational methods used for the initial concept C-8 nozzle calculations were also employed here. The exhaust pressure of 0.411 psi was also retained. The inlet nozzle width n was varied so that the total nozzle inlet area was equal to the heat pipe vapor space flow area. The distance m from the inlet to the throat was taken be to 1/4 of n.

As the vapor temperature dropped, the nozzles became larger due to the lower density of the lithium vapor, but the overall impact on engine volume remained minimal. The nozzle thickness increased in accordance with the increasing thickness of the heat pipe/reservoir from 0.58 in. to 1.21 in. The nozzle exit width varied over a small range from 1.38 in. to a maximum of 1.57 in. at 2450°F. At this temperature, 6.7% of the engine circumference was occupied by the nozzles. The percentage was less at other vapor temperatures.

The throat width increased from 0.086 in. to 0.754 in. as the vapor temperature dropped from 2835°F to 2122°F, while the entrance width increased from 1.48 in. to 3.55 in. The nozzle half angle was less than 5 deg in all cases.

The weight of the nozzles plus plenum ranged from about 2 lb to 4 lb as the vapor temperature dropped. Less than 1/2 lb of thermal insulation was needed around the nozzles in all cases. The thermal capacity of the insulation ranged from 110 Btu to 180 Btu.

COOLING SYSTEM OPTIMIZATION

The previously described calculations define the characteristics of the cooling system conceptual design as a function of of steady-state heat pipe vapor temperature. The characteristics with the greatest impact on engine design and performance are: system size, weight, and volume.

In Figure 32, cooling system thickness is plotted as a function of the heat pipe vapor temperature. The thickness reaches a minimum of 1.11 in. at about 2600°F. In Figure 33, the total system weight (not including the carbon-carbon liner) and the displaced fuel weight (weight of fuel which would be displaced if the excess volume occupied by the cooling system were accommodated at the expense of fuel) are plotted against vapor temperature. Again, a minimum is evident in both curves at around 2600°F, where the weight is 119 lb and the displaced fuel weight about 15 lb.

The optimum vapor temperature at which cooling system thickness, weight, and volume (as expressed by the displaced fuel weight) are minimized is therefore 2600°F. From Figure 31, the associated liner temperature is 3405°F.

The consequences of operating at below-optimum vapor temperatures in order to further reduce the liner temperature are readily determined from Figures 31, 32, and 33. In Table 19, characteristics of the conceptual design are compared at the optimum temperature of 2600°F and at a vapor temperature of 2300°F. It is evident that liner temperatures lower than that corresponding to the optimum heat pipe vapor temperature are attainable at the expense of cooling system size and weight.

OVERALL CHARACTERISTICS OF OPTIMIZED CONCEPTUAL DESIGN

Characteristics of the optimized conceptual design are presented below. (The characteristics actually correspond to a vapor temperature of 2588°F, because this is the closest temperature to 2600°F for which design calculations were performed.)

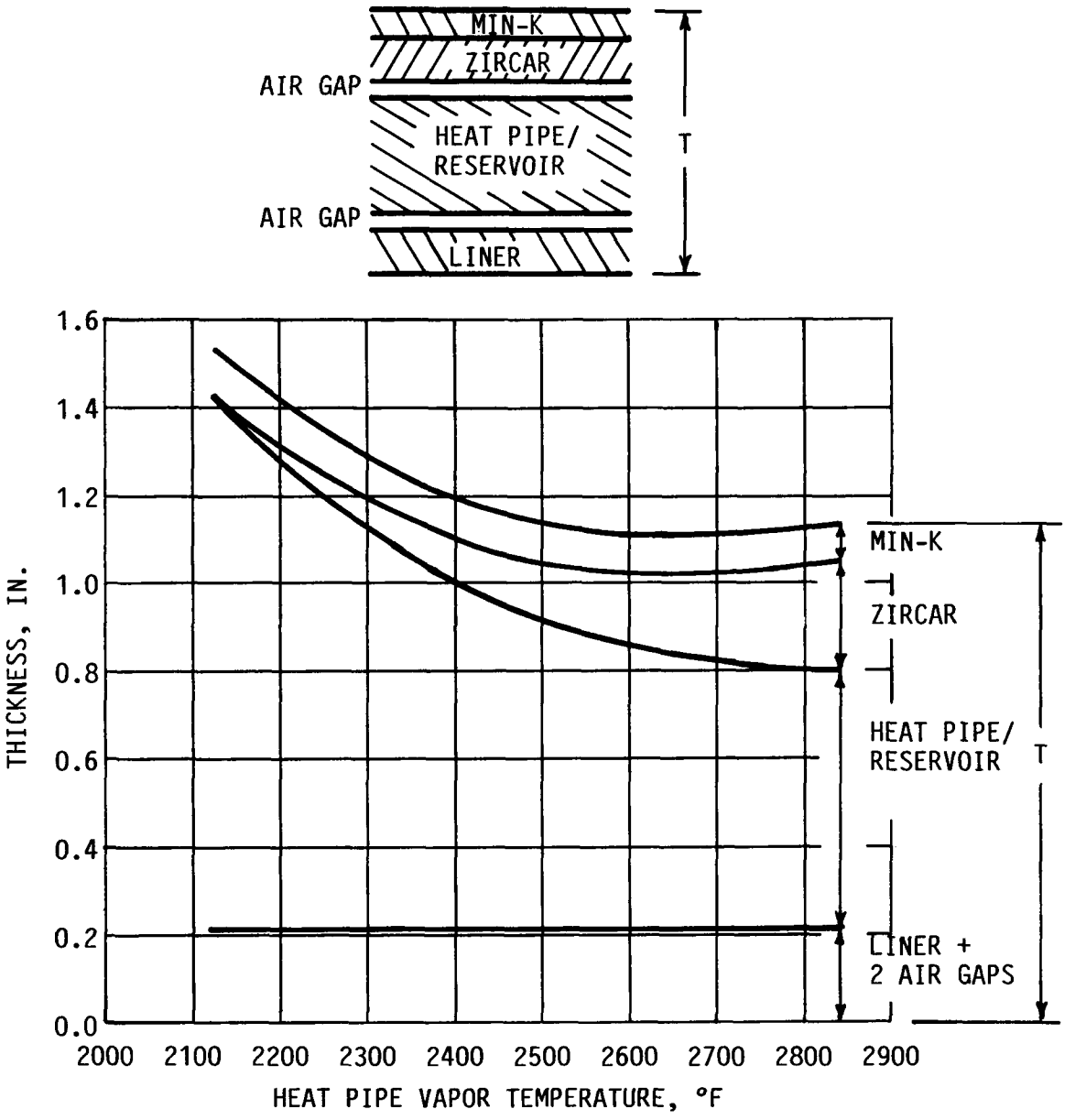

Figure 32. Cooling System Thickness Versus Heat Pipe Vapor Temperature for Conceptual Design

The radial temperature distribution across the cooling system thickness is shown in Figure 34. The temperature at the liner inner surface is 3400°F. It drops 280°F across the liner thickness and another 520°F across the first air gap to 2600°F at the heat pipe inner surface. A further drop of 12°F to 2588°F occurs across the wick thickness. The temperature remains at approximately 2588°F across the reservoir thickness, and drops another 28°F across the second air gap to 2560°F at the inner surface of the ZIRCAR insulation. A further drop of

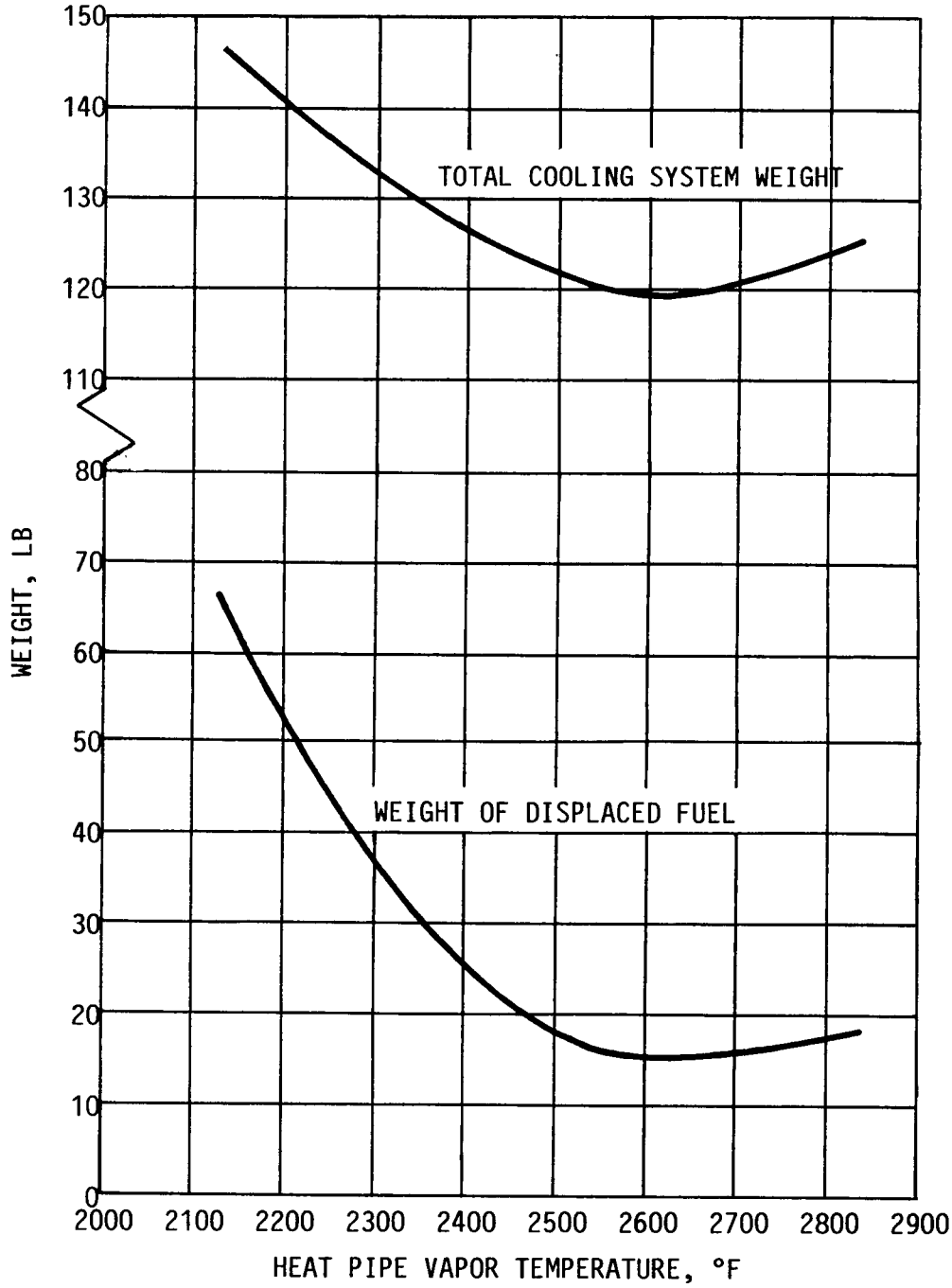

Figure 33. Cooling System Weight and Displaced Fuel Weight Versus Heat Pipe Vapor Temperature for Conceptual Design

560°F to 2000°F occurs across the ZIRCAR thickness, followed by a 1700°F drop to 300°F across the thickness of the MIN-K insulation.

Table 19. Conceptual Design Characteristics at Optimum and Below-Optimum Heat Pipe Vapor Temperatures

Characteristic	Vapor Temperature, F	
	2600(Optimum)	2300
Liner Temperature, F	3405	3300
Cooling System Thickness, in.	1.11	1.28
Cooling System Weight, lb	119	133
Displaced Fuel Weight, lb	15	37

A preliminary layout of the optimized conceptual design is given in Figure 35. Overall features are illustrated in the pictorial of Figure 36. Major design characteristics are presented in Table 20.

TRANSIENT BEHAVIOR

The design studies which have been described thus far have all been based on steady-state cruise conditions. In these studies, the heat loads needed to size the lithium reservoir were estimated by integrating the liner heat rate at a given steady-state liner temperature over the transient and steady-state flight times.

During the transient climb period, liner heat fluxes may be several times steady-state values, causing liner temperatures to rise significantly above steady-state levels. Therefore, transient studies were carried out to establish the temperature history of the optimized conceptual design during and subsequent to the climb transient.

ANALYTICAL MODEL

A model for the one-dimensional analysis of the cooling system temperature was developed, based on the finite-difference method (15). With this technique, the physical system is divided into a discrete number of segments. Nodes within or on the boundaries of the segments are assigned a temperature. The net heat leakage into each segment during a specified time interval produces a temperature change in that

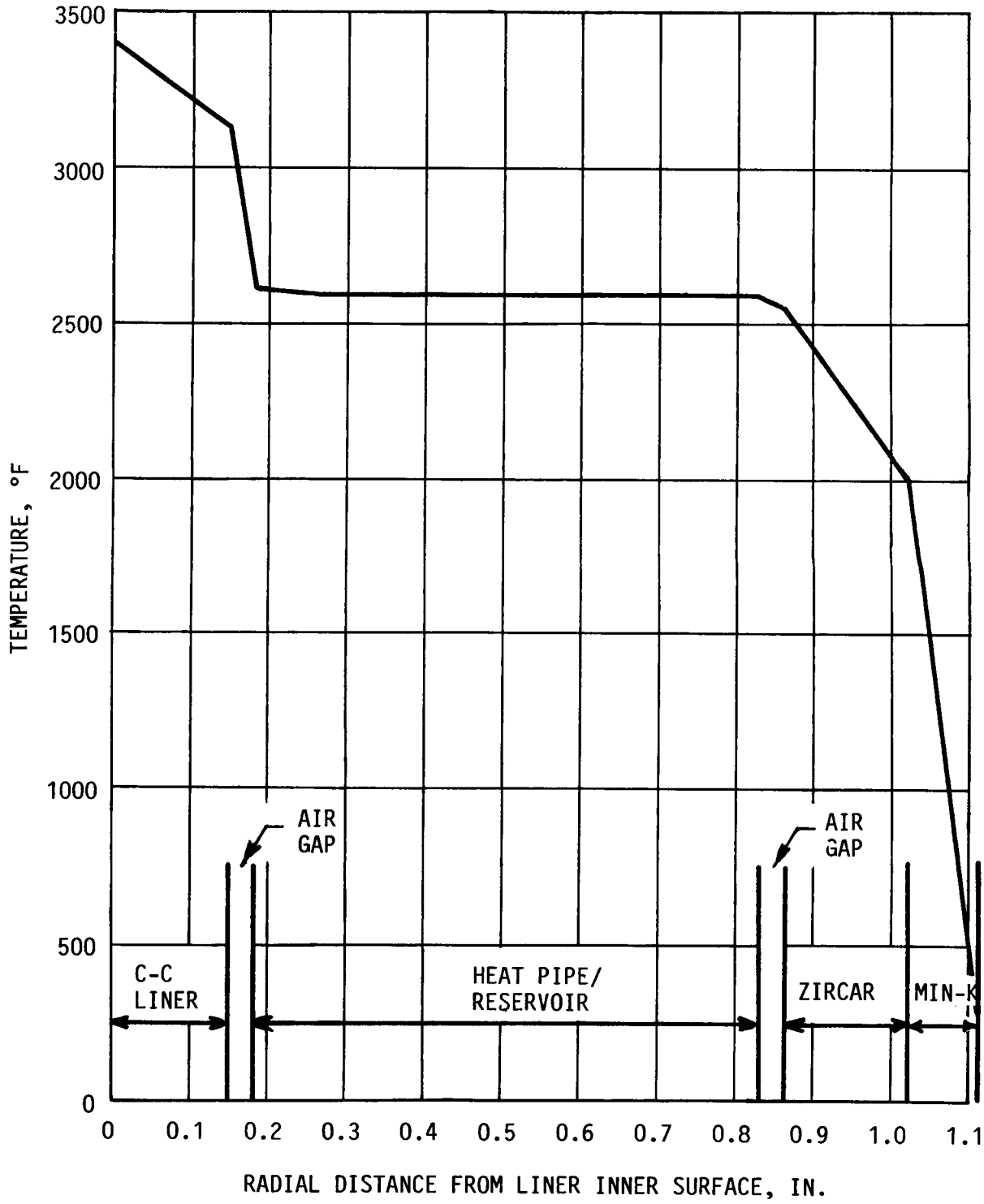

Figure 34. Temperature Distribution Across Thickness of Optimized Conceptual Design

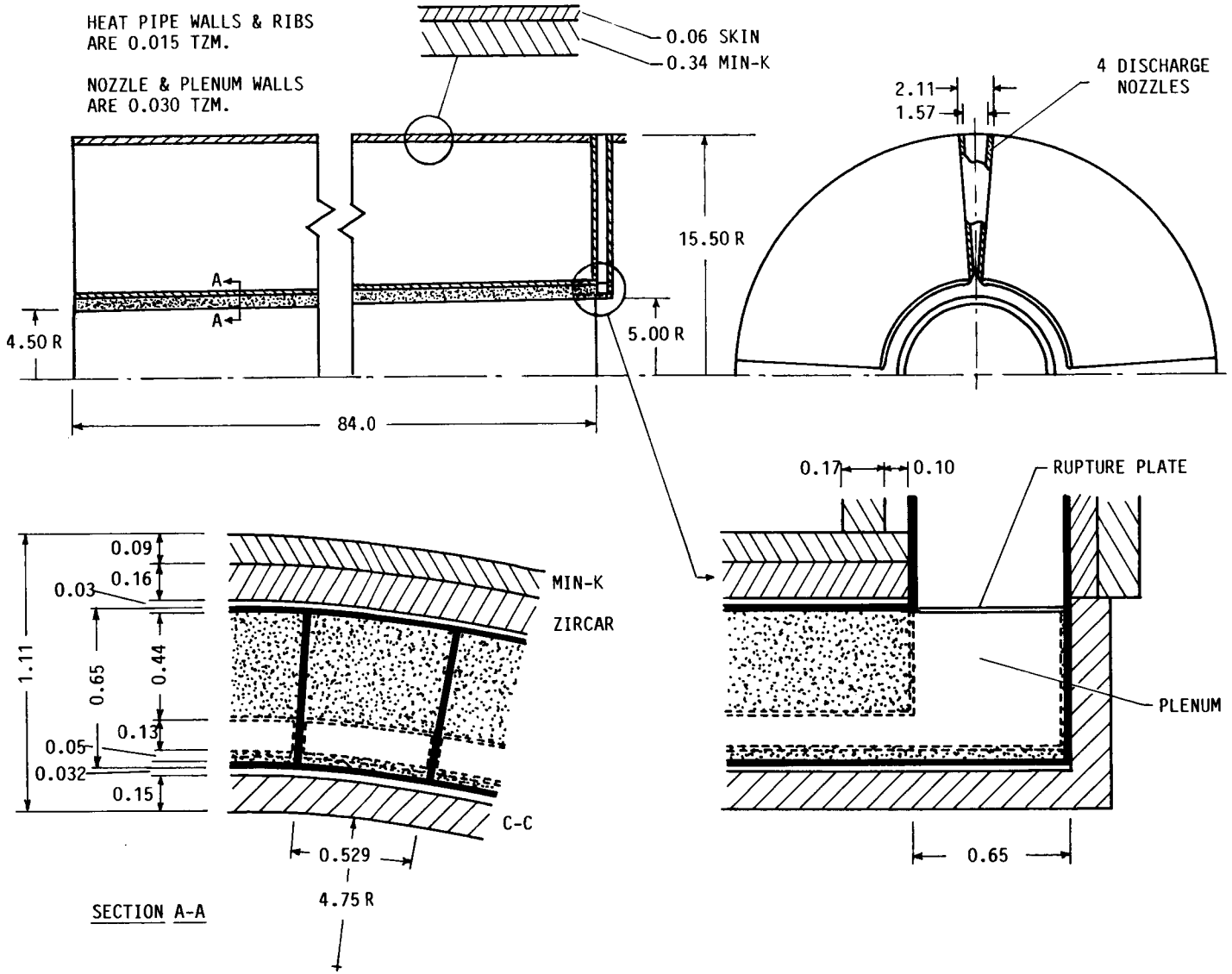

Figure 35. Preliminary Layout of Optimized Conceptual Design

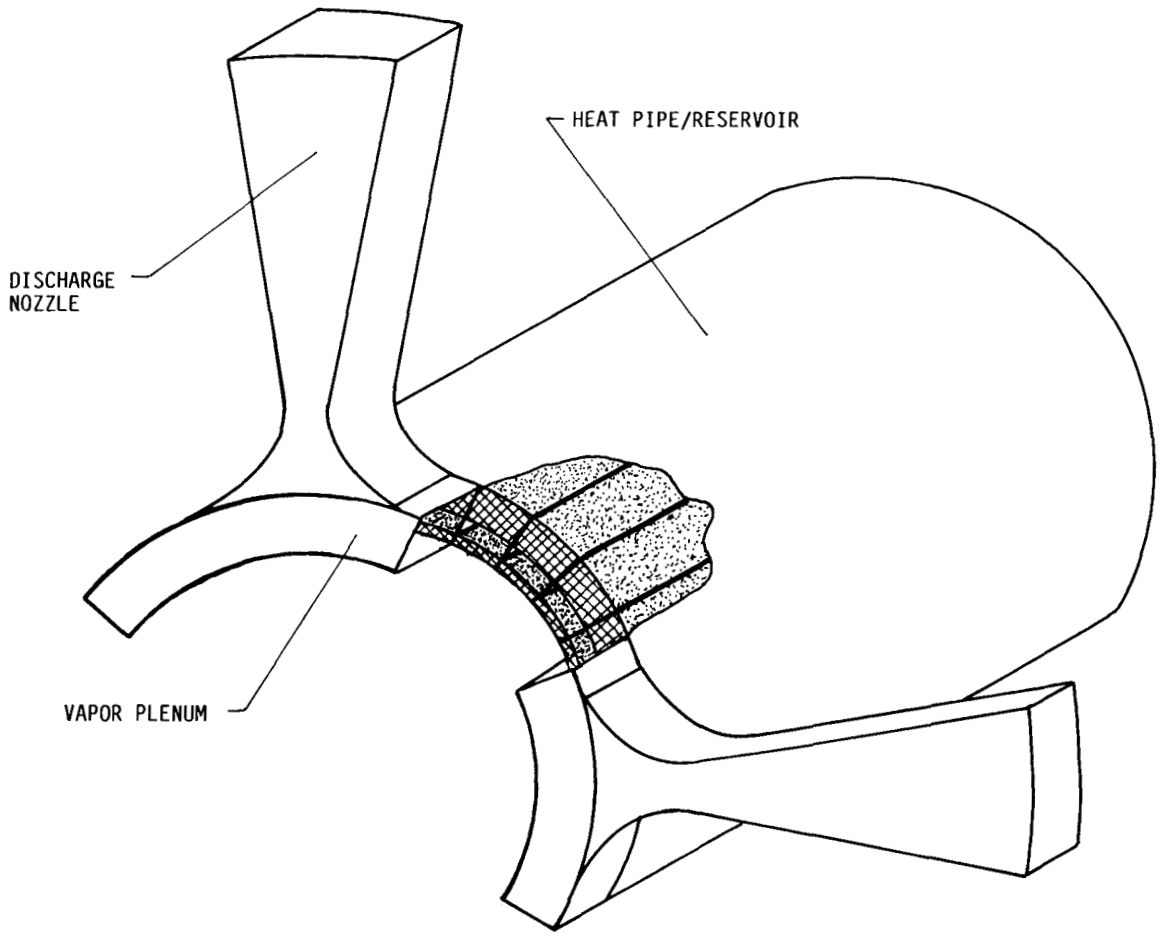

Figure 36. View of Cooling System Conceptual Design Looking Forward

segment. At segment boundaries, the heat flow to and away from the boundary must be the same.

With these basic ground rules, the temperature at each node after a given time increment can be estimated from the temperature at the start of the increment. The temperature distribution through the system is then determined by "marching out" the solution, increment by increment.

The cooling system model is illustrated in Figure 37. Five basic components have been included: the combustor liner, the air gap, the heat pipe wick, the heat pipe vapor space, and the lithium reservoir. These components are stacked between the combustion chamber and the thermal insulation. The time- and temperature-dependent heat flux incident on the liner is given by the Case B equations on page 15. The heat flux leaving the reservoir through the thermal insulation was assumed to be zero. The initial system temperature was assumed to be 90°F.

Table 20. Characteistics of Optimized Conceptual Design

	Weight, lb	Volume, in^3
Heat Pipe/Reservoir	110.3	1803.5
Nozzles and Plenum	2.3	38.1
Thermal Insulation	7.0	792.1
Total Cooling System	119.6	2633.7
Liner	26.6	382.0
Total	146.2	3015.7
Excess Volume		417.1
Displaced Fuel Weight	15.4	

Thermal Capacity, Btu

	Sensible	Latent	Total
Heat Pipe/Reservoir	59,030	134,220	193,250
Liner	33,920		33,920
Thermal Insulation	2,210		2,210
Total	95,160	134,220	229,380

Heat Pipe/Reservoir Structure

	Heat Pipe		Reservoir	
	TZM Felt	TZM Screen	TZM Felt	TZM Screen
Thickness, in.	0.040	0.010	0.430	0.010
Porosity, %	90	65	90	65
Pore Diameter, micron	190	30	190	30

Table 20. (continued)

Heat Leakage to Interior, Btu	
From Heat Pipe/Reservoir	10,000
From Skin	2,000
From Nozzles	230
Total	12,230
Temperature and Pressure	
Liner Temperature, °F	3400
Heat Pipe Vapor Temperature, °F	2588
Heat Pipe Vapor Pressure, psia	25.9
Lithium Discharge Nozzles	
Number of Nozzles	4
Total Flow Rate, lb/sec	0.0583
Nozzle Thickness, in.	0.650
Nozzle Width at Inlet, in.*	1.623
Nozzle Width at Throat, in.*	0.182
Nozzle Width at Exhaust, in.*	1.567
Radial Distance from Inlet to Throat, in.	0.406
Radial Distance from Throat to Exhaust, in.	9.262
Nozzle half-angle, deg	4.28

* Internal dimensions. Add 0.060 in. for external dimensions.

Table 20. (continued)	
Heat Transport Limits	
Sonic	
Axial Heat Flux, Btu/in²-sec	120.6
Axial Heat Flux at Sonic Limit, Btu/in²-sec	785.7
Entrainment	
Pore Diameter for No Entrainment, micron	≤282
Capillary Pumping	
Axial Temperature Drop, °F	6.3
Diameter of Curvature in TZM Felt, micron	225
Diameter of Curvature in TZM Screen, micron	42
Boiling	
Superheat in Heat Pipe Wick, °F	11
Superheat at Which Boiling Starts, °F	218

There are a total of 15 temperature nodes, distributed as follows: nodes 0 to 5, liner; nodes 6 to 8, wick; nodes 9 to 14, reservoir. The spacing Δx between liner nodes is $0.150/5 = 0.030$ in.; the spacing Δy between wick nodes is $0.065/2 = 0.0325$ in.; and the spacing Δz between reservoir nodes is $0.455/5 = 0.091$ in. The vapor space thickness is 0.130 in., while the air gap thickness L is variable.

The heat flux across the air gap includes a radiation component and a conduction component, and is the same on either side of the gap. The gap thickness is a function of an initial specified value and the temperature expansion coefficients of the adjacent liner and wick segments. The minimum gap thickness was taken as 0.001 in., which corresponds roughly to the

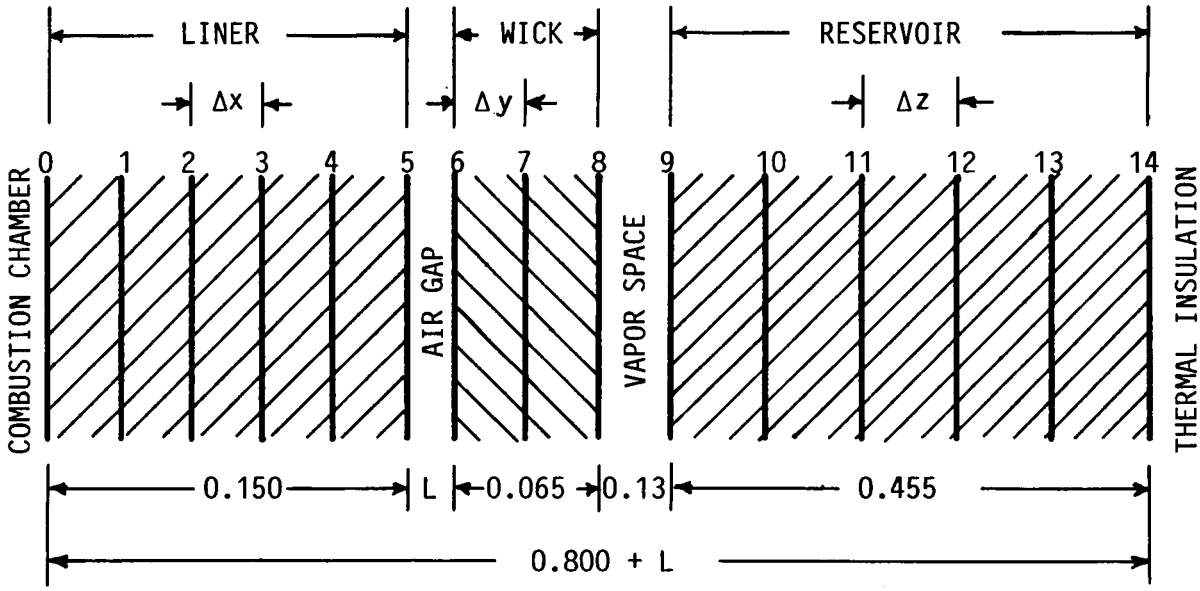

Figure 37. Finite-Difference Model for Transient Analysis of Optimized Conceptual Design

effective spacing between two 40-microinch-finish surfaces in contact under zero pressure. A constant air gap thickness option was also included, so that the effect of both fixed and variable airgaps could be assessed.

The heat flux across the vapor space between the wick and reservoir includes a radiation component and a convection component, and is the same on either side of the vapor space. (Conduction across the relatively thick vapor space is neglected.) Initially, the vapor temperature and pressure are too low to sustain continuum flow, and convective heat transfer is negligible. When the vapor temperature rises, convective heat transfer gradually increases as transition and finally continuum flow conditions are encountered.

As long as the wick boundary temperature exceeds that of the adjacent reservoir boundary temperature, the convective heat transfer component was assumed to be given by the heat flux corresponding to the sonic limit. Once the wick and reservoir boundary temperatures become equal, radiative heat transfer no longer exists. Convective heat transfer was then determined by energy balances on the wick and reservoir segments adjacent to the vapor space, subject to the criteria that the heat flux and temperature are the same on either side of the vapor space.

Solution of the finite difference equations requires that the density, specific heat, and thermal conductivity of the liner, wick, and reservoir be known as a function of tempera-

ture. This data for the carbon-carbon, TZM, and lithium which comprise the model components was obtained from Appendix C. Average property values for a component were found by weighting the property value of a given constituent by its volume fraction, and summing the weighted values of all the constituents. One-half of the TZM rib segments spanning the vapor space were allocated to the wick and one-half to the reservoir.

During the temperature transient, the lithium present in the heat pipe wick and reservoir will melt at 367°F. The heat of fusion (186 Btu/lb) was accomodated in the model by assuming that, at 367°F, the specific heat of lithium is equal to the heat of fusion. That is, at 367°F, 186 Btu is required to raise the temperature of 1 lb of lithium by 1°F.

The stability of finite-difference equation solutions requires that the parameter $M = \Delta\ell^2/\alpha\Delta t$ be larger than 2, where $\Delta\ell$ is the segment width, Δt is the time increment, and α is the thermal diffusivity. The maximum allowable time increment is thus determined by M, $\Delta\ell^2$, and α. For the cooling system model of Figure 37, the wick is the critical component in determining Δt, because of the small segment thickness Δy in the wick. It was found that the stability of solutions could be assured by letting $\Delta t = 0.005$ sec.

The temperature at a given node n and time t + Δt was calculated from the following generalized equation.

$$T'_n = \left(1 - \frac{2}{M_n}\right)T_n + \frac{2A}{M_n}T_{n+a} + \frac{B}{M_n}\left(T_{n+1} + T_{n-1}\right) + C\left(\frac{2\Delta\ell}{k_n M_n}\right)q_n \qquad (26)$$

where
- t = current time
- Δt = time increment
- T_n = temperature at node n and time t + Δt
- T_n = temperature at node n and time t
- T_{n+a} = temperature at node n+a and time t
- T_{n+1} = temperature at node n+1 and time t
- T_{n-1} = temperature at node n-1 and time t
- k_n = thermal conductivity at node n and time t
- α_n = thermal diffusivity at node n and time t
- $\Delta\ell$ = distance between successive nodes
- $M_n = \Delta\ell^2/\alpha_n\Delta t$
- a, A, B, C are functions of the node number n
- q_n = heat flux at node n and time t

Equation (26) applies to any node provided that values of a, A, B, C, q_n, and $\Delta\ell$ for that node are used. The values assigned to these parameters for the various nodes are given in Table 21.

Table 21. Node Parameters for Equation (26)

Node	a	A	B	C	$\Delta\ell$	q_n
0	1	1	0	1	Δx	Eq.(5)-(7)
1-4	0	0	1	0	Δx	0
5	-1	1	0	-1	Δx	$q_{ra}+q_{ca}$
6	1	1	0	1	Δy	$q_{ra}+q_{ca}$
7	0	0	1	0	Δy	0
8 ($T_8>T_9$)	-1	1	0	-1	Δy	$q_{rv}+\xi$
8 ($T_8=T_9$)	-1	1	0	-1	Δy	q_c
9 ($T_8>T_9$)	1	1	0	1	Δz	$q_{rv}+\xi$
9 ($T_8=T_9$)	1	1	0	1	Δz	q_c
10-13	0	0	1	0	Δz	0
14	-1	1	0	0	Δz	0

In Table 21, q_c has the form

$$q_c = k_8 k_9 \left[\frac{M_9(T_7 - T_8) + M_8(T_9 - T_{10})}{k_8 M_8 \Delta z + k_9 M_9 \Delta y} \right] \qquad (27)$$

and q_{ra} = radiation heat flux across air gap
q_{rv} = radiation heat flux across vapor space
ξ = heat flux at sonic limit
q_{ca} = conduction heat flux across air gap

TRANSIENT STUDIES

The analytical model described in the previous section was used to conduct transient studies of cooling system temperatures. The temperature history was determined over a time interval of 99 sec, covering the climb transient period of 72 sec plus 27 sec of the steady-state cruise phase. It was assumed that, when the wick and reservoir temperatures reach 2600°F and the discharge of lithium vapor begins, these temperatures remain constant thereafter at 2600°F. This is strictly true only if the heat flux at the start of lithium discharge is equal to the steady-state heat flux.

In the steady-state design studies, sufficient sensible thermal capacity was provided to raise the heat pipe temperature to the lithium discharge temperature at 72 sec, the end of the transient climb period. In the transient studies, the lithium discharge temperature may be reached before or after 72 sec, depending on the actual temperature history which develops during the transient.

If lithium discharge starts prior to 72 sec, the higher heat fluxes during the transient will produce a flow rate higher than the design steady-state value, and the lithium will be depleted prior to flight termination. To avoid this situation, the reservoir size can be enlarged to increase the cooling system thermal capacity, and hence the time required to "fill" the reservoir to the desired discharge temperature.

If lithium discharge starts after 72 sec, more lithium is present than needed to cool the liner for the prescribed flight time. If the discharge starts only a few seconds after the start of steady-state cruise, the excess thermal capacity may be regarded as a desirable factor of safety for the cooling system. On the other hand, a delay of 10 sec or more in the lithium discharge time indicates that the reservoir size may be reduced to lower the cooling system thermal capacity and weight.

The transient temperature distribution is dependent on the thermal resistance of the heat flow path through the liner and cooling system, and on the thermal capacity of the lithium reservoir. The major contributions to the thermal resistance are the air gap between the liner and the heat pipe/reservoir, and the liner itself. Therefore, the transient studies concentrated on how the peak liner temperature and lithium discharge time are influenced by changes in the air gap and liner thermal resistance, and in the reservoir thickness.

Since the air gap resistance is affected by the thickness of the air gap and the emissivity of the boundary surfaces, these parameters were varied during the transient calculations. The liner thermal resistance is affected by its thickness and thermal conductivity, and these parameters were also varied.

The initial air gap thickness will generally increase with temperature, since the TZM heat pipe/reservoir has a higher expansion coefficient than the carbon-carbon liner. Therefore, the conductive resistance across the air gap increases with time. In the transient studies, the initial gap thickness was varied. Additionally, some studies were conducted with a fixed gap thickness to evaluate the impact of a fixed gap width on the peak liner temperature.

In the steady-state design studies, an emissivity of 0.8 on both of the air gap boundary surfaces (carbon-carbon and

TZM) was assumed. Over the temperature range of 2000°F to 3000°F, the emissivity of oxidation-resistant coatings used on reinforced carbon-carbon is about 0.85 (16). For the W-3 silicide coating used on TZM, the emissivity at 2500°F is about 0.73. However, the addition of a titanium carbide topcoat increases the emittance to about 0.83 (7). In the transient studies, emittance values of 0.8 and 0.9 were used, spanning the probable range of interest.

The liner thermal resistance is lowered by a reduction in liner thickness and an increase in thermal conductivity. The effect of each of these options was studied. The liner segment thickness Δx was the parameter which was changed to reduce the liner thickness.

If the transient heat load increases as the result of design modifications which lower the liner temperature, the reservoir will "fill up" more quickly, and the discharge of lithium vapor will occur earlier. By increasing the reservoir thickness, the reservoir will fill more slowly, delaying the onset of lithium vapor discharge. The effect of an increase in the reservoir thickness was studied by varying the reservoir segment thickness Δz.

Characteristics of Transient Cases

A total of 18 transient cases were run, starting with case 3. In Table 22, the values of the variable design parameters used in each case are given, along with the calculated peak liner temperature and lithium discharge time.

The following symbols are used in Table 22.

ϵ = emissivity of air gap boundary surfaces
Δx = segment thickness in liner
Δz = segment thickness in reservoir
l_o = initial width of variable thickness air gap at 90°F
l = width of constant thickness air gap
k = thermal conductivity of carbon-carbon liner
T_l = peak liner temperature
t_d = lithium discharge time

In case 15, the liner thermal conductivity is arbitrarily given the value 2k in order to assess the effect of increasing liner conductivity. The value of 0.001 in., used in some cases for l_o or l, approximates the effective gap thickness for two 40-microinch-finish surfaces in contact at zero pressure (5).

Cases 10 and 13, with emissivities of 0.9 and 0.8 and a variable gap width with an initial thickness of 0.030 in., are most representative of the optimized conceptual design. The

Table 22. Design Parameters, Peak Liner Temperatures, and Lithium Discharge Time for Transient Runs

Case	ϵ	Δx, in.	Δz, in.	l_o, in.	l, in.	k	T_l, °F	t_d, sec
3	0.9	0.030	0.110	0.001	-	k(C-C)	3854	73
4	0.8	0.030	0.110	0.001	-	k(C-C)	3886	75
5	0.8	0.030	0.091	0.001	-	k(C-C)	3959	67
6	0.9	0.030	0.110	-	0.032	k(C-C)	3844	91
7	0.9	0.030	0.091	-	0.032	k(C-C)	3863	75
8	0.8	0.030	0.091	-	0.032	k(C-C)	3910	81
9	0.8	0.030	0.110	-	0.032	k(C-C)	3898	99
10	0.9	0.030	0.091	0.030	-	k(C-C)	3869	76
11	0.9	0.030	0.091	0.060	-	k(C-C)	3876	78
12	0.9	0.030	0.091	0.001	-	k(C-C)	3924	65
13	0.8	0.030	0.091	0.030	-	k(C-C)	3913	81
14	0.9	0.024	0.091	0.030	-	k(C-C)	3867	70
15	0.9	0.030	0.091	0.030	-	2k(C-C)	3816	65
16	0.8	0.030	0.091	-	0.001	k(C-C)	3729	50
17	0.8	0.030	0.110	-	0.001	k(C-C)	3698	56
18	0.8	0.030	0.130	-	0.001	k(C-C)	3653	63
19	0.8	0.030	0.150	-	0.001	k(C-C)	3596	70
20	0.8	0.030	0.160	-	0.001	k(C-C)	3549	74

peak temperature is in the range 3870°F to 3910°F, and the lithium discharge time is in the range 76 sec to 81 sec. Comparison of cases 10 through 12 shows that the peak liner temperature is minimized at an initial gap width of 0.030 in.

In cases 3 through 14, the various design parameter changes result in relatively modest changes in peak liner temperature and, with the exception of cases 5, 12, 14, and 15, the lithium discharge time exceeds 72 sec, the start of the steady-state cruise period.

Cases 16 through 20 show that, if even nominal contact can be maintained between the liner and the heat pipe/reservoir during the transient, the peak liner temperature can be reduced to 3550°F at a lithium discharge time of 74 sec. However, the

reservoir thickness must be increased by 76% to achieve this peak temperature reduction. The resulting increase of lithium in the reservoir could extend the cooling time during steady-state cruise by an estimated 50%. The steady-state liner temperature for this case is around 3110°F.

The slip-joint design of Figure 38, with three separate heat pipe/reservoir segments held in contact against the liner by circumferential tension springs, represents one approach to maintaining a constant thickness air gap.

Temperature Histories for Case 10

Representative temperature histories for four key cooling system locations are shown in Figure 39 for case 10. The temperature of the inner liner surface in contact with combustion gas reaches 2000°F within 1 1/2 sec. This rapid temperature rise is desirable, since it acts to limit the liner heat flux and hence the heat load. The temperature continues to rise, peaking at 3869°F at about 66 sec, then drops rapidly to below 3500°F after the start of the cruise phase at 72 sec. The temperature of the outer liner surface follows the general trend of the inner liner surface, peaking at 3325°F.

The temperature of the outer wick surface (adjacent to the vapor space) rises rapidly to about 1200°F after 16 sec, and more slowly to 1313°F after 47 sec. The slow rise occurs

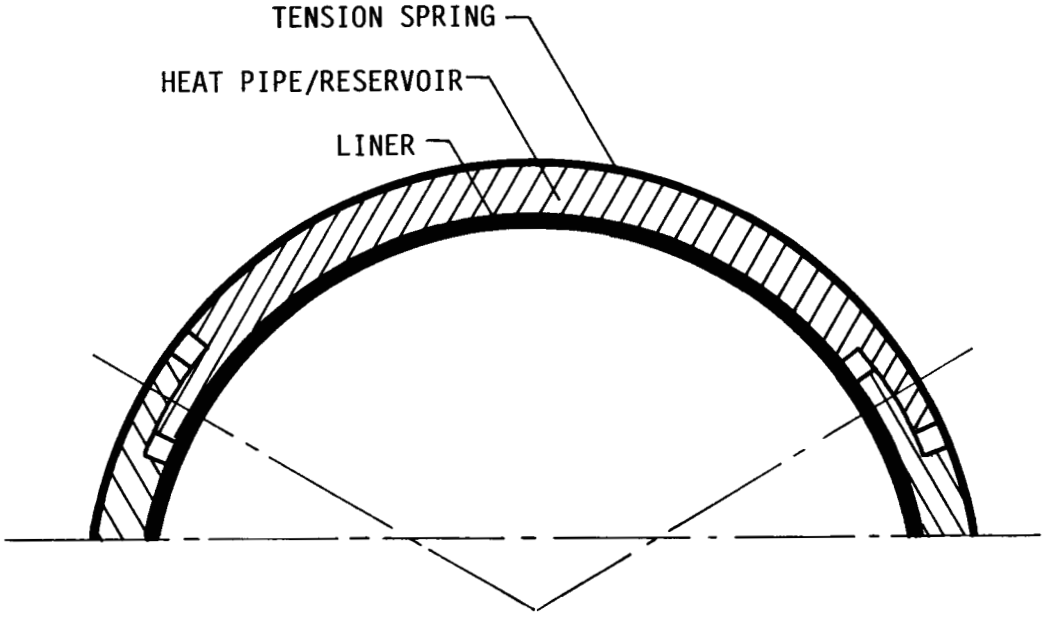

Figure 38. Slip-Joint Design Configuration for Heat Pipe Cooling System

C-2

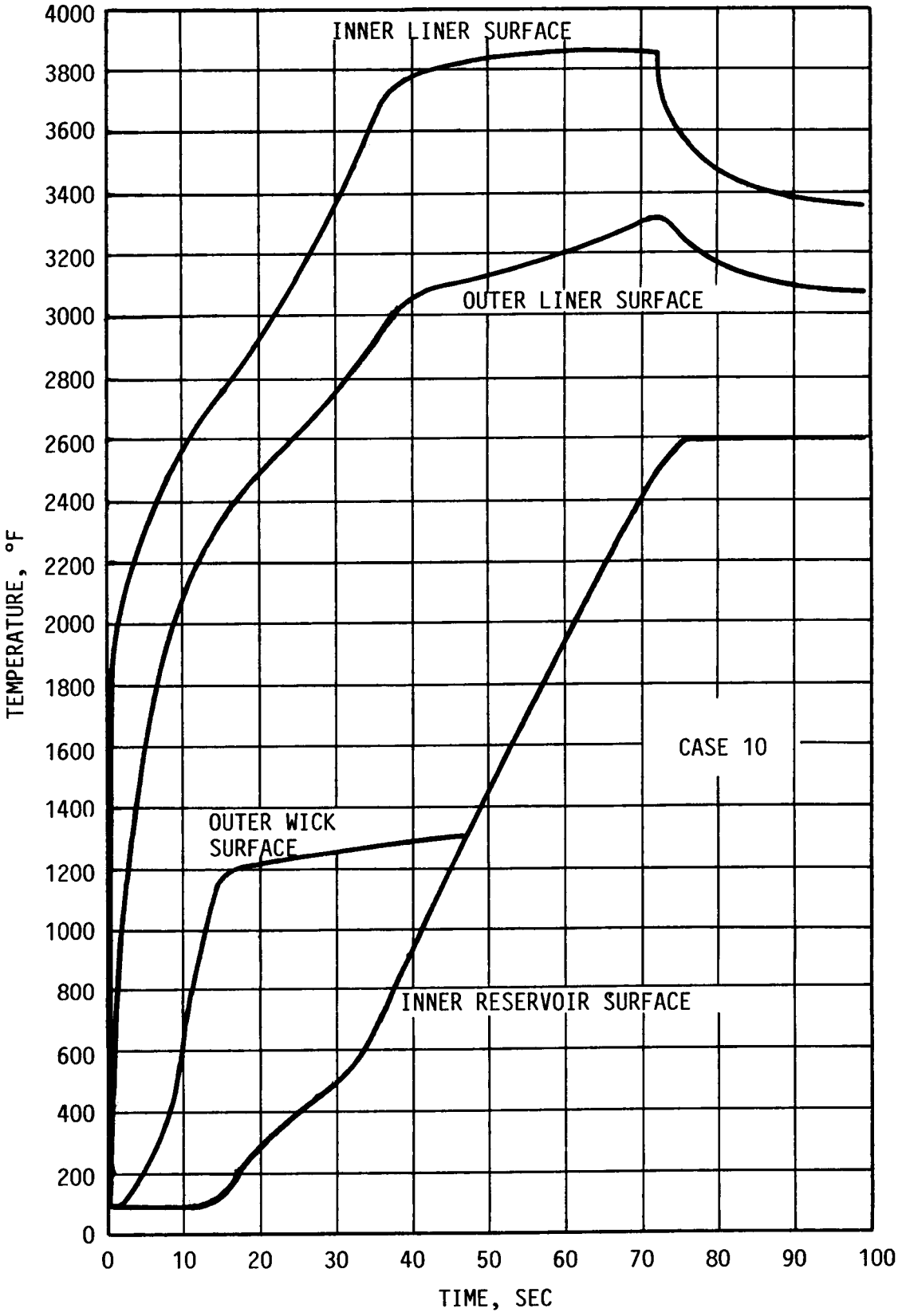

Figure 39. Cooling System Temperatures Versus Time for Case 10

during this period because heat is being transferred from the wick primarily at the sonic limit. The wick temperature is about 1800°F below that of the liner. At 47 sec, the temperatures of the wick and reservoir surfaces on either side of the vapor space become equal, and the heat pipe becomes fully operational. Thereafter, the wick/reservoir temperature reaches the lithium discharge temperature of 2600°F after 76 sec, and then remains constant.

For the first 12 sec, there is no change in the temperature of the inner reservoir surface. The temperature then starts to rise as heat transfer from the hotter adjacent wick surface increases. The reservoir and wick temperatures on either side of the vapor space merge at 1313°F after 47 sec.

Spacial Temperature Distribution for Case 10

In Figure 40, the temperature distribution across the cooling system thickness is shown after several time intervals. After 1 sec, the hot side of the liner has risen to 1860°F, while the cold side is at 480°F. The temperature has not yet changed in the wick or reservoir. After 25 sec, the liner surface temperatures have risen to 3140°F and 2620°F, the wick temperature is around 1250°F, and the reservoir has reached 400°F. After 47 sec, the liner surface temperatures are at 3820°F and 3120°F, and the facing wick and reservoir surfaces have reached a common temperature of 1313°F.

After 66 sec, the liner temperature has peaked at 3869°F, the cooler surface is at 3260°F, and the wick/reservoir temperature has reached 2240°F. After 76 sec, the liner surface temperatures are 3830°F and 3260°F, and the wick/reservoir interface temperature has reached the lithium discharge temperature of 2600°F. Finally after 83 sec, the liner surface temperatures have dropped to 3430°F and 3160°F, and the entire reservoir is now at a uniform temperature of 2600°F.

The large temperature difference across the liner thickness resulting from the high initial heating rate can produce significant thermal stress. After 1 sec, the temperature difference is 1380°F. From Equation (38), the tensile thermal stress is 13,800 psi at the outer radius of the carbon-carbon liner and the compressive stress is 16,800 psi at the inner radius. When combined with the hoop stress of 14,800 psi (see page 33), the total tensile stress is 28,600 psi.

From reference 9, the tensile strength of carbon-carbon is 32,000 psi and the compressive strength is 23,000 psi. Pending more detailed analysis, it appears that thermal stress in the liner during the initial phase of flight is high but tolerable.

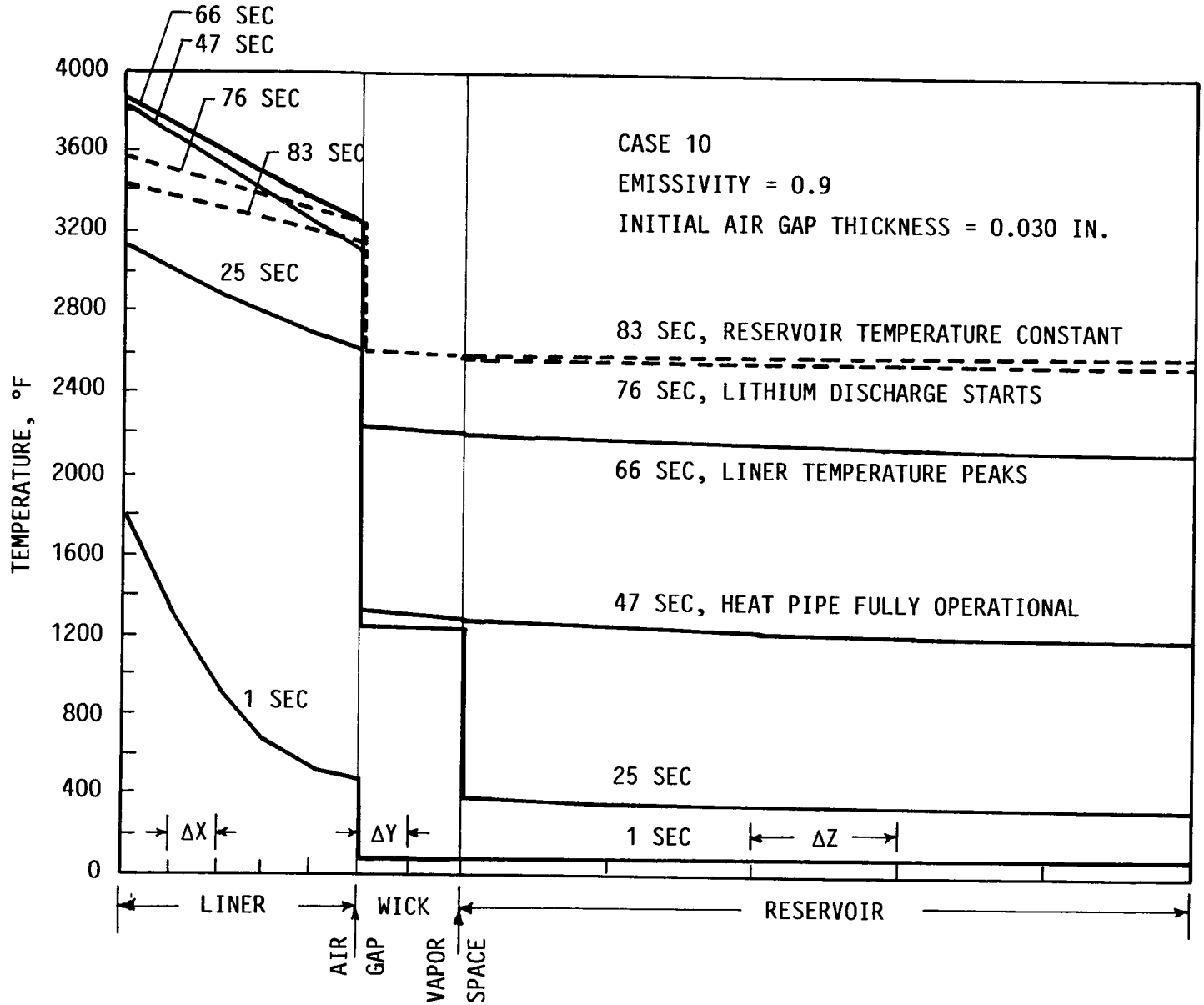

Figure 40. Temperature Distribution Across Cooling System at Various Times For Case 10

Comparison of Transient Histories for Cases 10, 11, and 12

In Figure 41, the inner surface temperature histories for the liner and reservoir are shown, indicating the effect of emissivity and initial air gap width. An increase in emissivity from 0.8 to 0.9 (cases 13 and 10) reduces the peak liner temperature by about 40°F and reduces the lithium discharge time by 6 sec. An increase in the initial air gap width from 0.001 in. to 0.030 in. (cases 12 and 10) reduces the peak liner temperature by about 50°F while increasing the lithium discharge time by 11 sec.

The liner heat flux histories are given in Figure 42. The heat flux drops to a minimum of 53-67 Btu/ft^2-sec after 16 sec, rises to a peak of 96-120 Btu/ft^2-sec after 36 sec, drops off again to a minimum of 15-17 Btu/ft^2-sec after 72-73 sec (the end of the climb transient), and finally recovers to approach steady-state values of 25-28 Btu/ft^2-sec. The increase in heat flux and heat load resulting from a reduction in the thermal resistance across the air gap is clearly evident. The transient and total heat loads are somewhat greater than the initial heat load estimates, which were based on integrating the heat flux over time at a constant steady-state temperature.

Heat Pipe Heat Transport Limits

During the climb transient, the heat pipe vapor and liquid flow radially along a very short flow path (less than an inch), and heat fluxes parallel to the flow path are very low (less than 1 Btu/in^2-sec.). Therefore, limitations on heat transport due to inadequate capillary pumping or entrainment are not expected.

The maximum superheat in the thin (0.050 in.) heat pipe wick is estimated to be around four times the steady-state superheat of 10°F, or around 40°F. The superheat at which boiling starts is 218°F at a vapor temperature of 2600°F. (See Table 20.) At the lower vapor temperatures encountered during the climb transient, even higher superheat is required for boiling. Therefore, the inception of boiling in the heat pipe wick is not expected to inhibit heat pipe heat transport during the transient.

Concluding Remarks

The transient studies have shown that the liner temperature of the optimized conceptual design will exceed 3500°F for 40-50 sec during the climb transient, peaking at 3800-3900°F. Generally, the heat pipe vapor temperature at which the discharge of lithium vapor is initiated (2600°F) is reached shortly after the start of the steady-state cruise phase. The liner temperature approaches the steady-state values of 3350-3400°F around 15 sec after the start of steady-state cruise.

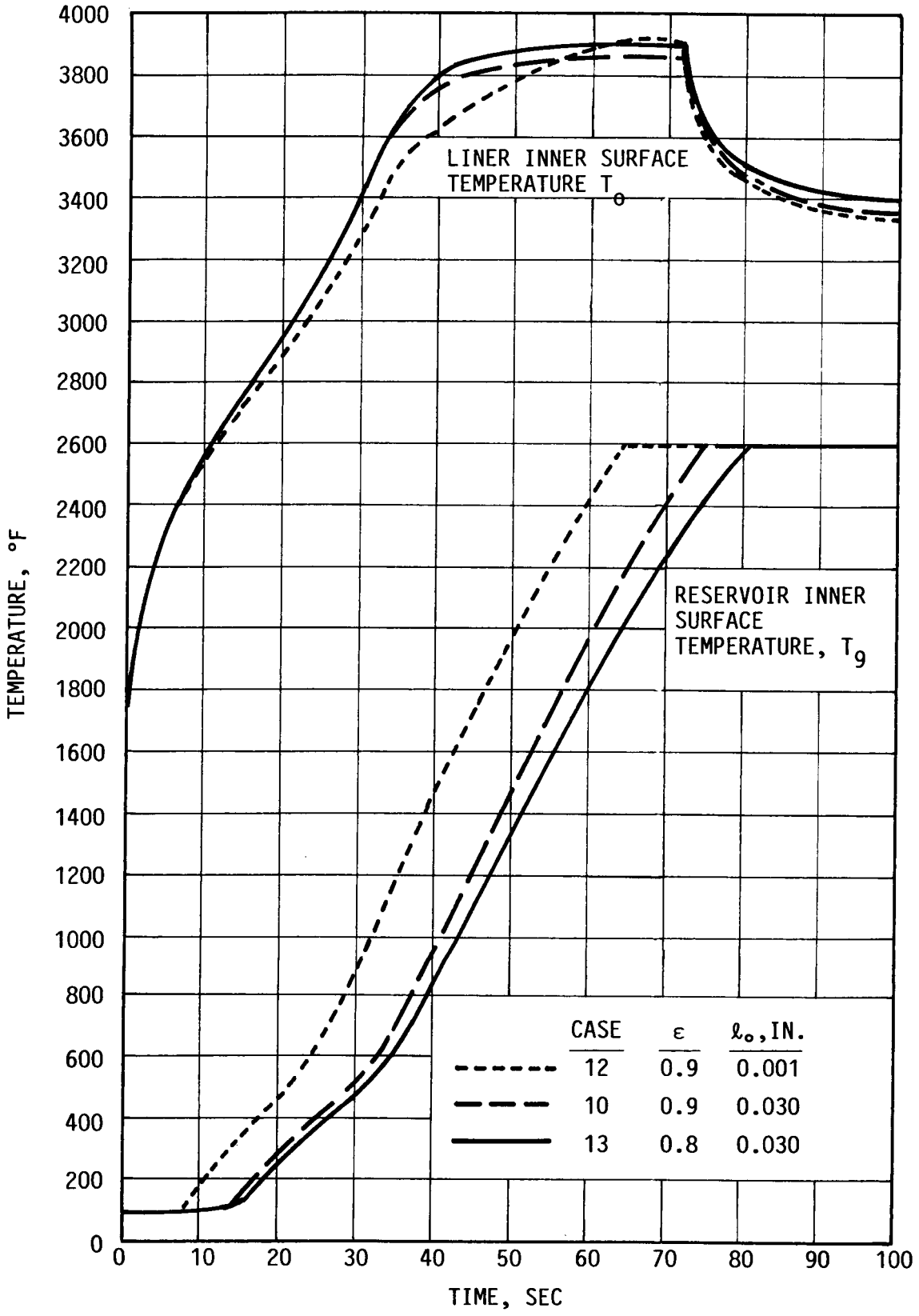

Figure 41. Temperature Histories for Cases 10, 11, and 12

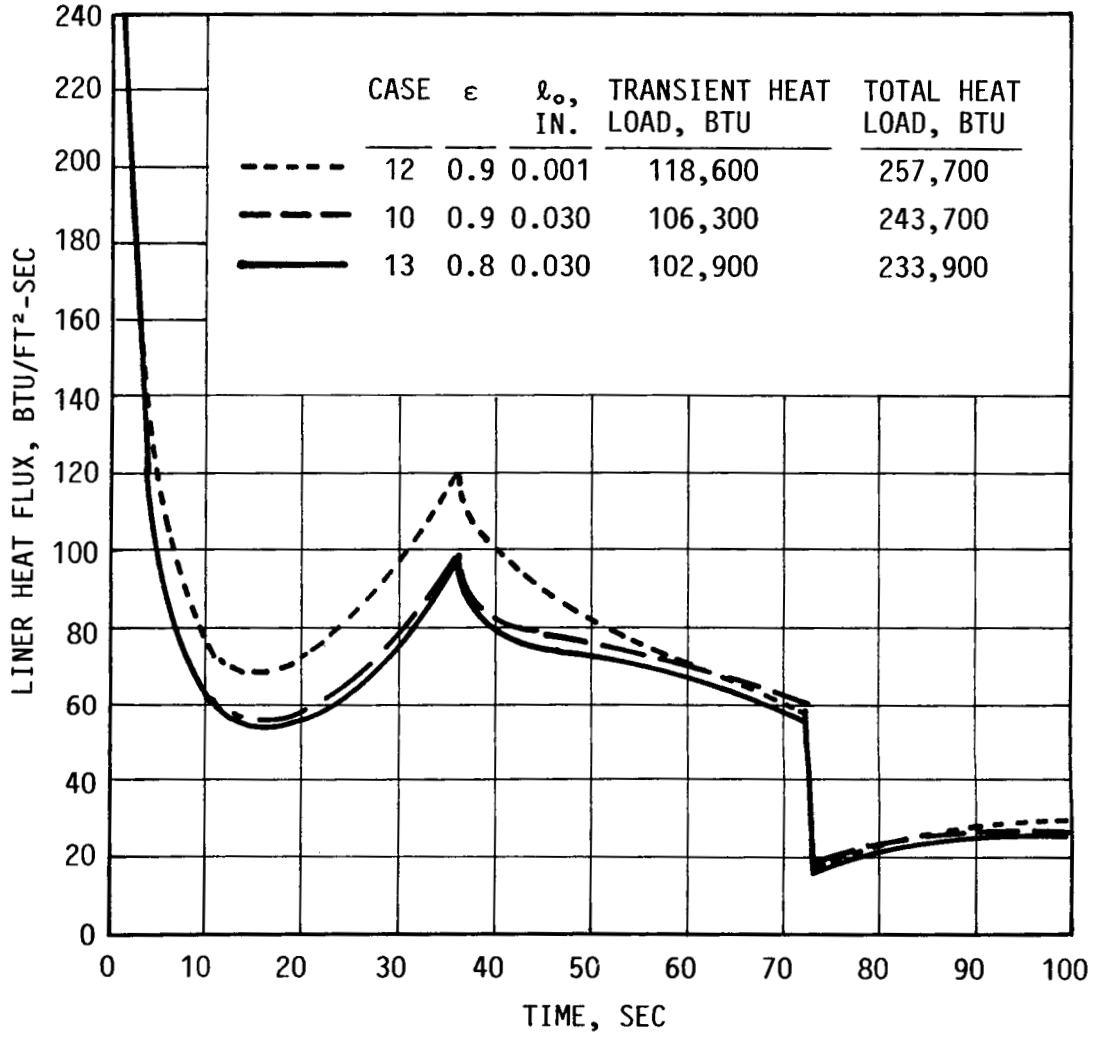

Figure 42. Liner Heat Flux Histories for Cases 10, 11, and 12

These results are based on the engine climb trajectory given in Appendix A, and can be expected to be modified for other trajectories.

If the liner and heat pipe/reservoir can be maintained in contact during flight, the peak liner temperature can be reduced to 3550°F with a lithium discharge time of 74 sec. However, a 70% increase in reservoir width is needed to achieve this temperature reduction. The steady-state liner temperature for this situation approaches 3100°F.

ASSESSMENT OF CONCEPT POTENTIAL

INTRODUCTION

At hypersonic cruise speeds on the order of Mach 6, the temperature of scramjet combustor liners can exceed 4000°F. Even higher liner temperatures are probable during the transient climb phase. Because of its excellent high temperature strength properties, coated carbon-carbon has been considered for use as the liner structural member. However, the upper temperature limit on available oxidation-resistant coatings is about 3000°F. Efforts are currently under way to extend the usable temperature range to 3500-3700°F. The present design approach is to use coated carbon-carbon of sufficient thickness to allow for ablation during flight.

An alternate approach to liner design is to cool the liner to a temperature at which coated carbon-carbon will survive without significant ablation. Cooling with liquid metal heat pipes has been considered for this purpose because there is then no need for external pumps or power. Additionally, liquid metal heat pipes operate at moderate vapor pressures while at elevated temperature, and have the capability to transport heat at high rates.

Initial studies for the Naval Surface Weapons Center indicated that a liner heat pipe cooling system should operate in the temperature range 2200-3000°F. In this temperature range, lithium is a superior heat pipe fluid, and also exhibits superior heat sink characterisics by virtue of its high specific heat and latent heat of vaporization. Lithium was therefore selected as both the heat pipe and heat sink fluid. TZM molybdenum was then selected as the cooling system construction material because of its compatiblity with lithium, good high temperature strength, and substantially higher thermal conductivity than other refractory alloys. On surfaces exposed to the air, the TZM is protected by an oxidation-resistant silicide coating.

CANDIDATE COOLING CONCEPTS

Five candidate heat pipe cooling concepts for scramjet combuster liners were considered, based on results of the earlier NSWC studies. One concept utilizes the TZM surface of the cooling system itself as the liner. In the other four concepts, the cooling system surrounds and cools a carbon-carbon liner. Heat is dissipated from the cooling system by one or more of the following techniques: an increase in temperature of heat-absorbing components, vaporization and discharge of the lithium heat pipe fluid, radiation from the external engine surface to the environment.

The four cooled carbon-carbon liner concepts were found to be substantially lighter, with less volume, than the combined liner-cooling system concept. Each of the four cooled liner concepts relies on the sensible thermal capacity of the cooling system and adjacent structure to absorb the transient liner heat load generated during the climb phase. The steady-state heat load generated during the cruise phase is dissipated by radiation from the engine surface in one case, and by the vaporization and discharge of lithium in the other three cases.

Both the surface radiator and lithium discharge approaches to steady-state heat dissipation are feasible. Heat dissipated from a surface radiator requires that the heat pipe extend from the cooled liner to the external surface. Heat dissipated by lithium discharge requires only that the heat pipe surround the liner, with connecting nozzles to direct the vaporized lithium to external or internal surface discharge points.

For missions of several minutes duration, such as have been considered here, heat dissipation by lithium vaporization and discharge requires less volume than the surface radiation mode. This fact, plus the more complex configuration for radiative heat dissipation, lead to selection of the lithium discharge mode. It is estimated that vaporization and discharge of lithium could be the preferable heat dissipation mode for flight times up to 10-20 minutes in length.

For longer missions, the need to accommodate increasing quantities of lithium will eventually cause the weight and volume for the lithium discharge mode to exceed that for the surface radiation mode, whose weight and volume are invariant with flight time. At that point, surface radiation may well become the preferable heat dissipation mode despite its greater complexity and impact on engine design. Heat dissipation by surface radiation may also be the preferable mode for missions which call for reusable equipment capability.

The three cooled carbon-carbon liner concepts utilizing the vaporization and discharge of lithium for dissipation of the steady-state heat load differ in the details of construction of the heat pipe/reservoir shell which surrounds the liner. In the first concept, a conventional heat pipe structure adjacent to the liner transfers heat into a separate but contiguous lithium reservoir which is connected to the lithium vapor discharge nozzles. In the second concept, the heat pipe and reservoir are integrated into a single structure with a common vapor flow passage which connects to the discharge nozzles. In the third concept, the heat pipe wick and lithium reservoir are combined into a single entity along with a vapor flow passage connected to the discharge nozzles.

The latter two concepts, both of comparable weight and volume, were selected in preference to the separate heat

pipe/reservoir concept because of lower weight and volume and simpler fabrication potential. The integrated heat pipe/reservoir concept was selected over the even simpler combined wick/reservoir concept because of uncertainty over whether the transfer of heat across the relatively thick wick/reservoir of the latter concept could trigger destructive boiling during the climb transient.

CHARACTERISTICS OF SELECTED SYSTEM CONCEPT

The integrated heat pipe/reservoir concept which was selected was analyzed to find the optimum operating temperature, and then subjected to a transient analysis to determine is temperature history.

The optimum operating temperature, at which cooling system weight and volume are minimized, is about 2600°F. The associated temperature of the carbon-carbon liner during steady state operation is aboout 3400°F.

Radial air gaps separate the cooling system from the carbon-carbon liner on one side and from thermal insulation on the other. These air gaps are exposed to atmospheric pressure. Thus, there is no net pressure differential across the cooling system thickness. The carbon-carbon liner acts as the pressure vessel to contain gas pressure within the combustor.

The thickness of the cooling system between the inner radius of the carbon-carbon liner and the outer radius of the thermal insulation is 1.1 in., compared to a nominal thickness of 1.0 in. between the same components for the reference uncooled combustor. The increased volume of the heat-pipe-cooled system, if accommodated at the expense of fuel, would displace 15 lb of fuel. The total cooling system weight (not including the carbon-carbon liner) is 120 lb.

During the initial climb transient, the liner temperature peaks at between 3800°F and 3900°F, the exact values depending on such system characteristics as the surface emissivity on either side of the air gap between the liner and heat pipe, the initial air gap thickness, and the lithium reservoir thickness. The liner temperature remains above 3500°F for about 40 sec during the climb transient period of 72 sec.

The discharge of lithium vapor through the exhaust nozzles is initiated when the vapor temperature reaches 2600°F. This occurs between 65 and 99 sec after initiation of the climb transient, the precise time again dependent on the previously mentioned design characteristics. Climb trajectory modifications which result in lower liner heat fluxes, and design alternatives which permit the liner and cooling sytem to remain in contact, will be reflected in lower peak liner temperatures.

INTEGRABILITY AND FABRICABILITY

The heat pipe cooling system is heavier and occupies more volume than the uncooled liner and associated insulation of the reference system. The excess weight and volume must be balanced against the reduction in liner temperature and increased liner longevity made possible by introduction of the heat pipe cooling system.

Fabrication and installation of the liner/cooling system will be facilitated by the 0.032 in. gap between the liner and cooling system at room temperature. The four discharge nozzles extending between the heat pipe cooling shell surrounding the liner and the engine surface must be accommodated within the engine midsection. They occupy 6.7% of the vehicle circumference. The nozzles can be located at and secured to a radial bulkhead at the end of or between fuel tanks, with minimal disruption to engine structural design. To insure that there is no net radial pressure on the heat pipe cooling shell, small-diameter bleed tubes will connect the air gaps on either side of the shell to the atmosphere at the vehicle surface.

It appears that the heat pipe cooling system can be integrated with the engine structure with minimal impact on overall engine design.

The heat pipe cooling system includes three major subsystems: the heat pipe/reservoir shell, the vapor plenum, and the discharge nozzles.

The heat pipe/reservoir shell consists of a slightly conical double shell of TZM molybdenum which surrounds the carbon-carbon liner. It can be fabricated as a flat sandwich structure which would be rolled to the desired conical shape, and then welded together along adjacent longitudinal edges.

The sandwich structure can be sealed shut at one end of the cone by welding on an annular TZM sheet. The ring-shaped TZM plenum would be welded to the other end of the cone, with provision for the vapor space in the sandwich shell to open freely into the plenum. The wick structure extends over the interior walls of the plenum to assure that the vapor within the plenum is in equilibrium with the liquid lithium. The sealed structure would be evacuated and loaded with lithium through a separate fill tube, to be welded shut after loading. The four discharge nozzles, including the rupture plates, would then be welded in place. The bleed tubes which extend between the two air gaps and the external surface would be welded to each side of the cooling system. Thermal insulation around the heat pipe/reservoir and the discharge nozzles would be added after installation.

The system can be installed by sliding it over the carbon-carbon liner. Axial aligning lugs on the plenum would fit into holes in a carbon-carbon plate at the aft end of the combustor section. A front carbon-carbon closure plate with aligning holes would then be added at the front of the system, the holes slipping over lugs on the front end of the system. The discharge nozzles would be secured by TZM mounting brackets to a midsection bulkhead of the engine.

RELIABILITY AND SURVIVABILITY

Prior to operation, the lithium in the combustor liner cooling system will be in solid form, and the vapor space will be under high vacuum. If all the welds are sound, the system should remain in this condition for an indefinite period prior to use.

During operation, the system will activate automatically as heat incident on the combustor liner penetrates into the cooling system. The system is designed to function normally under the stresses and accelerations encountered during flight.

If a small leak should develop in the system during flight, the lithium leaking out will act to lower system pressure and temperature. Since all of the cooling channels are connected through the plenum, the effect of a leak in one channel will be shared by all. The system should then continue to function adequately, at a somewhat lower pressure and temperature than normal.

If the leak develops during the climb transient, the resulting premature discharge of lithium will reduce the operating time during which cooling is effective. If the leak develops during the steady-state cruise period, little or no change in operating time would be expected because the system is designed to discharge lithium during this period. The leakage rate through the discharge nozzles would then tend to be lower because of the reduced system pressure resulting from the leak, offsetting the additional discharge path created by the leak.

The combustor cooling system is thus expected to be highly reliable and survivable under expected flight conditions, even if minor leaks should develop.

The system should be designed so that all the lithium is contained within the wick and reservoir structure at the discharge temperature. If excess lithium were present, it would accumulate in the vapor space and, upon opening of the discharge nozzles, would be rapidly dissipated into the atmosphere. While this occurrence is probably tolerable, the excess liquid lithium represents an unnecessary weight penalty and the waste of a valuable heat sink.

The cooling system has been designed to avoid the accumulation of excess lithium by charging the system with enough to just fill all the wick and reservoir pores at the discharge temperature of 2600°F. At lower temperatures, the higher density of the liquid lithium will cause it to occupy less than the available volume in the wick/reservoir.

During the early part of the climb transient, before the temperature of the liquid lithium has increased substantially, the liquid-vapor interface will be within the coarse-pored sections of the heat pipe and reservoir wicks. In these sections, the maximum available capillary pressure is less than the pressure drop produced in the liquid lithium by the vehicle acceleration. Therefore, the liquid will be forced toward the rear while the interface moves into the fine-pored section of the wicks, where sufficient capillary pressure will be generated to balance the acceleration pressure drop. The net result is that during the initial part of the climb transient, the liquid column will occupy less than the full wick/reservoir length.

This situation can be avoided by increasing the thickness of the fine-pored section to about 30% of the total thickness. The liquid-vapor interface will then lie within the fine-pored section of the wick during the initial transient, and capillary pressure will be sufficient to withstand the pressure drop due to vehicle acceleration over the full liquid column length. The required thickness increase can be accomplished in the wick by doubling the thickness of the fine-pored layer to 0.020 in.

This solution could also be applied to the reservoir, but would result in a 30 lb weight penalty. In lieu of this reservoir design change, the liquid column in the reservoir will grow longer as the lithium temperature increases, finally occupying the full reservoir length.

The effect of a shorter liquid lithium column in the reservoir on system temperature during the transient is expected to be minimal. Vapor evaporating from the wick surface which would ordinarily condense in the now empty reservoir section will simply flow to where the liquid heat sink is now located and condense there. Somewhat higher system temperatures may then be expected, due to the higher heat flux incident on the reduced reservoir heat transfer area.

If experimental investigation of cooling system behavior during the startup transient results in higher than expected peak temperatures, the alternative approach of redesigning the reservoir wick structure with a thicker fine-pored layer would then be considered.

SAFETY

Since the lithium contained in the cooling system is in solid form until the melting point of 367°F has been reached, and the internal vapor pressure is less than atmospheric pressure until the temperature has exceeded 2400°F, the system poses no safety risks during normal handling and storage at ambient temperature. Accidental penetration of the system, resulting in the inflow of air, could produce some oxidation or nitriding of the solid lithium. The influx of water could trigger a more vigorous reaction, and should be avoided.

During flight, the accidental release of lithium could trigger reactions with the air in the adjacent air gaps. A leak would produce some lithium oxide and lithium nitride smoke, with little other effect expected. However, the effect of lithium and these compounds on carbon-carbon, thermal insulation, and other adjacent materials should be explored further. A massive release of lithium could generate a significant quantity of heat through reactions with oxygen and nitrogen, but because the total charge of lithium is only about 15 lb, the total energy release would be small compared to the energy-generating potential of the engine fuel.

COST

The cost of a cooled carbon-carbon liner can be expected to be lower than that of an uncooled liner, because of less stringent operating temperatures and minimal or negligible ablation. However, the cost of the heat pipe/reservoir cooling system must now be added. Fabrication procedures for the cooling system will be complicated by the need to work with TZM molybdenum, an oxidation-prone material at elevated temperatures. Nonetheless, these procedures are considerably less complex than the tedious and time-consuming methods used to fabricate carbon-carbon structural members.

Overall, the cost of a cooled carbon-carbon liner plus the cooling system may exceed that of an uncooled liner. The extra cost would be buying a lower temperature, more durable liner with increased resistance to the combustion gas environment.

RELATION OF COOLING SYSTEM REQUIREMENTS TO CURRENT STATE-OF-ART

Unique Aspects of Operation

The combustor liner cooling system utilizes the same principles of capillary pumping as are used in heat pipes, but incorporates a number of unique features not found in typical heat pipe cooling systems.

The internal construction itself is unique, with a lithium heat sink reservoir situated across the lithium vapor space from the normal heat pipe wick. Two distinct modes of operation are involved.

In Mode A, which exists during the climb transient, heat is transferred radially across the vapor space gap from the wick to the reservoir by evaporation and condensation of the lithium heat transport fluid. The lithium condensate returns from the reservoir to the wick via fine-pored screening on the surface of the radial ribs. Vapor and liquid flow are thus restricted to the radial direction, with flow path lengths of fractions of an inch. In addition, a static liquid head develops in the axial direction as a combined result of vehicle acceleration and gravity, which manifests itself as a substantial liquid pressure drop in the axial direction.

Mode B occurs during steady-state cruise, after the discharge of lithium vapor has started. Vapor which evaporates from the wick now flows axially along the vapor space passage, and then radially through the discharge nozzles to the atmosphere. Liquid lost from the wick by evaporation is replenished by the radial flow of liquid from the reservoir, along the screened ribs. When the reservoir has been depleted, continuing evaporation results in the eventual depletion of liquid lithium from the wick. In Mode B, there is no axial liquid pressure drop, since there is no acceleration.

Heat Transport Limits

Proper operation of the cooling system during both the climb transient (Mode A) and steady-state cruise (Mode B) requires that heat transport rates not exceed limits due to boiling, entrainment, and loss of capillary pumping. The radial heat flux into the cooling system, once the liquid in the wick has melted, varies from a peak of about 100 Btu/ft^2-sec during Mode A to around 26 Btu/ft^2-sec during Mode B. These heat fluxes are well below levels at which lithium heat pipes have successfully operated without the inception of boiling. Entrainment during Modes A and B can be avoided by using wick pore sizes below 200 microns, a requirement readily met with 200-mesh screening.

During Mode A, capillary pumping requirements are established by the axial liquid pressure drop due to vehicle acceleration and gravity. Capillary pressure corresponding to a wick pore size under 40 microns is needed to balance this pressure drop. Pore diameters of 19 microns have been achieved by drawing down multilayers of 400-mesh screening, and even smaller pore sizes are available in specially-woven screens.

Material Compatibility Considerations

During cooling system operation, liquid lithium must be compatible with the TZM containment and wick structures for a period of perhaps 10 minutes at peak temperatures of around 2625°F. Lithium-TZM heat pipe operation has been demonstrated for thousands of hours at 2700°F. Therefore, lithium-TZM compatibility requirements for the cooling system are well within demonstrated capabilities.

The external TZM surfaces of the cooling system are exposed to air in the adjacent gaps, and hence require a protective coating against oxidation. The molybdenum-disilicide-based W-3 coating should adequately meet cooling system requirements, since this coating has protected TZM against oxidation for over 50 hours at 2597°F (14).

The heat pipe cooling system has been designed to maintain the temperature of the carbon-carbon combustor liner at 3350-3400°F during steady-state cruise. During the climb transient, the liner temperature exceeds 3500°F for 45-50 seconds, peaking at 3830-3900°F. Through the use of special designs which maintain contact between the liner and cooling system, peak liner temperatures may be reduced to 3550°F, and steady-state temperatures to 3100°F.

The current operational temperature limit of coated carbon-carbon is around 3000°F. Development programs now in progress indicate the potential for coated carbon-carbon operating times of several hours at 3500-3700°F. Realization of this potential will permit the development of carbon-carbon combustor linings which, in conjunction with heat pipe cooling, exhibit little or no recession during missions of the type which have been considered.

CONCLUSIONS

The heat pipe combustor liner cooling system which has been investigated limits steady-state liner temperatures to 3400°F or less, and peak transient temperatures to the 3800-3900°F range. More sophisticated designs in which the liner and cooling system remain in contact can reduce these temperatures by 300°F. This capability, in conjunction with the successful development of high-temperature coated carbon-carbon, will permit the design of combustor liners with little or no recession over mission lifetimes.

The alternative approach of designing uncooled liners results in liner temperatures well in excess of 4000°F over the entire mission lifetime, with substantial in-flight ablation of the liner.

The heat pipe cooling system is largely compatible with mission and engine design needs. The total weight, including the liner, is less than 150 pounds. Accommodation of the cooling system volume displaces about 15 pounds of fuel, compared to an uncooled system. The cooling system is largely confined to the radial space between the liner and fuel, with the exception of the radial discharge nozzles which extend to the engine surface.

Heat transport requirements of the cooling system, its configuration, fabricability, and compatibility of the TZM and lithium used in the system are consistent with current technology.

The principal uncertainty relates to the lack of operating experience with the integral lithium reservoir/heat pipe structure during the transient and steady-state phases of flight. Resolution of this uncertainty requires experimental demonstration of cooling concept feasibility.

RECOMMENDATIONS

Experimental Studies

It is recommended that an experiment be carried out to demonstrate the feasibility of the selected heat pipe combustor liner cooling concept. The test article would include a flat section of an integral heat pipe/reservoir connected to a single discharge nozzle. Initial tests could be conducted in a radiant heating facility, to be followed by testing in a high Mach number wind tunnel.

The heat pipe/reservoir fluid would not necessarily be lithium, or even a liquid metal. The critical aspect is to demonstrate that the temperature of an integral heat pipe/reservoir structure subjected to external heating can be controlled within specified limits. The control mechanism would initially be the heat absorption capability of the structure, followed by the controlled discharge of the heat pipe/reservoir vapor.

Alternate Cooling Concepts

Additional study of alternate candidate cooling concept C-4 is also recommended. Concept C-8, the preferred concept, incorporates the integral heat pipe/reservoir arrangement. Concept C-4 employs a simpler arrangement, consisting of a single combined lithium wick/reservoir and adjacent vapor space. It was not selected because of uncertainty over whether destructive boiling could occur in the relatively thick wick/reservoir during the climb transient. Transient studies of concept C-4 are recommended to resolve this uncertainty. If

boiling is not encountered, concept C-4 would represent an attractive alternative to the selected concept.

Studies of a segmented cooling system in which continuous contact is maintained with the liner are also recommended. This system has the potential to reduce peak and steady-state liner temperatures by another 300°F.

Study of the design option in which lithium is discharged directly into the combustion gas is also warranted. Potential benefits of this design approach include: improved engine integrability, and possible augmentation of engine performance from exothermic reactions of the discharged lithium with nitrogen and oxygen.

Finally, longer mission flight times will enhance the attractiveness of concept C-7, in which the steady-state heat load is dissipated by a surface radiator. Further studies of this concept for such missions is recommended.

PART II

HEAT PIPE COOLING FOR LEADING EDGE OF ENGINE INLET

INTRODUCTION

The air inlets of scramjet engines are required to have sharp leading edges in order to maximize compression of the inlet air. As a result, aerodynamic heat fluxes at the leading edge stagnation line may be on the order of hundreds of Btu/ft^2-sec. Stagnation line temperatures of uncooled leading edges may then reach several thousand °F.

Heat pipe cooling of wing leading edges of hypersonic aircraft has previously been considered for leading edge radii as small as 1/4 in. (6). The feasibility of heat pipe cooling for leading edges has also been demonstrated, in both radiant heating and wind tunnel tests (17). The purpose of the studies reported herein was to evaluate the feasibility of heat pipe cooling for small-radii leading edges characteristic of scramjet engine inlets.

DESIGN CONCEPT

The design concept which was investigated is shown in Figure 43. The leading edge was assumed to be configured as a two-dimensional wedge with a leading edge radius of 0.035 in. The outer surface of the wedge is parallel to the flight direction, and the inner surface inclines at an angle of 5 deg. The angle of attack was assumed to be zero.

The nose surface, the outer surface, and the inner surface of the leading edge are subjected to aerodynamic heating. At the same time, heat is being radiated away from these surfaces. The rear surface was assumed to be perfectly insulated. As the surface temperature increases, the aerodynamic heating rate decreases while the radiation heat transfer rate increases. At the radiation equilibrium temperature, the aerodynamic and radiation heating rates are equal, and net heat transfer to the surface is zero. For surface temperatures in excess of the radiation equilibrium temperature, surface radiation will exceed aerodynamic heating, and the surface then acts as a heat dissipator.

In the design concept under consideration here, heat absorbed on the nose and inner surfaces is transferred to the outer surface for dissipation. The outer surface was selected as the heat sink because the aerodynamic heating rate, and hence the radiation equilibrium temperature, is lowest there.

To facilitate heat transfer from the heat absorbing surfaces to the heat dissipation surface, the leading edge is fabricated as a heat pipe. The hollow interior is lined with a

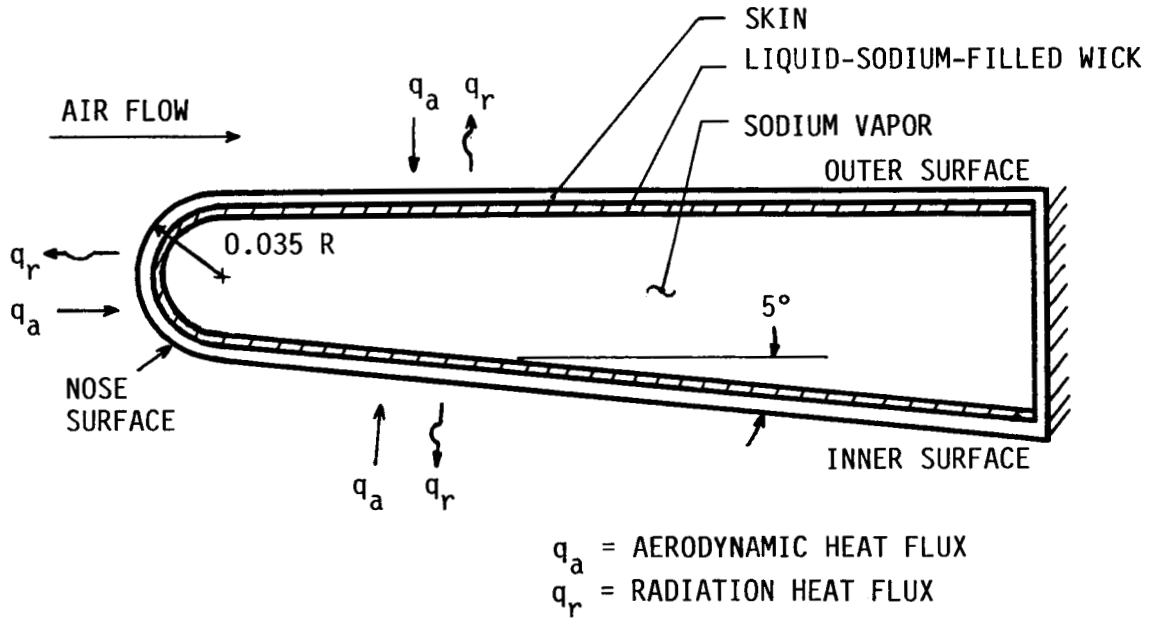

Figure 43. Design Concept for Heat-Pipe-Cooled Engine Inlet Leading Edge

porous wick. Liquid sodium fills the wick pores, and sodium vapor occupies the remaining internal volume.

Heat incident on the nose and inner surface is then transferred to the outer surface with minimal temperature drop by evaporation of liquid sodium from the wick on the nose and inner surfaces and the subsequent condensation of sodium vapor on the wick section which lines the outer surface. Sodium condensate returns through the wick by capillary action to the heat-absorbing surfaces.

AERODYNAMIC HEATING RATES

Aerodynamic heat fluxes were calculated at the stagnation line of the leading edge, and at points 2 in. aft of the leading edge on the inner and outer surfaces. The heat fluxes were obtained for the same trajectory conditions which were used in the combustor liner cooling studies of Part I, using the formula

$$q = h(H_r - H_w) \tag{28}$$

where q = aerodynamic heat flux, Btu/ft^2-sec

h = heat transfer coefficient, lb/ft^2-sec
H_r = recovery enthalpy, Btu/lb
H_w = wall enthalpy, Btu/lb

Data on h and H_r versus time were provided by the Langley Research Center. Wall enthalpy data corresponding to specific surface temperatures was obtained from air tables (18).

The stagnation line heat flux is shown as a function of mission time and surface temperature in Figure 44. Similar data are given in Figure 45 for the inner and outer surfaces. The plotted points in these figures represent the original calculated aerodynamic heating data. The curves are plots of equations which were fitted to the data. These equations are of the form

$$q = a + bt + ct^2 + (d + et + ft^2)(T_w + 460) \qquad (29)$$

where q = aerodynamic heat flux, Btu/ft^2-sec
t = elapsed time, sec
T_w = surface temperature, °F
a through f are curve-fitting coefficients

Values of the curve-fitting coefficients are given in Table 23.

The heat flux values at 180 sec were used as the steady-state values. The steady-state heat flux equations take the form

$$q = 540.7 - 0.176(T_w + 460) \; ; \quad \underline{\text{Stagnation Line}} \qquad (30)$$

$$q = 21.31 - 0.00759(T_w + 460) \; ; \quad \underline{\text{Inner Surf., 2 in. back}} \qquad (31)$$

$$q = 5.359 - 0.00198(T_w + 460) \; ; \quad \underline{\text{Outer Surf., 2 in. back}} \qquad (32)$$

STEADY-STATE DESIGN STUDIES

LEADING EDGE LENGTH

The leading edge length is equal to the length required for the heat absorbed at the nose and inner surfaces to be dissipated by radiation from the outer surface. The length decreases with an increase in surface temperature. It also

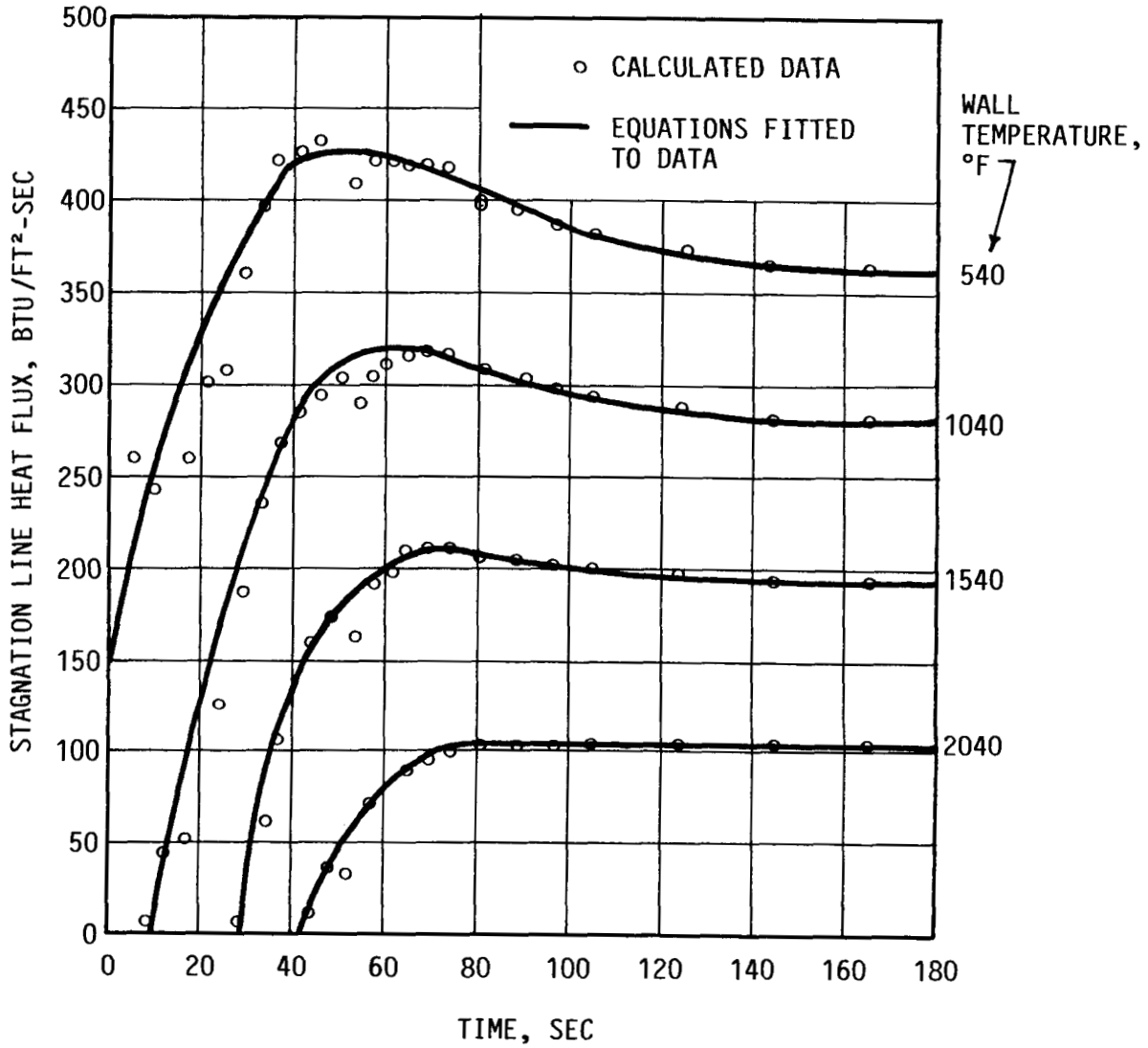

Figure 44. Aerodynamic Heat Flux at Stagnation Line of Engine Inlet Leading Edge

depends on the extent of radiative heat interchange between the leading edge surfaces and adjacent engine components. At a sufficiently high temperature, radiative heat transfer from the inner surface will exceed aerodynamic heating to that surface. The inner as well as the outer surface will then act as a dissipative heat sink for heat absorbed at the nose surface.

Radiant interchange with adjacent surfaces can be characterized by the radiant interchange factor, defined here as the ratio of the actual radiation heat transfer rate from a surface to the rate at which radiant energy is emitted from that surface.

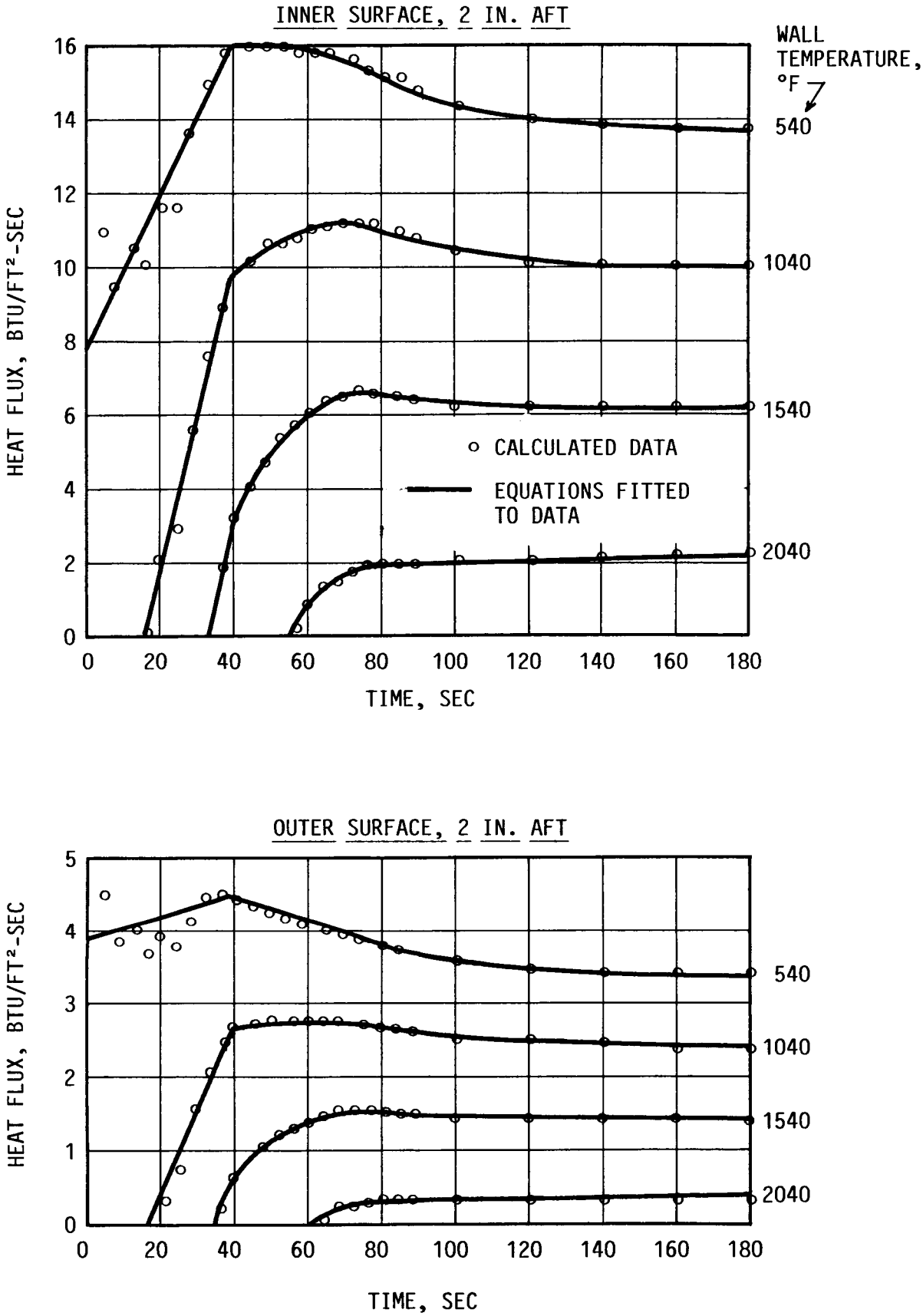

Figure 45. Aerodynamic Heat Flux on Inner and Outer Surfaces

Table 23. Coefficients for Aerodynamic Heat Flux Equations

Range *	a	b	$cx10^4$	$dx10^3$	$ex10^4$	$fx10^8$
Stagnation Line						
A	769.8	-1.179	-101.0	-600.7	108.0	-7267
B	787.7	-1.850	-45.0	-467.4	58.0	-3100
C	802.6	-3.149	94.1	-268.5	10.9	-320
Inner Surface, 2 In. Back						
A	36.86	-0.260	16.0	-29.9	5.25	-250
B	38.42	-0.292	14.25	-23.18	3.35	-195
C	32.05	-0.1293	3.87	-12.0	0.5117	-14.83
Outer Surface, 2 In. Back						
A	17.01	-0.3068	23.15	-12.82	2.99	-190
B	13.76	-0.1707	9.46	-8.216	1.423	-86.0
C	8.216	-0.0336	0.985	-3.215	0.1428	-4.117

* A: 0<sec<40 sec
* B: 40<sec<80 sec
* C: 80<sec<180 sec

The leading edge length was found from an energy balance in which the sum of the net heat transfer rates at the nose, inner, and outer surfaces is equal to zero. For each surface, the net heat transfer rate equals the difference between the aerodynamic heating rate and the radiation heat transfer rate. A positive value for the net heat transfer rate denotes that the surface is acting as a heat source, while a negative value denotes that the surface is acting as a heat sink.

From page 30, Reference 6, the net heat transfer rate at the nose surface can be expressed as

$$Q_n = \frac{RB}{72}\left[0.874q_s - 0.598\Omega_n\left(\frac{T_w + 460}{1000}\right)^4\right] \tag{33}$$

where T_w = wall temperature at stagnation line, °F
Ω_n = radiation interchange factor for nose surface
q_s = aerodyn. heat flux at stagnation line, Btu/ft^2-sec
R = nose radius, in.
B = leading edge span, in.
Q_n = net heating rate on nose surface, Btu/sec

In Equation (33), the temperature over the nose surface is assumed to be constant.

Performing the energy balance over the leading edge surfaces and using Equation (33), it may be shown that

$$L = \frac{144Q_n/B}{0.381(\Omega_o + \Omega_i)\left(\frac{T_w + 460}{1000}\right)^4 - (q_o + q_i)} \tag{34}$$

where L = leading edge length (less nose radius), in.
q_o = aerodyn. heat flux on outer surface, Btu/ft^2-sec
q_i = aerodyn. heat flux on inner surface, Btu/ft^2-sec
Ω_o = radiation interchange factor for outer surface
Ω_i = radiation interchange factor for inner surface

In Equations (33) and (34) the surface emissivity, with a value of 0.8, has been incorporated into the radiation terms. It was further assumed that all surfaces are at the same temperature T_w, ignoring temperature drops through the wall and wick at each surface. Because of the small net heat flux at the inner and outer surfaces, the temperature drops at these surfaces are small and may be ignored. The temperature drop at the stagnation line (as will be indicated shortly) is around 70°F. The effect of ignoring the higher temperature on the nose surface is to somewhat overestimate the length L for a specified surface temperature, or, for a specified length, to somewhat overestimate the surface temperatures.

Calculation of the leading edge length requires that the radiation interchange factors for each surface be specified. Insufficient information was available to determine these factors.

For calculational purposes, the following assumptions were made. The outer surface does not "see" any surrounding surfaces with which radiation can be interchanged, so that $\Omega_o = 1$. In Figure 46, the heat transfer rate to the nose surface per unit span length is shown as a function of wall temperature and the radiation interchange factor Ω_n. Since the heat transfer

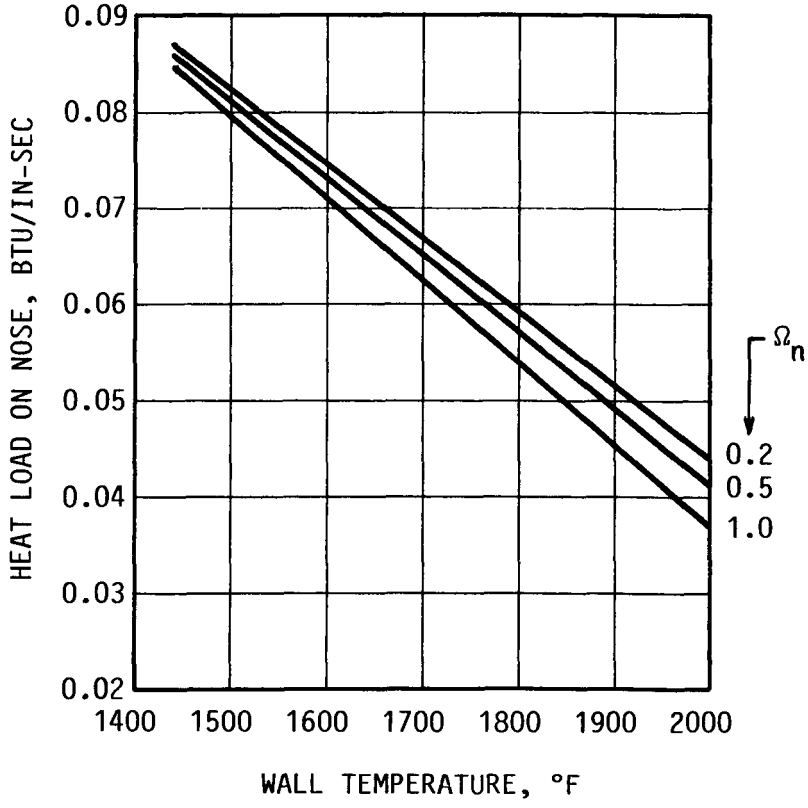

Figure 46. Heat Transfer Rate to Nose Per Unit Span Length

rate is relatively insensitive to Ω_n, Ω_n was also taken to be equal to 1. The radiant interchange factor Ω_i for the inner surface was allowed to vary parametrically in the calculation of the leading edge length.

In Figure 47, the leading edge length is shown as a function of wall temperature for various values of Ω_i. It is desirable to maintain the wall temperature at a level below 1750°F, at which superalloy construction of the leading edge is feasible. For design purposes, taking into account that the actual stagnation line temperature will exceed the indicated wall temperatures by the sum of the temperature drops through the wall and heat pipe wick, a wall temperature of 1650°F was selected, along with a value of 0.5 for Ω_i. The leading edge length (less the nose radius) is then 2.0 in.

MATERIALS SELECTION

At the steady-state design temperature level of 1650°F, superalloy construction appears to be feasible for the heat-pipe-cooled leading edge. On the basis of prior studies (6), the superalloy Haynes 25 was selected as the wall and wick fabrication material, and sodium as the heat pipe fluid.

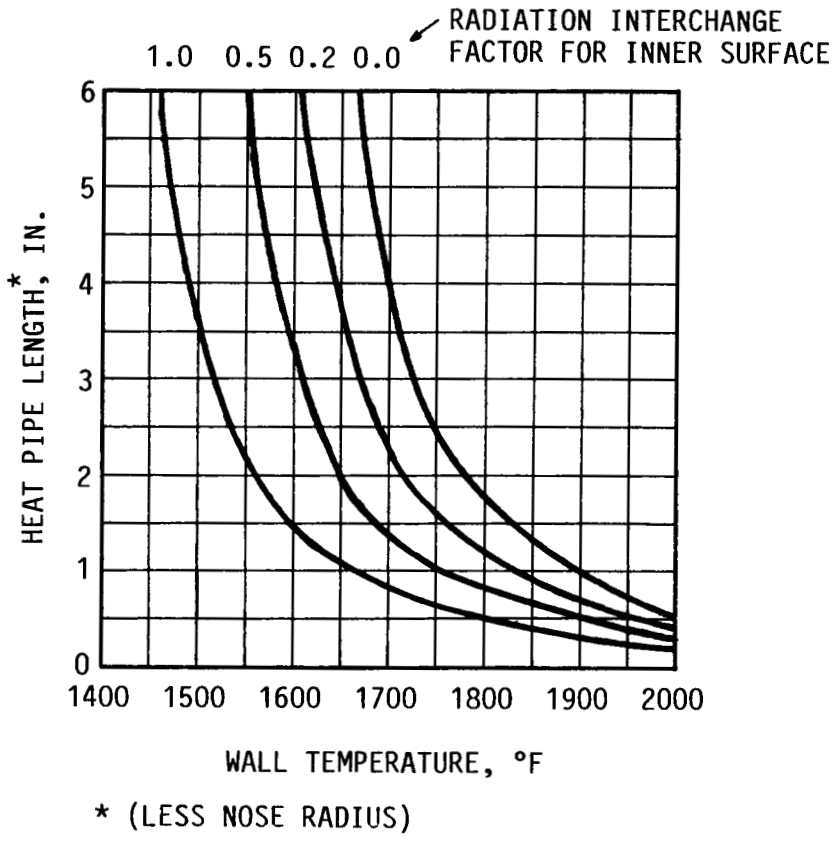

Figure 47. Heat Pipe Cooling System Length

Haynes 25 is expected to be chemically compatible with liquid sodium, and exhibits adequate strength and oxidation resistance at anticipated operating temperatures. Sodium possesses the desired combination of good resistance to boiling and moderate vapor pressure at these temperatures. In contrast, the low vapor pressure of lithium limits the practicality of its use here. Haynes 25 properties were obtained from Reference 6, and sodium properties from Reference 11.

TEMPERATURE DROP AT STAGNATION LINE

The temperature drop through the wall and wick at the stagnation line was calculated on the basis of one-dimensional cylindrical geometry, using the following equations.

$$\Delta T_{wall} = 300\left[q_s - 0.381\left(\frac{T_w + 460}{1000}\right)^4\right]\frac{R}{k_s}\ln\left(\frac{R}{R - t_s}\right) \qquad (35)$$

$$\Delta T_{wick} = 300\left[q_s - 0.381\left(\frac{T_w + 460}{1000}\right)^4\right]\frac{R}{k_w}\ln\left(\frac{R - t_s}{R - t_s - t_w}\right) \qquad (36)$$

$$k_w = \phi k_l + (1 - \phi)k_s \qquad (37)$$

where ΔT_{wall} = temperature drop through wall, °F
ΔT_{wick} = temperature drop through wick, °F
t_s = wall thickness, in.
t_w = wick thickness, in.
k_s = thermal conductivity Haynes 25, Btu/hr-ft-°F
k_l = thermal conductivity liq. sodium, Btu/hr-ft-°F
k_w = thermal conductivity of wick, Btu/hr-ft-°F
ϕ = wick porosity

The wall thickness was taken to be 0.010 in. The wick thickness was taken to be 0.011 in., consisting of two layers of 200-mesh screen adjacent to the wall and one layer of 400-mesh screen. The wick porosity was taken to be 0.651. T_w was taken to be the design temperature of 1650°F.

The temperature drops through the wall and wick at the stagnation line were found to be

$$T_{wall} = 36.7°F$$

$$T_{wick} = 37.5°F$$

Adding the sum of these temperature drops to the design temperature of 1650°F gives a wall temperature at the stagnation line of 1724°F.

OXIDATION

The oxidation rate of Haynes 25 is 0.4 mil/1000 hr at 1400°F, and 0.9 mil/1000 hr at 1600°F (6). At the stagnation line temperature of 1724°F, the oxidation rate was estimated to be on the order of 4 mil/1000 hr, or less than 0.001 mil over a 10 minute mission. Hence, oxidation of the heat-pipe-cooled leading edge is not expected to be a problem.

THERMAL STRESS

The thermal stress in the wall at the stagnation line is a maximum at the inner radius, and was calculated from the formula (19)

$$\sigma_t = \frac{E\alpha\Delta T_{wall}}{2(1 - \nu)}\left(1 + \frac{b - a}{3a}\right) \qquad (38)$$

where σ_t = thermal stress, psi
E = elastic modulus, psi
α = coefficient of expansion, in./in.-°F
ν = Poisson's ratio = 0.3
b = outer radius of nose wall = 0.035 in.

a = inner radius of nose wall = 0.025 in.

For Haynes 25, Equation (38) yields a thermal stress of 4510 psi. This figure may be compared with an estimated yield strength of 10,000 psi, and an estimated ultimate strength of 30,000 psi, for Haynes 25 at 1800°F.

BUCKLING PRESSURE

The pressure needed to buckle the nose section of the leading edge was calculated from Equation (16) of Reference 6.

$$\Delta P_b = \frac{E}{4(1 - \nu^2)}\left(\frac{t_s}{\bar{r}}\right)^3 \frac{1}{14.7} \tag{39}$$

where ΔP_b = buckling pressure, atm
t_s = wall thickness, in.
$\bar{r}$ = mean wall radius, in.

From Equation (39), a pressure differential of 11,400 atm would be required to buckle the nose section, a figure far above anticipated stagnation pressures.

BENDING STRESS

At 1650°F, the vapor pressure of sodium is 17.2 psi. Since the air pressure surrounding the leading edge is almost zero at operational altitudes, a pressure differential of around 17 psi will exist across the leading edge wall. This pressure differential will produce bending stress in the wall, of magnitude given by Equation (19) of Reference 6.

$$\sigma_b = \left(\frac{W_v + t_s}{t_s}\right)^2 \frac{\Delta P}{2} \tag{40}$$

where σ_b = bending stress, psi
ΔP = pressure differential across wall, psi
t_s = thickness of wall & chordwise supporting ribs, in.
W_v = spanwise spacing between supporting ribs, in.

Letting ΔP = 17.2 psi, t_s = 0.010 in., and W_v = 0.19 in., the bending stress from Equation (40) is 3440 psi. The combined bending and thermal stress is 7950 psi, well below the yield and ultimate stress figures previously given for Haynes 25 at 1800°F.

Therefore, chordwise ribs 0.010-in.-thick and spaced 0.19 in. apart were included in the leading edge design.

HEAT TRANSPORT LIMITS

Sonic, entrainment, boiling, and capillary pumping heat transport limits were calculated and compared to actual heat transport rates and/or related parameters. The calculations were performed on the basis of methods presented in References 6, 12, and 13.

It was assumed that sodium vapor generated at the nose section of the leading edge condenses at the same rate on the outer surface, and that the chordwise flow of vapor from the nose section is relatively unaffected by the flow of vapor between the inner and outer sections. Axial heat fluxes corresponding to the vapor space area at the nose section exit were used in the calculations.

The liquid sodium condensate flows chordwise through the wick along the outer surface toward the nose, along the nose surface, and then along the inner surface toward the rear of the leading edge. Determination of the capillary pumping limit required evaluating the capillary pressures (equal to the difference between the vapor and liquid pressures) at each end of the leading edge, and then selecting the larger value.

The sonic and entrainment limits were represented as axial heat fluxes (heat transfer rate per unit vapor space area), and compared to the actual axial heat flux. The boiling limit was presented as the surface heat flux at the wall/wick interface at which boiling is initiated, and compared to the actual net heat flux at the wall/wick interface. The capillary pumping limit was presented in terms of the diameter of curvature at the liquid-vapor interface needed to produce the required capillary pressure, and compared with the actual effective diameter of the wick pores.

The actual wick pore radius at the liquid-vapor interface was taken to be 20 micron, which is characteristic of 400-mesh screening. The flow passage section of the wick consisted of two layers of 200-mesh screen. The boiling limit was calculated for a nucleation site radius of 3 micron, and a conservatively small radius of curvature of 20 micron.

Results of the heat transport limit calculations are given in Table 24. It is evident that heat transport limits are not encountered within the heat-pipe-cooled leading edge under steady-state conditions.

CONCEPTUAL DESIGN

The conceptual design of the heat-pipe-cooled leading edge is shown in Figure 48. The nose radius is 0.035 in., and the overall chordwise length is somewhat more than 2 in. The leading edge is fabricated from Haynes 25, and sodium is the

Table 24. Heat Transport Limits for Leading Edge	
	Axial Heat Flux, Btu/in²-sec
At Sonic Limit	237.1
At Entrainment Limit	79.0
Actual	2.51
	Surface Heat Flux, Btu/ft²-sec
At Boiling Limit	580.5
Actual	226.4
	Radius of Curvature, micron
At Capillary Pumping Limit	584.5
Wick Pore Radius	20.0

heat pipe fluid. The wall thickness is 0.010 in., the wick thickness is 0.011 in., the end plate thickness is 0.030 in., and the rib thickness is 0.010 in. The ribs are spaced 0.19 in. apart. The wick is fabricated from two layers of 200-mesh screen and one layer of 400-mesh screen.

The weight of the leading edge conceptual design is 0.32 lb/ft of span length, and 1.86 lb/ft^2 of planform area.

TRANSIENT STUDIES

Studies were conducted to establish 1) the temperature history of the leading edge, and 2) its heat transport capability, during the transient phase of flight.

TEMPERATURE HISTORY

Analytical Model

Key features of the analytical model used to predict the temperature history of the leading edge are shown in Figure 49.

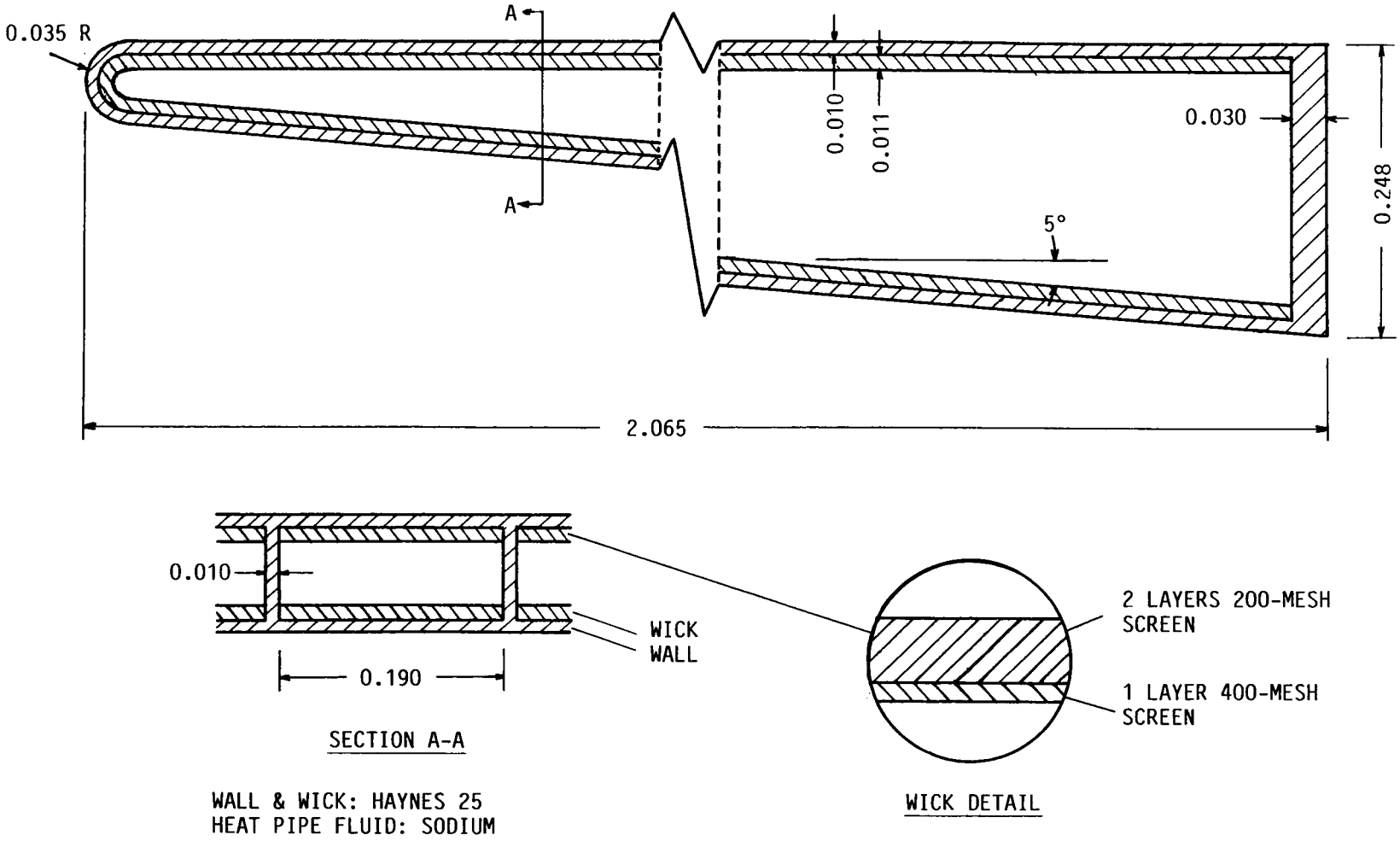

Figure 48. Conceptual Design of Heat-Pipe-Cooled Engine Inlet Leading Edge

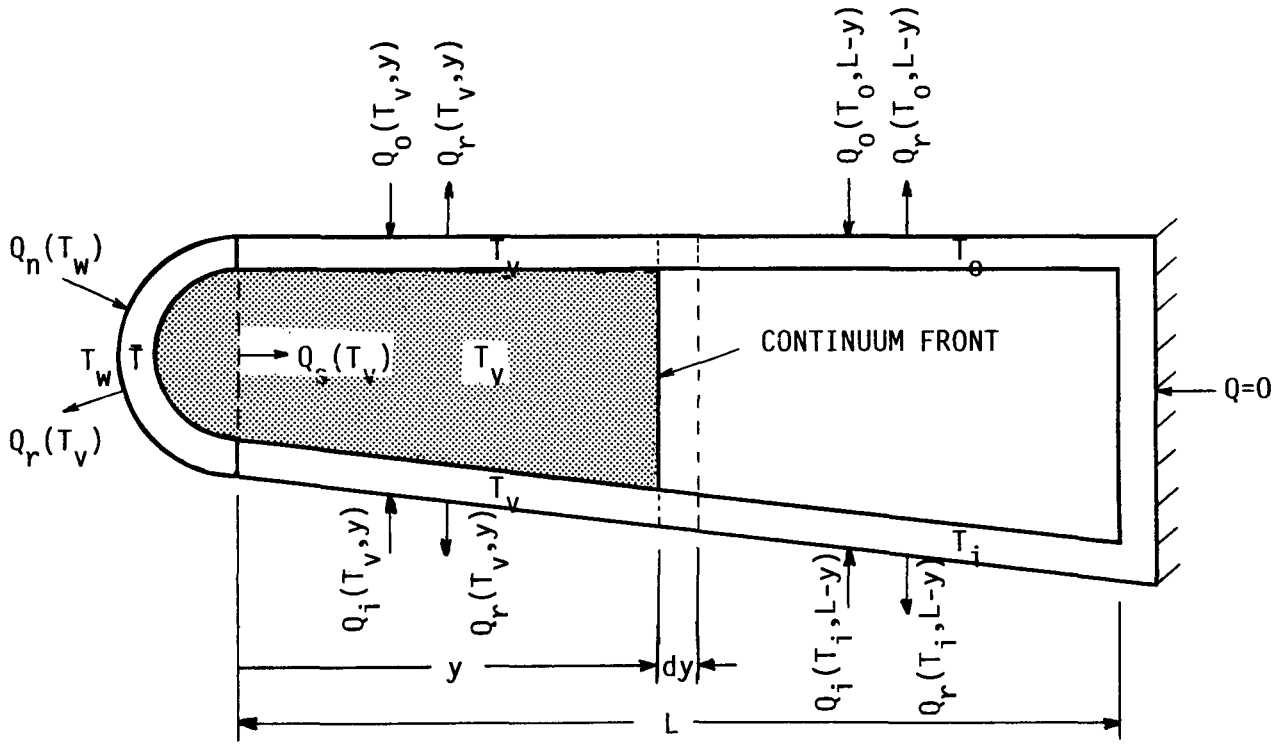

Figure 49. Analytical Model for Study of Leading Edge Temperature History

The wall and wick are homogenized into a single structure, whose temperature-dependent thermal properties are found by weighting the property of each component by its volume fraction. Net surface heating rates (aerodynamic heating minus radiation) at the nose, inner, and outer surfaces are time- and temperature-dependent.

The nose section is characterized by a mean temperature. Surface and vapor temperatures at the stagnation line are estimated by adding to and subtracting from the mean temperature 1/2 the steady-state temperature drop through the wall and wick.

Three distinct phases occur during the temperature transient.

In Phase 1, the sodium vapor density is not high enough to sustain continuum flow, and internal heat transfer by vaporization and condensation of the sodium is negligible. Each leading edge segment-the nose, the inner surface, and the outer surface-is heated independently, at a rate determined by its net surface heating rate and thermal capacity. The thermal capacity of the nose portion of the ribs is allocated to the nose section, while the remaining rib thermal capacity is divided equally between the inner and outer surface sections.

In Phase 2, the sodium vapor density is high enough to sustain continuum flow, and a hot continuum vapor front moves into the leading edge interior as shown in Figure 49. The net heating rate of the nose section is now equal to the net surface heating rate less the rate of heat removal by evaporating sodium, which occurs at the sonic limit. The temperature behind the continuum front is taken to be uniform and equal to the the sodium vapor temperature. Heat enters the continuum region from the nose section at the sonic limit. Depending on the continuum temperature, heat is also added to or lost from the continuum region via the portion of the inner and outer surfaces which lie within the region.

Heat absorbed within the continuum region during a time increment dt raises the temperature over length y by dT_v, and extends the continuum region by the length increment dy. Ahead of the continuum front, the inner and outer surface temperatures continue to increase by the same mechanisms as in Phase 1.

In Phase 3, the continuum region occupies the entire length of the leading edge, and the entire region is at the sodium vapor temperature. Now, the net heat input rate from the nose, inner, and outer surfaces is equal to the rate of heat absorption in the entire leading edge structure. In Phase 3 only, the thermal capacity of the end plate is added to the total thermal capacity.

The equations which govern the temperature history of the leading edge according to the analytical model which has been described are listed below.

Criterion for Continuum Flow

The onset of continuum flow, signifying the start of Phase 2, was estimated to occur when the mean free path in sodium vapor is 0.01 times the vapor space dimension at the nose section exit. The relationship between the mean free path and vapor properties is given by Equation (36) of Reference 6. Using the perfect gas equation to represent the vapor density and setting the mean free path equal to $0.01D_v$, the following equation can be derived.

$$T_c = 2479M\left(\frac{D_v P_c}{\mu_v}\right)^2 - 460 \qquad (41)$$

where D_v = minimum vapor space dimension, in.
μ_v = vapor viscosity, lb/hr-ft
M = molecular weight of vapor
T_c = vapor temperature at start of continuum flow, °F
P_c = vapor pressure at T_c, psi

For a given D_v, Equation (41) defines a relationship between T_c and P_c. These parameters also satisfy the vapor pressure equation

$$\log_{10} P_c = C - \frac{D}{T_c + 460} \tag{42}$$

where C and D are constants specific to the vapor under consideration (12).

Equations (41) and (42) constitute a set of simultaneous equations for T_c and P_c. These equations were solved for sodium vapor, using the following constants.

$$M = 23$$
$$C = 5.6883$$
$$D = 9396$$

The minimum vapor space dimension D_v was varied over the range 0.010 to 0.060 in. Results of the calculations were correlated by the equation

$$T_c = 1258.1 - 10{,}099 D_v + 85{,}100 D_v^2 \tag{43}$$

Letting $D_v = 0.028$ in., the design value for the vapor space thickness at the nose section exit, $T_c = 1042°F$.

Equations for Stagnation Line Temperatures

Wall and vapor temperatures at the stagnation line were calculated from the following equations.

$$\Delta T = 300\left[q_s - 0.381\Omega_n\left(\frac{T_v + 460}{1000}\right)^4\right]\frac{R}{k_n}\ln\left(\frac{R}{R - t_s - t_w}\right) \tag{44}$$

$$T_w = \bar{T} + \Delta T/2 \tag{45}$$

$$T_v = \bar{T} - \Delta T/2 \tag{46}$$

where ΔT = temperature drop across wall and wick at stagnation line, °F
q_s = aerodynamic heat flux at stagnation line, Btu/ft^2-sec
T_v = vapor temperature, °F
T_w = surface temperature at stagnation line, °F

Ω_n = radiation interchange factor for nose surface = 1
R = nose radius, in.
t_s = wall thickness at stagnation line, in.
t_w = wick thickness at stagnation line, in.
k_n = mean thermal conductivity of nose section, Btu/hr-ft-°F
$\bar{T}$ = mean temperature of nose section, °F

The mean temperature $\bar{T}$ is found from the Phase 1, 2, and 3 equations. (See below.)

Equations for Phase 1 Temperatures

The temperatures of the nose, outer surface, and inner surface during Phase 1 were found from the following equations.

$$d\bar{T} = (Q_n/C_{tn})dt \tag{47}$$

$$dT_o = (Q_{oo}/C_{tw})dt \tag{48}$$

$$dT_i = (Q_{ii}/C_{tw})dt \tag{49}$$

where t = time, sec
$\bar{T}$ = mean temperature of nose, °F
T_o = temperature of outer section, °F
T_i = temperature of inner section, °F
Q_n = net heat load on nose surface, Btu/sec
Q_{oo} = net heat load on outer surface, Btu/sec
Q_{ii} = net heat load on inner surace, Btu/sec
C_{tn} = thermal capacity of nose section, Btu/°F
C_{tw} = thermal capacity of inner section, Btu/°F, and also
= thermal capacity of outer section, Btu/°F

Equations for Phase 2 Temperatures and Continuum Front Position

System temperatures and the location of the continuum front in Phase 2 were found from the following equations.

$$d\bar{T} = \left(\frac{Q_n - \xi A_v}{C_{tn}}\right)dt \tag{50}$$

$$dT_o = \frac{Q_{oo}(L - y)}{C_{tw}(L - y)}\,dt \tag{51}$$

$$dT_i = \frac{Q_{ii}(L - y)}{C_{tw}(L - y)}\,dt \tag{52}$$

$$dy = \frac{[\xi A_v L + (Q_{oo} + Q_{ii})y]dt - 2C_{tw}(y)L[\bar{T} - (T_w + T_v)/2]}{[2C_w(T_v) - C_w(T_o) - C_w(T_i)]} \quad (53)$$

where ξ = sonic limit, Btu/in^2-sec
A_v = vapor space area at nose section exit, in^2
L = length of outer and inner surface, in.
y = position of continuum front, in.
$C_{tw}(y)$ = thermal capacity of length y of inner section, Btu/°F, and also
= thermal capacity of length y of outer section, Btu/°F
$C_{tw}(L-y)$ = thermal capacity of length L-y of inner section, Btu/°F, and also
= thermal capacity of length L-y of outer section, Btu/°F
$C_w(T_v)$ = heat required to raise temperature of inner or outer surface from 90°F to T_v, Btu
$C_w(T_o)$ = heat required to raise temperature of outer surface from 90°F to T_o, Btu
$C_w(T_i)$ = heat required to raise temperature of inner surface from 90°F to T_i, Btu
$Q_{oo}(L-y)$ = net heat load over length L-y of outer surface, Btu/sec
$Q_{ii}(L-y)$ = net heat load over length L-y of inner surface, Btu/sec

Equations for Phase 3 Temperatures

The system temperatures in Phase 3 were calculated from the following equations.

$$\bar{T} = \frac{(Q_n + Q_{oo} + Q_{ii})dt + C_{tn}\bar{T} + C_{tw}(T_w + T_v)/2}{C_{tn} + C_{tw}} \quad (54)$$

$$T_o = T_i = T_v \quad (55)$$

In Equation (54), the thermal capacity C_{tw} is equal to the sum of the thermal capacities of the inner and outer sections, plus the thermal capacity of the end plate.

Results

The temperature history was calculated by converting the above equations to finite difference form and then marching out solutions for successive time increments Δt. Temperature histories were calculated for various values of the leading edge length L and the radiation interchange factor Ω_i for the

inner surface. The time increment used in the calculations was 0.004 sec for the first 100 sec, and 0.020 sec thereafter.

Figure 50 shows the transient characteristics of a 2-in.-long leading edge with an inner surface radiation interchange factor of 0.5. The peak stagnation line surface temperature and vapor temperature are 1715°F and 1655°F respectively, while the corresponding steady-state values are 1695°F and 1638°F. Thus, temperatures at the stagnation line peak at about 20°F above the steady-state values.

Phase 1 continues until the vapor temperature reaches 1040°F, when continuum flow is predicted to start. At this point the stagnation line surface temperature is about 1 1/2°F greater than the vapor temperature. The temperature of the inner surface has risen to 828°F, and that of the outer surface to 657°F.

Phase 2 commences at 10 sec and continues until 23 sec. During this time interval, the continuum front reaches the rear of the leading edge (y = 2 in.). The temperature behind the front is equal to the vapor temperature of around 1040°F. Ahead of the front, the temperature reaches 1051°F in the inner section, and 844°F in the outer section.

Phase 3 starts at 23 sec, and continues thereafter. The continuum front position remains constant at 2 in. from the nose section exit (i.e., at the end plate of the leading edge). Since the entire length of the inner and outer sections has now been traversed by the continuum front, the temperatures of these sections merge with that of the sodium vapor.

The peak and steady-state surface temperatures at the stagnation line are shown in Figure 51 as a function of L and Ω_i. For Ω_i = 0.5, the value used for design purposes, the peak temperature drops from 1715°F to 1652°F as L increases from 2 in. to 4 in. If Ω_i = 0.8, the peak temperature varies from 1670°F to 1604°F over the same range of L. Conversely, a smaller value of Ω_i yields higher peak and steady-state temperatures.

It appears that peak leading edge temperatures can be limited to 1700°F or less by utilizing heat pipe cooling with sodium as the heat pipe fluid. The leading edge length required to achieve this temperature goal is dependent on the extent of radiative interchange between the inner leading edge surface and its surroundings.

Since the temperature differential across the leading edge thickness is less than 1°F during Phase 1, thermal stress is negligible. The most critical thermal stress condition occurs during Phase 3 at about 80 sec, when the temperature difference is about 36°F and the leading edge temperature has peaked.

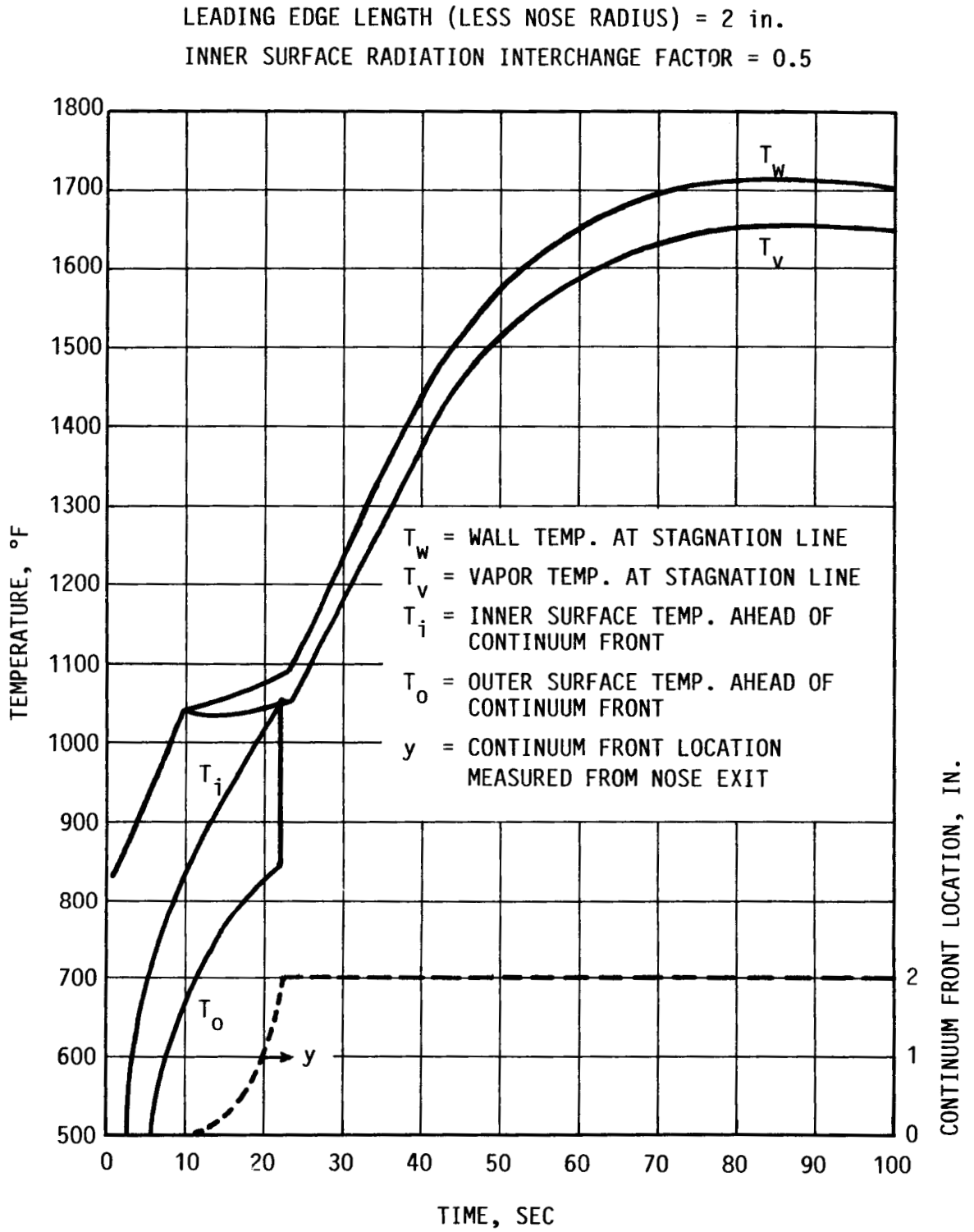

Figure 50. Transient Behavior of Heat Pipe Cooling System for Leading Edge

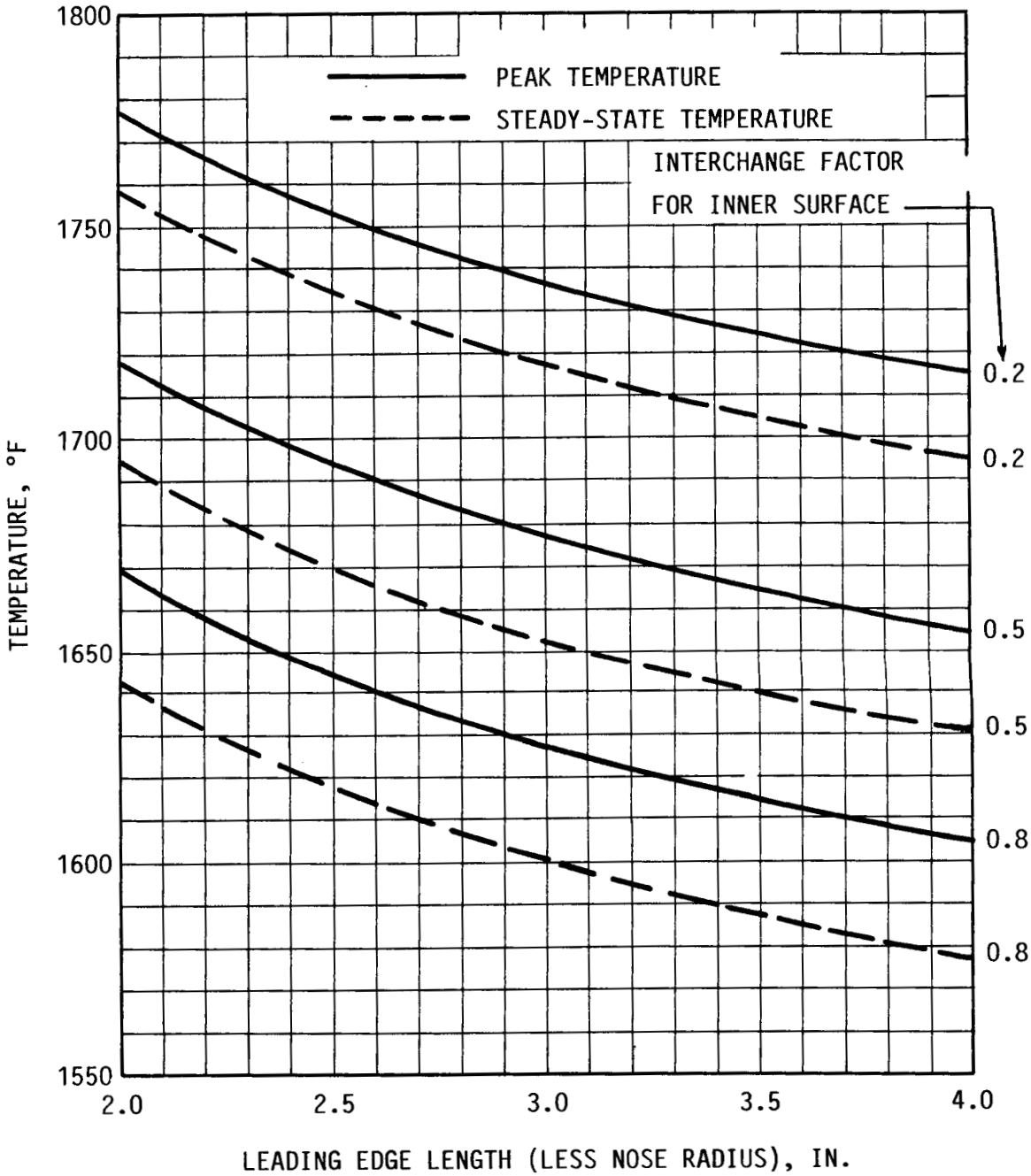

Figure 51. Peak and Steady-State Temperatures at Stagnation Line of Engine Inlet Leading Edge

From Equation (38), the maximum thermal stress is a tensile stress of 5990 psi at the inner radius. From page 125, the bending stress is 3440 psi, and is compressive at the inner radius. The net tensile stress is then 2550 psi, well below the yield stress of 16,700 psi for Haynes 25 at 1650°F. Thus,

thermal stress is not excessive during the transient phase of flight.

HEAT TRANSPORT LIMITS DURING TRANSIENT

Heat pipe heat transport limits were calculated and compared with actual heat transport rates and/or related parameters during the temperature transient. Calculations were performed generally using the same methods as were employed for determining the steady-state heat transport limits. However, some modifications were necessary, as will now be described.

Modifications for Transient Case

The sonic and entrainment limits represent the axial heat flux (heat transport rate per unit minimum vapor space area) at which sonic velocity is reached and vapor starts to entrain liquid from the wick, respectively. These limits must be compared with the actual axial heat flux leaving the nose section. The latter heat flux was found by subtracting the rate at which heat is absorbed in the nose section from the net incident heating rate on the nose surface.

The boiling limit represents the heat flux at the wall/wick interface at which boiling is initiated in the heat pipe liquid. What was actually calculated is the net heat flux at the stagnation line which would initiate boiling in the wick. It may be shown that this figure is 0.542 times the boiling limit calculated at the wall/wick interface on the basis of rectilinear geometry. A further correction should be made to account for heat absorption in the wall of the nose section, which would increase the stagnation line heat flux required to initiate boiling. This latter correction was ignored here, resulting in conservatively lower estimates of the stagnation line heat flux at which boiling starts.

The capillary pumping limit calculation determines the maximum pressure difference between the heat pipe vapor and liquid, which in turn establishes the minimum diameter of curvature at the liquid-vapor interface. The actual wick pore diameter must be less than the minimum diameter of curvature. Actual heat transfer rates at the liquid-vapor interface must be used in the capillary pumping limit equation. Therefore, heat transfer rates incident on the nose and inner sections of the leading edge must be reduced by the heat absorption rates in these sections.

During Phase 2 of the transient, when the continuum front is advancing through the leading edge interior, a substantial fraction of the vapor generated at the nose section condenses on the wick at the continuum front, in addition to that which condenses along the wick length behind the front. The average fluid velocity in the condensing region is then larger than is

the case when condensation occurs uniformly over the entire condenser length. This effect was allowed for in the equations by assuming adiabatic (noncondensing) flow when calculating the axial fluid pressure drops. The fluid velocities are then constant and equal to their entrance values, assuring a conservatively high estimate of the frictional pressure drops. The liquid pressure drop due to vehicle acceleration and gravity was included in the liquid pressure drop calculations.

Results

Results of the transient heat transport limit calculations are given in Figures 52 and 53. In Figure 52, the sonic and entrainment limits are plotted against time, along with the actual axial heat flux. During Phase 2, the axial heat flux is equal to the sonic limit. The axial heat flux is seen to be always less than or equal to the sonic and entrainment limits.

In Figure 53, the stagnation line boiling limit is compared with the actual net stagnation line heat flux, and the minimum diameter of curvature at the liquid-vapor interface required for capillary pumping is compared with the wick pore diameter of the 400-mesh screen used at the liquid-vapor interface. The boiling limit is seen to be always well above the stagnation line heat flux. The diameter of curvature remains well above the wick pore diameter, reaching its lowest value at the end of Phase 2 (at 23 sec).

The data presented in Figures 52 and 53 indicates that disruptions in heat transport through the leading edge interior due to heat pipe heat transport limitations should not occur during the climb transient.

CONCLUDING REMARKS

The analysis presented in this report indicates that the use of heat pipe cooling techniques in the design of scramjet inlet leading edges is feasible. By fabricating the leading edge as a hollow shell with a sodium-filled porous wick liner, heat incident on the nose and inner surface of the leading edge can be dissipated from the outer surface with a minimal temperature drop.

With a leading edge radius of 0.035 in. and an overall length of 2-3 in., peak leading edge temperatures can be held to 1700°F or less. Thermal and bending stresses are held to tolerable levels by the use of thin (0.010 in.) walls and wicks, and closely spaced (0.2 in.) chordwise ribs. The leading edge can then be fabricated from an oxidation-resistant

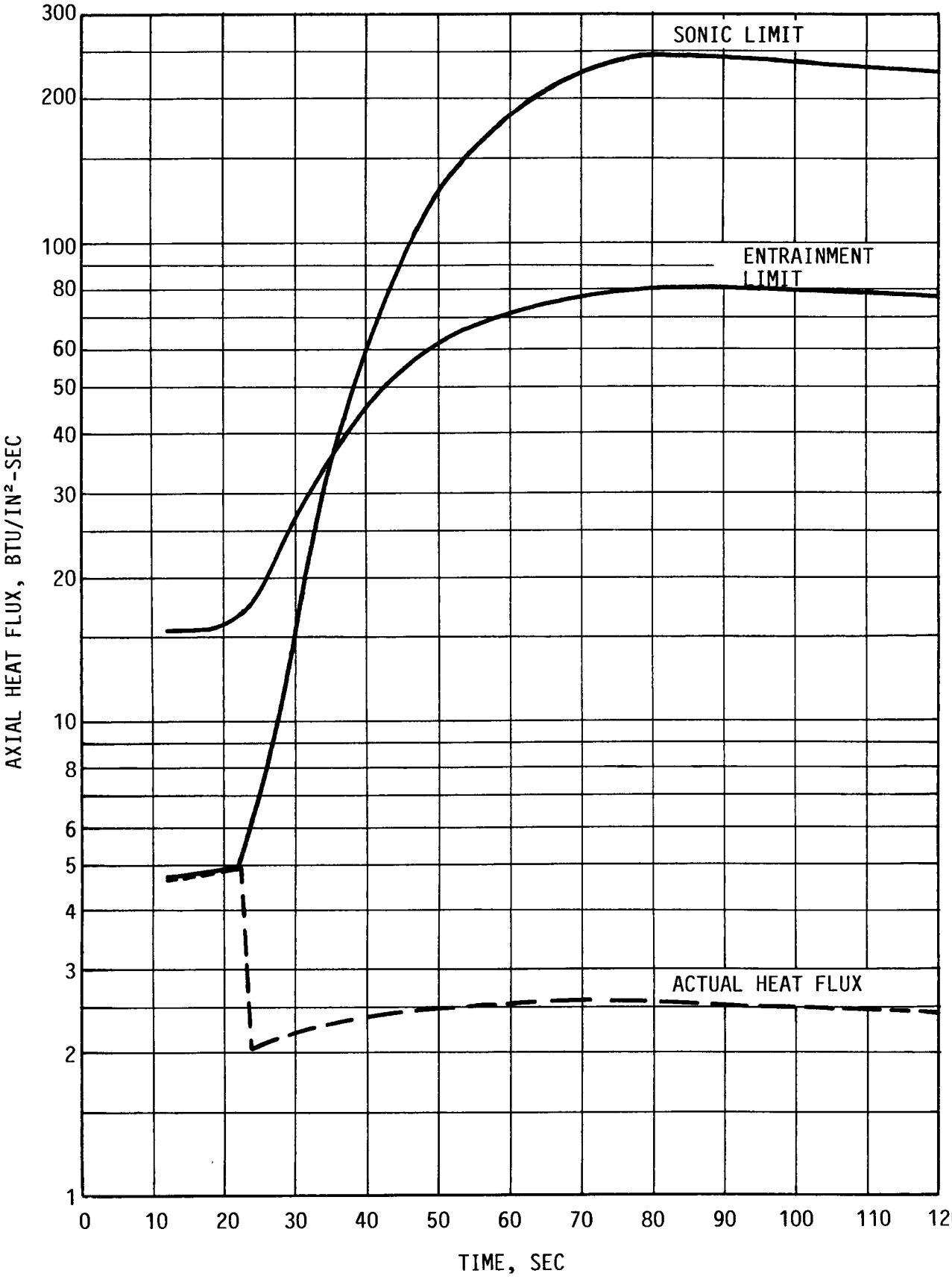

Figure 52. Sonic and Entrainment Limits During Climb Transient

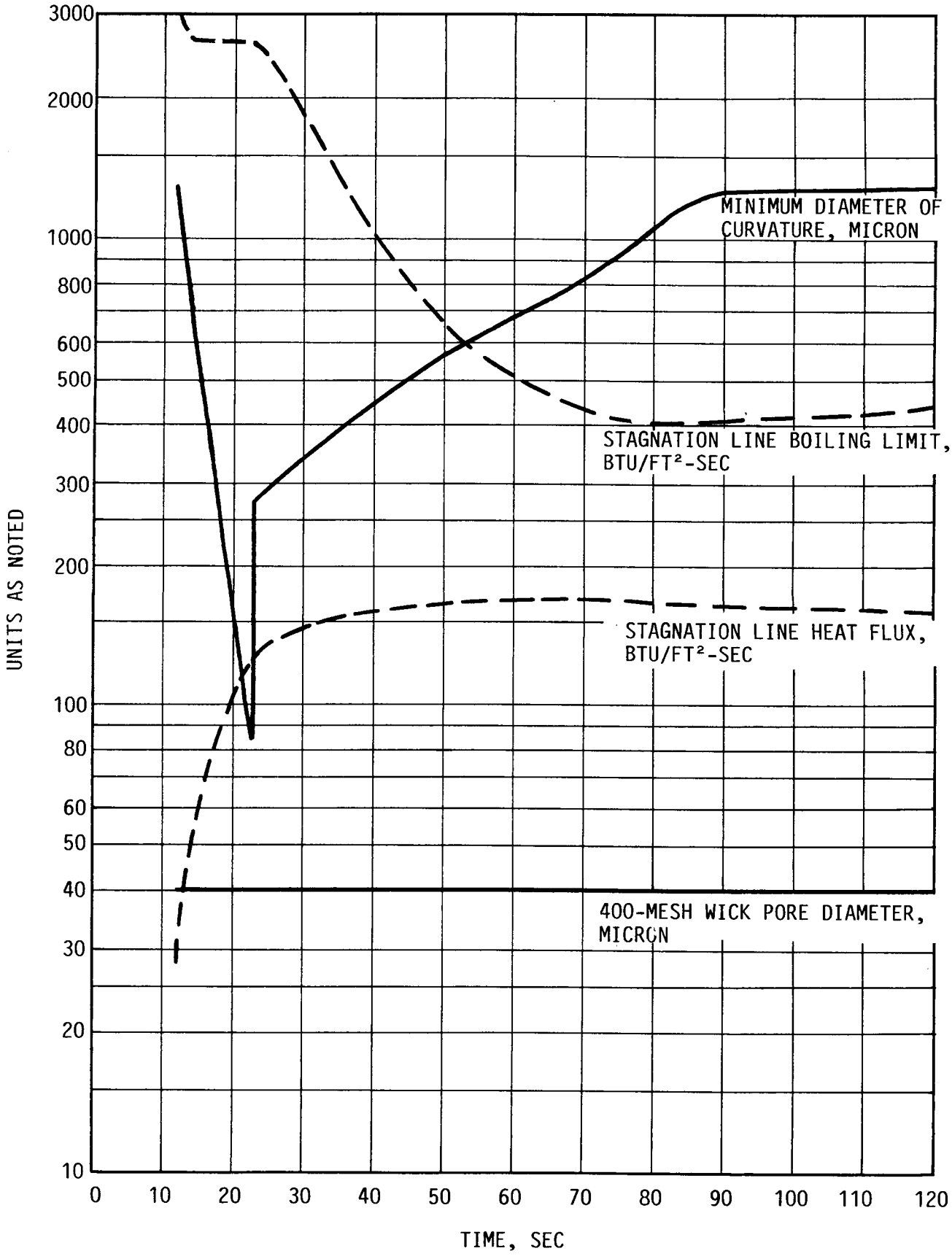

Figure 53. Boiling and Capillary Pumping Limits During Climb Transient

superalloy such as Haynes 25. Overall weights are on the order of 2 lb/ft^2 of planform area.

It is recommended that a feasibility demonstration of heat pipe cooling for a small-radius engine inlet leading edge be carried out, using superalloy construction and sodium as the heat pipe fluid. Additional analytical studies to identify the minimum feasible radius of heat-pipe-cooled leading edges are also recommended.

APPENDIX A - REVIEW OF PRIOR WORK

The work on heat pipe cooling systems for scramjet combustor liners presented in the main part of this report represents the continuation of an earlier study conducted for the Naval Surface Weapons Center under Purchase Order N 60921-83-M-G788.

Study objectives were to determine if heat pipe cooling for scramjet combustor liners is feasible, and to identify design concepts warranting further investigation.

Design criteria were provided by the Johns Hopkins Applied Physics Laboratory. Included were: engine size and configuration, trajectory data, and combustor liner heat flux data. The engine size and configuration were approximately as shown in Figure 4, page 10. The trajectory and liner heat flux data are given in Table A1.

In one design option, the combustor liner consisted of a 0.125 in. layer of carbon-carbon coated with a 0.070 in layer of pyrolytic graphite. The heat pipe cooling structure surrounded the liner and was assumed to be in perfect thermal contact with the liner. In the other option, the heat pipe cooling structure itself served as the combustor liner. TZM molybdenum was selected as the cooling system structural material, and lithium as the heat pipe and heat sink fluid.

Three types of heat sinks were considered: sensible lithium, vaporizing lithium, and radiation. The manner in which the heat sinks were integrated with the liner and heat pipe for the first option is shown in Figure A1. The same configurations apply for the second option, except that the separate carbon-carbon liner is not present.

Cooling system characteristics which are common to the carbon-carbon and TZM (heat pipe) liner options are summarized in Table A2. The cooling system temperature for the carbon-carbon liner option is 1250°F lower than the liner temperature because of the low thermal conductivity of the pyrolytic graphite liner coating.

A total of 18 heat pipe cooling concepts were analyzed in a scoping study on the basis of a figure of merit (FOM). The FOM was defined as the sum of the increase in engine weight and decrease in fuel weight resulting from substitution of the heat pipe liner cooling system for a comparable uncooled liner. The figure of merit for five concepts was found to be at least 50% lower than the FOM for the other 13 concepts.

The characteristics of these five concepts are given in Table A3. The candidate concepts identified in Table A3 were

PRECEDING PAGE BLANK NOT FILMED

Table A1. Trajectory and Liner Heat Flux Data

Time	Altitude	Mach No.	Air Pressure	Liner Temperature, °F			
sec	1000 ft		psi	140	1840	2740	3540
				Liner Heat Flux, Btu/ft²-sec			
4	3.52	3.192	12.92	973.0	285.2	-	-
8	10.60	3.345	9.88	862.2	261.3	-	-
12	17.85	3.612	7.39	867.1	305.8	-	-
16	25.09	3.805	5.45	771.4	288.9	1.1	-
20	32.24	4.163	3.95	842.9	385.0	111.9	-
24	39.20	4.385	2.84	752.6	380.9	157.9	-
28	45.87	4.688	2.06	731.4	419.8	234.7	55.2
32	52.22	4.955	1.52	670.3	415.6	263.8	117.6
36	58.02	5.177	1.15	571.7	363.6	239.4	119.9
40	63.17	5.350	0.90	489.3	316.9	214.1	115.2
44	67.64	5.491	0.73	424.7	279.0	192.1	108.5
48	71.46	5.605	0.61	375.7	249.7	174.6	102.3
52	74.69	5.702	0.52	338.0	226.7	160.4	96.5
56	77.42	5.786	0.46	309.8	209.6	149.8	92.2
60	79.41	5.860	0.41	288.5	196.5	141.7	88.9
64	81.64	5.926	0.38	271.9	186.4	135.4	86.3
68	83.27	5.974	0.35	256.7	177.0	129.4	83.7
72	84.64	5.994	0.32	177.7	110.2	70.0	31.3
80	86.80	5.997	0.29	146.7	89.3	55.0	22.0
88	88.38	5.997	0.27	136.1	82.8	51.4	21.2
100	90.04	5.996	0.25	128.1	78.5	49.3	21.2
120	91.71	5.996	0.23	121.5	75.1	47.9	21.6
140	92.68	5.995	0.22	118.0	73.8	47.3	21.9
160	93.28	5.995	0.22	115.8	72.7	47.0	22.2
180	93.67	5.995	0.21	114.4	72.0	46.6	22.3
202	93.97	5.995	0.21	113.2	71.3	46.2	22.1
358	93.97	5.995	0.21	113.2	71.3	46.2	22.1

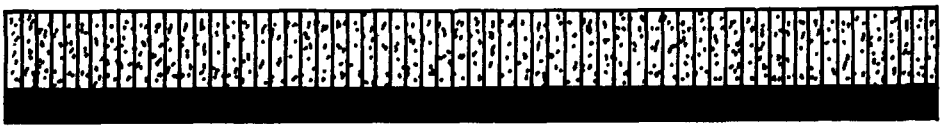

HEAT SINK INTEGRATED WITH COMBUSTOR HEAT PIPE

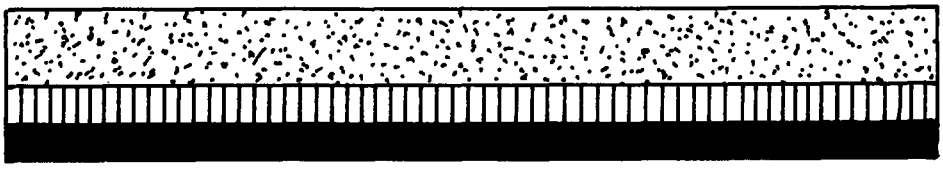

HEAT SINK + COMBUSTOR HEAT PIPE

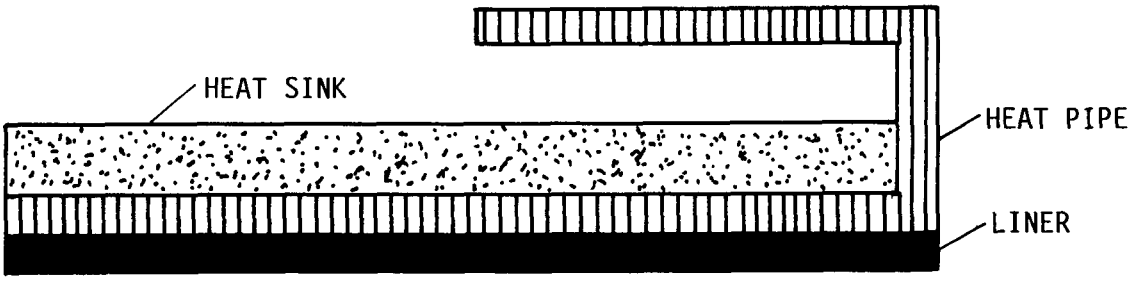

HEAT SINK + COMBUSTOR & RADIATOR HEAT PIPES

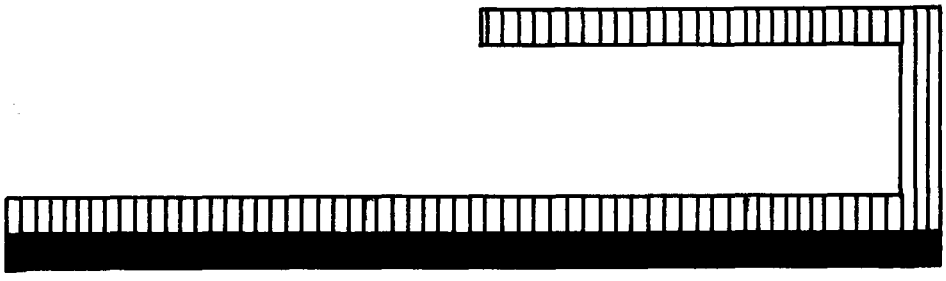

COMBUSTOR HEAT PIPE & RADIATOR HEAT PIPE

A separate carbon-carbon liner is not present when the heat pipe itself serves as the combustor liner.

Figure A1. Liner Cooling Concept Configurations

Table A2. Cooling System Characteristics		
Characteristic	C-C Liner	TZM Liner
Liner Temperature, °F	3500	3000
Heat Load, Btu	185,000	310,000
Peak Heat Flux, Btu/ft²-sec	140	230
Steady State Heat Flux, Btu/ft²-sec	24	40
Cooling System Temperature, °F	2250	3000
Heat Pipe & Heat Sink Fluid	Lithium	Lithium
Vapor Pressure, psia	6.6	95.7
Structural Material	TZM	TZM
Wall & Rib Thickness, in.	0.015	0.015

subjected to more detailed analysis in the Cooling System Integrability task of the current study program. A preferred concept was then selected for evaluation in the remaining program tasks.

Table A3. Characteristics of Candidate Cooling Concepts

Characteristic	C7	C8	C4	M6	C5
Figure of Merit, lb	29	54	70	60-75	81
Liner Material	C-C	C-C	C-C	TZM	C-C
Heat Sink Type	-	V	V	V	V
Combustor Heat Pipe	X	X|I	X|C	X	X
Radiator Heat Pipe	X	-	-	X	-
Cooling System Temp., °F	2250	2250	2250	3000	2250
Weight, lb	78	57	72	112-120	67
Volume, ft^3	0.83	0.77	0.78	0.98-1.08	1.02
Displaced Weight, lb	54	10	10	65	10
Displaced Volume, ft^3	0.75	0.66	0.66	0.79	0.66
Net Weight Increment, lb	24	47	62	47-55	57
Fuel Weight Decrement, lb	5	7	8	13-20	24
Heat Pipe Thickness, in.	0.211	-	-	0.180	0.211
Heat Sink Thickness, in.	-	-	0.494	0.203	0.466
Combined HP/HS Thickness, in.	0.211	0.511	0.494	0.383	0.677
Rib Spacing, in.	1.06	1.06	1.06	0.11-0.18	1.06
Radiator Area, ft^2	22.5	-	-	13.2	-
Radiator Length, ft	4.1	-	-	2.4	-

Notes: V denotes vaporizing lithium heat sink.
X denotes that indicated component is present.
|I denotes that indicated components are integrated as single structure.
|C denotes that the heat pipe wick and the lithium heat sink are a single combined entity.

APPENDIX B - RADIATOR AREA

The net heat transfer rate per unit area q from the radiator surface is equal to the radiation rate from the surface minus the aerodynamic heating rate on the surface, or

$$q = \varepsilon\sigma T_w^4 - h(T_r - T_w) \tag{B1}$$

where T_r = absolute recovery temperature
T_w = absolute radiator surface temperature
h = heat transfer coefficient
σ = Stefan-Boltzmann radiation constant
ε = surface emissivity

The surface temperature when q = 0 is called the radiation equilibrium temperature. From Equation (B1), T_r can then be expressed as

$$T_r = \frac{\varepsilon\sigma T_e^4 + hT_e}{h} \tag{B2}$$

where T_e is the absolute radiation equilibrium temperature.

Upon substitution of Equation (B2) into (B1), the net heat transfer rate q can be written

$$q = \varepsilon\sigma(T_w^4 - T_e^4)(1 + \beta) \tag{B3}$$

where

$$\beta = \frac{h(T_w - T_e)}{\varepsilon\sigma(T_w^4 - T_e^4)} \tag{B4}$$

From Equation (B2),

$$h = \frac{\varepsilon\sigma T_e^4}{T_r - T_e} \tag{B5}$$

On substitution of Equation (B5) into (B4), β may be written

$$\beta = \left(\frac{T_w - T_e}{T_r - T_e}\right)\left(\frac{T_e^4}{T_w^4 - T_e^4}\right) \tag{B6}$$

Also,

$$q = \frac{Q}{A_r} = \frac{q_l A_l}{A_r} \tag{B7}$$

where A_r = radiator area
A_l = liner area
q_l = liner heat flux
Q = net heat transfer rate

Upon substitution of Equation (B7) into (B3) and solving for A_r,

$$A_r = \frac{q_l A_l}{\varepsilon\sigma(T_w^4 - T_e^4)(1 + \beta)} \tag{B8}$$

The radiator area can be found from Equations (B6) and (B8) when T_w, T_r, and T_e are specified.

The recovery temperature is given by

$$T_r = T_s + r(T_t - T_s) \tag{B9}$$

where T_s = static temperature
T_t = total temperature
r = recovery factor

The total temperature (15) is given by

$$T_t = T_s\left(1 + \frac{\gamma - 1}{2} M^2\right) \tag{B10}$$

where M = Mach number
γ = ratio of specific heats at constant pressure and constant volume

Upon substitution of Equation (B10) into (B9),

$$T_r = T_s\left(1 + \frac{\gamma - 1}{2} rM^2\right) \tag{B11}$$

The recovery temperature T_r can be found from Equation (B11) for specified values of T_s, r, M, and γ. For air, $\gamma = 1.4$.

The radiation equilibrium temperature can be found from tables such as are given in Reference 4.

APPENDIX C - THERMAL PROPERTY DATA

Thermal property data for the liner, heat pipe, insulation, fuel, and fuel tank materials which were used in the cooling system concept design studies are presented here.

TZM MOLYBDENUM, LITHIUM, AND CARBON-CARBON (7, 11, 16, 20)

Curves were fitted to temperature-dependent property data for TZM molybdenum, lithium, and carbon-carbon to facilitate their use in the analytical studies. Thermal property equations for these materials were formulated in the following forms.

$$w = A + BT \tag{C1}$$

$$c = C + DT + ET^2 \tag{C2}$$

$$k = F + GT + HT^2 \tag{C3}$$

$$C_s = I + JT + KT^2 \tag{C4}$$

$$C_l = L + MT \tag{C5}$$

$$C_t = N + OT \tag{C6}$$

$$\alpha = P + QT \tag{C7}$$

where A through Q are thermal property constants

T = temperature, °F
w = density, lb/in^3
c = specific heat, Btu/lb-°F
k = thermal conductivity, Btu/hr-ft-°F
C_s = sensible thermal capacity = $\int_{90}^{T} c\,dT$, Btu/lb
C_l = latent thermal capacity, Btu/lb
C_t = total thermal capacity = $C_s + C_l$, Btu/lb
α = thermal expansion coefficient, in./in.-°F

The thermal property constants for TZM molybdenum and carbon-carbon are given in Table C1. The initial temperature used in the calculation of thermal capacity was 90°F.

Table C1. Thermal Property Constants for TZM Molybdenum and Carbon-Carbon

Constant	TZM Molybdenum	Carbon-Carbon
A	0.3618	0.058
B	-5.017×10^{-6}	0.0
C	0.0593	0.100*
D	7.33×10^{-6}	2.90×10^{-4}*
E	0.0	0.0*
F	74.17	3.16
G	-0.00833	0.00043
H	0.0	0.0
I	-5.37	-217.5
J	0.0593	0.417
K	3.67×10^{-6}	1.25×10^{-5}
L,M,N,O	0.0	0.0
P	1.825×10^{-6}	1.00×10^{-6}
Q	8.75×10^{-10}	0.0

* Applies for T≤1000°F.
For T>1000°F, let c = 0.1137*ln(T + 460) - 0.4384

Thermal property constants for lithium are given in Table C2. Data is presented separately for temperatures below the melting point of 367°F, at the melting point, and above the melting point. Again, the initial temperature used to calculate the thermal capacity was 90°F.

Below the melting point, mean values over the temperature range between 90°F and the melting point were used in specifying the density and specific heat. At the melting point, the specific heat was assumed to be equal to the heat of fusion (186 Btu/lb). With this assumption, the addition of a quantity of heat equal to the heat of fusion raises the temperature of 1 lb of lithium at the melting point by 1°F (nominally zero). The thermal capacity at the melting point was taken to be the sum of the thermal capacity from 90°F to the melting point plus the heat of fusion.

Table C2. Thermal Property Constants for Lithium			
Constant	Below MP	At MP(liq.)	Above MP
A	0.019	0.01939	0.01939
B	0.0	-2.008×10^{-6}	-2.008×10^{-6}
C	0.79	186.0	1.0
D	0.0	0.0	1.0
E	0.0	0.0	1.0
F	20.26	20.26	20.26
G	0.0149	0.0149	0.0149
H	-3.268×10^{-6}	-3.268×10^{-6}	-3.268×10^{-6}
I	-	-	37.83
J	-	-	1.00
K	-	-	0.0
L	-	-	10,230
M	-	-	-0.77
N	-	-	10,268
O	-	-	0.23

Above the melting point, the thermal capacity is equal to the sum of the thermal capacity at the melting point plus the thermal capacity from the melting point to the temperature in question.

SILICON CARBIDE (21)

For calculational purposes, the thermal conductivity and specific heat of silicon carbide and carbon-carbon, which are similar in magnitude, were assumed to be the same. The density of silicon carbide is 0.116 lb/in^3.

MIN-K AND ZIRCAR (16, 22)

MIN-K was used as the cooling system insulation at temperatures up to 2000°F. ZIRCAR (zirconia felt) was used at temperatures over 2000°F.

MIN-K

The density value used for MIN-K is 0.00926 lb/in^3, although even lighter forms are available. The thermal conductivity and specific heat are given in Table C3.

Table C3. Thermal Conductivity and Specific heat of MIN-K

Temperature °F	Thermal Conductivity Btu/hr-ft-°F		Specific Heat Btu/lb-°F
	Sea Level	80,000 ft	
0	0.019	0.009	0.135
500	0.020	0.010	0.230
1000	0.025	0.015	0.260
1500	0.035	0.026	0.275
2000	0.052	0.041	0.280

In the design calculations, thermal conductivity values at 80,000 ft altitude were used.

ZIRCAR

The density of ZIRCAR is 0.00868 lb/in^3. The specific heat is 0.13 Btu/lb-°F at 200°F, and 0.18 Btu/lb-°F at 4300°F. The thermal conductivity is given in Table C4.

Table C4. Thermal Conductivity of ZIRCAR

Temperature, °F	Thermal Conductivity, Btu/hr-ft-°F	
	Air	Vacuum
2000	0.108	0.053
2500	0.138	0.075
3000	0.175	0.108

In the design calculations, thermal conductivity values in air were used.

FUEL AND FUEL TANK (23, 24)

Properties of the engine fuel and fuel tank (see Table C5) were used in calculating the fuel temperature rise due to heat leakage from the liner cooling system and the engine skin.

The fuel was assumed to be Shelldyne H at a mean temperature of 200°F, and the tank was assumed to be constructed from titanium.

Table C5. Fuel and Fuel Tank Properties at 200°F

Property	Shelldyne H	Titanium
Density, lb/in^3	0.0369	0.1625
Specific Heat, Btu/lb-°F	0.387	0.113
Thermal Conductivity, Btu/hr-ft-°F	0.090	-

REFERENCES

1. Hunt, J.L., et al, "Hypersonic Airbreathing Missile Concepts Under Study at Langley," AIAA-82-0316. Presented at AIAA 20th Aerospace Sciences Meeting, Orlanda, Fla., Jan. 1982, p. 7.

2. Harder, I.E., et al, "Carbon-Carbon for Turbine Engine Applications," Advances in TPS and Structures For Space Transportation Systems, NASA CP-2315, Dec. 1983, p. 425.

3. Eckert, E.R.G. and Drake, R.M. Jr., Heat and Mass Transfer, McGraw-Hill, New York, 1959, p. 260.

4. Bartle, R.S. & Hanawalt, A.J., "A Manual for Determining Aerodynamic Heating of High-Speed Aircraft-Vol.II," Report No. 7006-3352-001, Bell Aircraft Corp., June 1959.

5. Minges, M.L., "The Temperature Dependence of the Thermal Contact Resistance Across Nonmetallic Surfaces," AFML-TR-69-1, Air Force Materials Laboratory, Wright-Patterson Air Force Base, Ohio, Oct. 1969.

6. Silverstein, C.C., "A Feasibility Study of Heat-Pipe-Cooled Leading Edges for Hypersonic Cruise Aircraft," NASA CR-1857, Nov. 1971.

7. Briggs, J.Z. & Barr, R.Q., "Arc-Cast Molybdenum TZM Alloy: Properties and Applications," High Temperatures-High Pressures, Vol. 3, 1971, pp. 363-409.

8. Salisbury, J.K. (ed.), Kent's Mechanical Engineering Handbook, Power-Vol., 12th Ed., Wiley, N.Y., 1950, p. 6-40.

9. Blosser, M.L., "Design Studies of Carbon-Carbon Shuttle Body Flap," Advances in TPS and Structures for Space Transportation Systems, NASA CP-2315, Dec. 1983, p. 597.

10. Faires, V.M., Applied Thermodynamics, MacMillan, N.Y., 1948, p. 170.

11. Weatherford, Jr., W.D., et al, "Properties of Inorganic Energy Conversion and Heat Transfer Fluids for Space Applications," WADD TR 61-96, 1961.

12. Silverstein, C.C., "Correlation of Heat Pipe Heat Transport Limits with Vapor Pressure," AIAA-85-0939. Presented at AIAA 20th Thermophysics Conference, Williamsburg, Va., June 1985.

13. Silverstein, C.C., "A Study of Heat Pipe Applications in Nuclear Aircraft Propulsion Systems," CR-72610, NASA Lewis Research Center, Cleveland, Ohio, Dec. 1969.

14. Tuominen, S.M. & Dahl, J.M., "Cyclic Oxidation Testing of Molybdenum Protected by Silicide Coatings," J. Less-Common Metals, Vol. 81, 1981, pp. 249-260.

15. Kreith, F., Principles of Heat Transfer, 2nd Ed., International Textbook Company, Scranton, Pa., 1967, pp. 175-188, 521.

16. "High Temperature Structures Research Investigation-Phase III," Task IV, MDC E2035, McDonnell Douglas Astronautics Co., St. Louis, Mo., Feb. 15, 1979.

17. Camarda, C.J. & Masek, R.V., "Design, Analysis, and Tests of a Shuttle-Type Heat-Pipe-Cooled Leading Edge," J. Spacecraft & Rockets, Vol. 18, No. 1, Jan-Feb. 1981, pp. 71-78.

18. Keenan, J.H., et al, Gas Tables, 2nd Ed., Wiley, New York, 1980.

19. Timoshenko, S. & Goodier, J.N., Theory of Elasticity, 2nd Ed., McGraw-Hill, New York, 1951, p. 414.

20. Davison, H.W., "Compilation of Thermophysical Properties of Liquid Lithium," NASA TN D-4650, NASA, Washington, D.C., July 1968.

21. Baumeister, T. (ed.), Standard Handbook for Mechanical Engineers, 7th Ed., McGraw-Hill, N.Y., 1967, pp. 6-208, 209.

22. "ZIRCAR Fibrous Ceramics High Temperature Thermal Insulation," Bulletin No. ZPI-207, ZIRCAR Products, Inc., Florida, N.Y., Aug. 1, 1978.

23. "Vaporizing and Endothermic Fuels for Advanced Engine Application," AFAPL-TR-67-114, Vol II, Part III, Feb. 1970, pp. 390-391.

24. Esbach, O.W. (ed.), Handbook of Engineering Fundamentals, 1st Ed., Wiley, N.Y., 1947, p. 1-126.

Standard Bibliographic Page

1. Report No.	2. Government Accession No.	3. Recipient's Catalog No.
NASA CR-4036		

4. Title and Subtitle	5. Report Date
HEAT PIPE COOLING FOR SCRAMJET ENGINES	December 1986
	6. Performing Organization Code
7. Author(s)	8. Performing Organization Report No.
Calvin C. Silverstein	CCS-115
9. Performing Organization Name and Address	10. Work Unit No.
CCS Associates P.O. Box 563 Bethel Park, PA 15102	11. Contract or Grant No. NAS1-17908
12. Sponsoring Agency Name and Address	13. Type of Report and Period Covered
National Aeronautics and Space Administration Washington, DC 20546	Contractor Report
	14. Sponsoring Agency Code 505-33-53-70

15. Supplementary Notes

Langley Technical Monitor: Robert R. McWithey
Final Report

16. Abstract

Liquid metal heat pipe cooling systems have been investigated for the combustor liner and engine inlet leading edges of scramjet engines for a missile application.

The combustor liner is cooled by a lithium-TZM molybdenum annular heat pipe, which incorporates a separate lithium reservoir. Heat is initially absorbed by the sensible thermal capacity of the heat pipe and liner, and subsequently by the vaporization and discharge of lithium to the atmosphere. The combustor liner temperature is maintained at 3400°F or less during steady-state cruise.

The engine inlet leading edge is fabricated as a sodium-superalloy heat pipe. Cooling is accomplished by radiation of heat from the aft surface of the leading edge to the atmosphere. The leading edge temperature is limited to 1700°F or less.

It is concluded that heat pipe cooling is a viable method for limiting scramjet combustor liner and engine inlet temperatures to levels at which structural integrity is greatly enhanced.

17. Key Words (Suggested by Authors(s))	18. Distribution Statement
Heat pipe, liquid metal, scramjet, leading edge cooling, combustor cooling	[redacted]N until December 1988 Subject Category 34

19. Security Classif.(of this report)	20. Security Classif.(of this page)	21. No. of Pages	22. Price
Unclassified	Unclassified	168	